Study on Neutronics Simulation Applicable to Various Design Requirements for Fast Spectrum Reactor

Jun-Shuang Fan

Graduate School of Engineering

Hokkaido University

A dissertation submitted for the degree of

Doctor of Philosophy in Engineering

February, 20, 2023

Abstract

Since the nuclear fission reaction was confirmed in 1938, human beings realized that the fission process can cause a self-sustaining chain reaction. After this point was verified through experiment, the age of nuclear power utilization started. The first commercial nuclear reactor plant *Shippingport Atomic Power Station* started to operate in 1957, and since then more than 60-year operation experience on nuclear power utilization has been accumulated. Currently, the development of nuclear reactors is in the process of moving from the third generation to the fourth generation. The majority of commercial power plant reactors are thermal-neutron reactors, i.e., using thermal neutrons (around 0.025 eV) to sustain a fission chain reaction and to output energy. The utilization rate of uranium resources by thermal neutrons is low due to the uranium nuclear properties. Therefore, fast-neutron reactors (fast reactors in short), which can greatly improve the utilization rate of uranium resources, have received widespread attention and been actively promoted. The fast reactors can fully utilize uranium resources by converting fertile material into fissile material, and therefore, this process is called as *breeding*. Besides, the minor actinide (MA) from fast reactor spent fuel is considerably less than it from conventional thermal reactor. With these unique features, fast reactor technology has been being actively promoted in all major industrial countries. Currently, U.S. and Japan are promoting the *Natrium* fast reactor project, and China is constructing demonstration fast reactors *Xiapu-1* and *Xiapu-2*.

In the research field of nuclear engineering, analysis strongly relies on computer software. The development of a new type of reactor (such as a fast reactor) begins with a conceptual design that explores a wide range of design parameter space, followed by several stages of design refinement, and eventually leads to a detailed design and plant construction. In the conceptual design stage, a large number of quick calculations are necessary for giving a solution, whereas in the detailed design stage, accuracy of the solution must be ensured. Therefore, software that is capable of meeting different demands at each stage of the design work would be essential.

The research summarized in this dissertation focuses on software that can be used in a variety of reactor designs. The first research is the development and verification of a software for neutronics analysis applicable to various design stages in fast reactor development. The second research is the development of a practical neutronics analysis method for the intermediate stage of fast reactor design, which could be regarded as a bridge between the conceptual design stage and the detailed design stage.

The software used in this dissertation is CBZ, which is a general-purpose reactor physics analysis code system, and it is independently developed at Hokkaido University. FRBurner is a fast reactor burnup calculation module that can realize various combinations of calculation methods through incorporating them with various modules and solvers in CBZ. This module is being verified against an OECD/NEA fast reactor neutronics analysis benchmark. This benchmark offers four sodium-cooled fast reactor concepts, which represent the general type of sodium-cooled fast reactors. Four key reactor physics parameters, effective neutron multiplication factor k_{eff},

effective delayed neutron fraction β_{eff}, sodium void reactivity $\Delta\rho_{\text{void}}$, and Doppler reactivity $\Delta\rho_{\text{Doppler}}$, are the focus and compared to reference results. Comparison with the reference results provided by other institutes indicates that the FRBurner module can provide acceptable results for general-type fast reactor physics analysis. Second, a comprehensive comparison of these methods is performed in order to reveal the features of each option on the calculation method. This helps users choose proper methods for wide range utilization. Moreover, the computing burden is taken into account to present desirable calculation conditions for the conceptual, intermediate, and detailed design stages. In addition to the solvers based on the transport and diffusion equations, a solver based on the simplified-P_3 equation (SP_3 equation) is added to CBZ. The SP_3 solver is positioned as an intermediate option between the transport and diffusion solvers. Aside from the verification part of study, the novelty of this study is that various methods that differ from whole-core step calculation theory, dimension of lattice model, burnup chain model, and libraries (which can be regarded as four aspects on calculation method) are thoroughly compared in the context of fast reactor applications. It is noteworthy that a series of calculation methods based on the SP_3 theory are used for fast reactor analysis in this research. Utilization of the SP_3 theory in fast reactor analysis has been limited in the past. People have started to use the SP_3 theory in fast reactor analysis very recently. Therefore, the accumulated data is insufficient, and this research fills the blank from the viewpoint of application.

Building on the first research, the reliability of the FRBurner module is well proved, and advantage of the SP_3 solver is exhibited as well. Then, an innovative reactivity calculation method is newly proposed through combining the SP_3 and perturbation theories. Equations of the SP_3-perturbation (SPP) method is derived at first, and then verification is carried with the same OECD/NEA benchmark after code implementation is finished. Although all reactivity calculation methods based on the perturbation theory could give component-wise reactivity, the SPP method has a physical meaning unclear term in its equation. Through tracing to the theoretical source of SP_3 and defining a new form of it, the physical meaning unclear term in the SPP method is eliminated. Thus, the component-wise reactivity calculation based on the SP_3 and perturbation theories is achieved firstly in the world. Through component-wise reactivity analysis, it is demonstrated that more accurate prediction of the scattering and leakage components of reactivity can be obtained with the new method comparing to the diffusion-perturbation method.

In summary, the author has developed and verified a software applicable to meet various demands on design requirements of fast reactors, and proposed a new method (SPP method) which is useful for the reactivity analysis. These two works together contribute to the nuclear engineering field significantly.

Contents

List of Figures

List of Tables

Acknowledgements

Looking back at my more than five years of life at Hokkaido University, I would like to express my deepest gratitude to my supervisor, Professor Go Chiba, for all the guidance, concern, and support during my master's and PhD periods. Chiba-sensei always helps me study patiently, no matter how busy he is. The help from Chiba-sensei is not only for study but also for life. I am grateful to have such a precious opportunity to study with Chiba-sensei, and I do feel fortunate.

I would like to thank Hokkaido University for supporting my research and life since 2021 through the DX fellowship program.

I want to express my gratitude to Prof. Tamotsu Kozaki, Prof. Kazuhiro Sawa, and Prof. Tomohiro Endo for their comments and instructions on my twice mid-term evaluations. Furthermore, the comments from Kozaki-sensei and Endo-sensei on several AESJ meetings are important to me as well.

I also want to say thanks to Dr. Kenichi Tada for his kindness during my entire internship at JAEA.

I would like to thank my family and my friends at Hokkaido University for helping me get through the tough time.

I must say thanks to my cute little cats, Tetsuko and Luna. I would finish my dissertation earlier if they could keep quiet at midnight.

Lastly, I would like to express my gratitude to my girlfriend, Zixuan Zhang. Her love, companionship, and support always help me feel the happiness of life.

Chapter 1

Introduction

1.1 Background

Nuclear reactors are devices which initiate and control nuclear reaction (fission reactor in most cases) to output power. Nuclear reactors can be categorized as thermal neutron reactors or fast neutron reactors according to the energy of the neutrons that sustain the fission chain reaction. The fast neutron reactor (fast spectrum reactor as well, or fast reactor in short) technology is given high expectations since the beginning of nuclear energy utilization. The fast reactors have obvious advantages in making full use of uranium resources and reducing transuranic elements (TRU). From the perspective of limited resources and a growing emphasis on environmental conservation, the benefits of fast reactors over light water reactors (LWRs) are obvious. The significance of fast reactor technology can be known from the fact that three of the six Generation IV nuclear reactors are fast reactors [1]. Many nations, including Japan, continue to develop the fast reactor technology as middle-long term projects [2].

The reactor physics analysis is one crucial part of the work for reactor design.

Generally speaking, the reactor physics analysis calculates key parameters such as reactor thermal or electric power, the effective neutron multiplication factor k_{eff}, the distribution of neutron flux ϕ (or angular neutron flux ψ), the reactivity coefficient $\Delta\rho$, etc. by calculating the reaction rate between neutrons and the various materials that make up the reactor. The essence of the reactor physics analysis is to obtain the neutron flux distribution within the reactor by describing the properties (cross-section) of each material and solving the *Boltzmann transport equation* [3] [4, p. 431], or *transport equation* in short.

Reactor physics analysis relies on computers and computational programs, the same as other engineering field calculations. Reactor physics analysis is time-consuming since it is necessary to take the interactions between almost all materials and neutrons into account even when the complicated geometric structure of the reactor is simplified.

There are two numerical methods to solve the transport equation from the perspective of computation: one is the *deterministic* method, and the other is the *stochastic* method, which is known as *Monte Carlo*. The deterministic method gives unique outputs with a series of input data, which means the result is predictable. The Monte Carlo uses random number to simulate the behavior of neutrons so that result relies on the number of simulations [5, p. 4]. The computation time of Monte Carlo is significantly longer than that of the deterministic method in general, and the prediction accuracy is higher than that of the deterministic method. This is because the deterministic method requires the discretization of the neutron energy, flight angle, space, and time. On the other hand, the discretization is not necessary for the Monte Carlo method.

Various computer programs (or code systems) have been developed since the

first use of nuclear energy. These code systems vary in the governing equation (theory), model, calculation strategy, nuclear data library, and other aspects. From the perspective of research, there is a need to use a consistent code system to conduct calculations ranging from fuel assembly or core design, nuclear fuel burnup calculation, nuclear fuel cycle strategy design, key parameter confirmation, etc. Then, it is possible to avoid the differences in calculation introduced by using various code systems.

1.2 Necessity of software development in this work

A brief introduction to several widely used fast reactor physics and burnup code systems is given here. This dissertation also explains about the CBZ software, which is a key tool and the focus of this dissertation.

REBUS (REactor BUrner System) [6] [7] is a nuclear reactor burnup analysis code system developed by ANL (Argonne National Laboratory, USA). This code system was initially developed for liquid metal fast breeder reactors in 1970. Till now, 50-year development yields various modifications and extensions. REBUS combines a neutronics model and a fuel cycle model to give complete integration of the in- and ex-reactor fuel cycle. There is no geometric information involved in the fuel cycle model. Therefore, the static neutronics calculation can rely on any other extensions to be performed. Currently, REBUS offers a zero- to three-dimensional model, the diffusion or transport theory solver, and a deterministic or Monte Carlo solution through combining with other extensions. As for the burnup calculation, users can set up the depletion chain according to their demands. The language of REBUS (and the auxiliary extension) is FORTRAN-77 and C.

ERANOS (European Reactor ANalysis Optimized calculation System) [8] [9] has been developed and validated for neutronic calculations for fast reactors. This code system consists of nuclear data libraries, a code for lattice calculation (ECCO), a whole-core flux solver, a burnup calculation module, some processing modules, some tools related to the perturbation theory and sensitivity analysis, and other function tools. ERANOS could carry out neutron-gamma coupled calculations with specific library files. It is intuitive to feel the difference between ERANOS and REBUS. ERANOS is more like an independent fast reactor physics code, and REBUS focuses on burnup calculation only. The ERANOS (and ECCO) code package offers four libraries based on JEFF-2.2 evaluated nuclear data files; the energy group structures of these libraries are 1968-group, 175-group, 172-group, and 33-group, respectively. ERANOS applies the classic two-step method to give the solution of reactor. On the cell/lattice calculation step, the ECCO code offers many types of geometry models, including 0-, 2-, and 3-dimensional lattice model options in several coordinate systems. Then, on the core flux calculation step, the diffusion, transport (S_N: method of discrete ordinates), and nodal variational transport options are available. The language of ERANOS is FORTRAN-77 either.

MARBLE (and its update version MARBLE2) [10] [11] [12] is an advanced framework which integrates some existing codes on fast reactor research works in Japan with some refinements. From 1978 to 1988, Japan and the U.S. together conducted a fast reactor research project, JUPITER. Japan analyzed almost all the JUPITER experiments with domestic code systems [13], and these code systems were previously part of MARBLE. The MARBLE framework is formed by capsuling existing codes and adding new codes. Five sub-systems are constructed for specific purposes, and SCHEME and ORPHEUS among them are for neutronics analysis and burnup analysis,

respectively [11]. On the lattice calculation (resonance self-shielding effect evaluation), MARBLE uses the SLAROM-UF [14] code as a plug-in solver. The feature of the SLAROM-UF code is that ultra-fine group calculation in resonance range, two energy group structure (70-g and 900-g) library files, and 0/1/2-dimensional geometry model calculation. On the eigenvalue/flux calculation, finite difference/nodal diffusion solver, and finite difference/nodal S_N transport solver in 1-, 2-, and 3-dimensional multiple coordinates system are available. SCHEME provides perturbation calculation, group-collapsing, effective cross-section processing, and other functions as well.

Multiple options on the calculation method are needed to achieve the goal of wide range utilization in fast reactor neutronic analysis. The existing fast reactor burnup or analysis code systems offer multiple options for users to choose from. However, there are not enough options offered in some aspects. Particularly, because the eigenvalue or flux solver of these code systems is only diffusion- and transport-based, the options on library files are not as free as other aspects. More importantly, the solver is capsuled as a ”black box” in some code systems so that users cannot check the calculation process or add new functions easily.

CBZ is a general-purpose reactor physics deterministic code system that is developed at Hokkaido University. FRBurner, which is developed through the work in this dissertation, is a fast reactor burnup calculation module in CBZ. In general, the unique features of CBZ or the FRBurner module are as follows.

- CBZ has its own multi-group nuclear data library (NDL) generation system based on FRENDY [15], which is a nuclear data processing code developed by JAEA and Nagoya University. Arbitrary number of energy groups from arbitrary evaluated nuclear data files (ENDF) can be prepared and used. It is

convenient for users to use the latest ENDF library immediately.

- Arbitrary nuclide transmutation chain models can be applied into CBZ. The detailed (or reference) transmutation chain consisting of all nuclides defined in the ENDF library can be used, and inventory calculations of any actinides or fission products in fuel are possible. Thus, nuclide inventory calculations for spent fuel, which are generally carried out separately from the reactor core calculations, can be carried out in a consistent way with the core calculations.

- Diffusion, transport (S_N), and simplified-P_N (SP_N) solvers for eigenvalue or flux calculation are available. Besides, various angular quadrature sets including energy-group-dependent sets can be chosen for the S_N solver.

- Multiple lattice model calculation functions have been implemented. Homogeneous (0-dimensional), cylinder (1-dimensional) and hexagonal (2-dimensional) models are available to use. On the lattice calculation, several resonance calculation methods such as the Dancoff factor method and Tone's method can be used.

- More importantly, CBZ is developed based on C^{++}, and solvers are created as classes. So that it is convenient to make modification and add new function. Since CBZ is a self-developed code system, extension is easy to be accomplished.

1.3 Research purpose and outline

The objective of this dissertation is to develop software to meet the demands of wide-ranging use in fast reactor physics analysis with innovative calculation capability. In

this dissertation, a fast reactor burnup calculation module with multiple calculation options is developed and verified. The features of each option on the calculation methodology are discussed through a comprehensive comparison. The efforts and discussion on theory are crucial parts of this dissertation. Although the SP_N theory has been applied on reactor physics analysis in decades (also on others field, like analyzing the radioactive cooling process of glass, crystal growth, radioactive transfer of photon in biological tissues, plasma spectroscopy, etc. [16]), there is no sufficient discussion on the use of SP_N in fast reactor physics analysis. The SP_N theory is used in LWRs applications mostly. Therefore, one of the focuses of this study is on the use of the SP_N method in fast reactor analysis. Then, a new method for reactor reactivity calculation based on the SP_N and perturbation theories is proposed. The categorization of reactivity with this new method is discussed in comparison with traditional diffusion and transport perturbation calculations. These two researches taken together can be viewed as a study of the advancement of fast reactor physics analysis.

The structure of this dissertation is arranged as follows. Chapter 1 introduces background and motivation. In Chapter 2, the development and verification of a fast reactor burnup calculation module are summarized. Several famous reactor physics code systems are briefly introduced to make a comparison on the calculation methodology as well in the Chapter 2. Chapter 3 contains the derivation, verification, and discussion of the novel reactivity calculation approach based on the SP_N and perturbation method. Chapter 4 summarizes the works in this dissertation from the perspective of the entire story as a conclusion, and considerations about potential future work are discussed.

Chapter 2

Development and Verification of Fast Reactor Calculation Module FRBurner

2.1 Introduction

Neutronics calculation methods have been well established by a number of studies over the past decades, and there are two main directions in the neutronics calculation field: the deterministic and Monte Carlo methods. FRBurner is developed as a fast reactor burnup calculation module in the CBZ code system [17], which is a deterministic code under development at Hokkaido University. While the fast reactor calculation code systems REBUS [7], ERANOS [8], and MARBLE [10] exist, the demand for a particular code system that enables diverse purpose (accuracy) calculations still exists for new reactor designs. For instance, it is desirable to use an identical code for preliminary design calculation with a low-resource-cost option

and final parameter confirmation calculation with a high-accuracy option both, so that consistency is maintained between calculations and computing resources are saved. Moreover, the demand for a new algorithm, nuclear data library, burnup chain model, etc., exists for our current and future works. It is difficult to meet such flexible demands without a self-developed code system.

An OECD/NEA fast neutronic analysis benchmark [18] was chosen for the verification work. Four sodium-cooled fast reactor cores, which contain three types of fuel—metallic fuel, MOX fuel, and carbide fuel—are provided in this report. In addition, two of these cores are large-sized with a thermal power of 3,600 MWth, and the others are middle-sized with a thermal power of 1,000 MWth. The diversity of the core type provides adequate universality, increasing the reliability of this verification work.

From the perspective of practical application, it is beneficial to understand the differences among the methodologies of a module, such as FRBurner, that has diverse calculation methodology options. Thus, the differences in (i.e., effects on) numerical results while applying a 0-dimensional/1-dimensional/2-dimensional lattice model, diffusion/transport theory for whole-core calculations, and a coarse/fine-energy group structure cross-section library are investigated in this work. This impact investigation would help potential users choose an appropriate methodology for diverse purposes.

For the purpose of illustrating the advantage of the SP_3 method, comparisons of the SP_3, diffusion, and transport methods on some reactor physics parameters are provided in this section as well. These comparisons can be regarded as a bridge leading to the next chapter.

2.2 Basic theory and numerical method

2.2.1 Multi-group library and its generation procedure

The FRBurner module uses a multi-group cross-section library called CBZLIB to calculate problem-dependent medium-wise multi-group (or effective) cross sections. CBZLIB consists of the infinite dilution cross sections (term for self-shielding effect evaluation in resonance calculation [19] [20] [21]), the scattering matrices with an arbitrary order of the Legendre expansion, and the self-shielding factors for the reactions of (n,n), (n,f), and (n,γ). The self-shielding factors for the elastic removal cross sections and for the current-weighted total cross sections are also included.

These multi-group library data are obtained from the ENDF-formatted evaluated nuclear data files and the *point-wise (resonance-reconstructed) ENDF* (PENDF) files with the NJOY-99 code [22] through the processing sequence of the BROADR, PURR, GROUPR and MATXSR modules. In the GROUPR module, the narrow resonance approximation is adopted, and the IWT = 8 weighting function [23, Pages 187, 237], which is adaptive for fast reactor study is chosen for multi-group constants calculation. The generated text files in the MATXS format are converted into the other text files in a specific format readable by CBZ. The PENDF files are generated by the FRENDY code developed at JAEA [15]. In this research, the author generates several multi-group libraries with different numbers of energy groups from several evaluated nuclear data libraries. Examples (**Figure 2.1**) of 70- and 280-energy group structures that are going to be used in this work are shown with the total cross-section of ^{235}U. These two energy group structures can be regarded as coarse- and fine-group structures, respectively. It is clear to find out that different energy group structures make changes on results since the cross-section values of them are quite different.

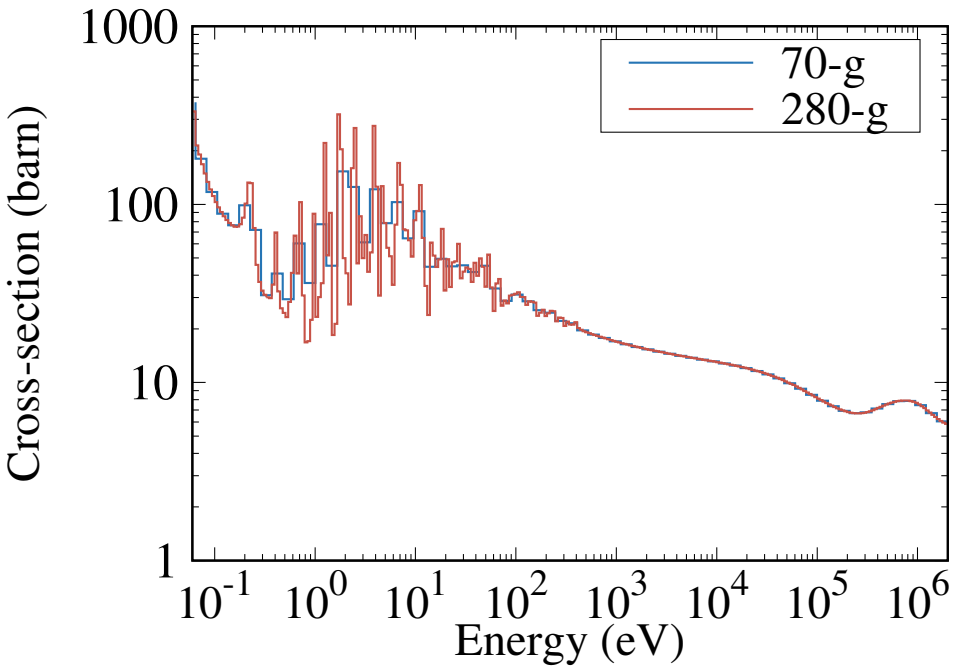

(a) Total cross-section of ^{235}U in a fast reactor inner-core region

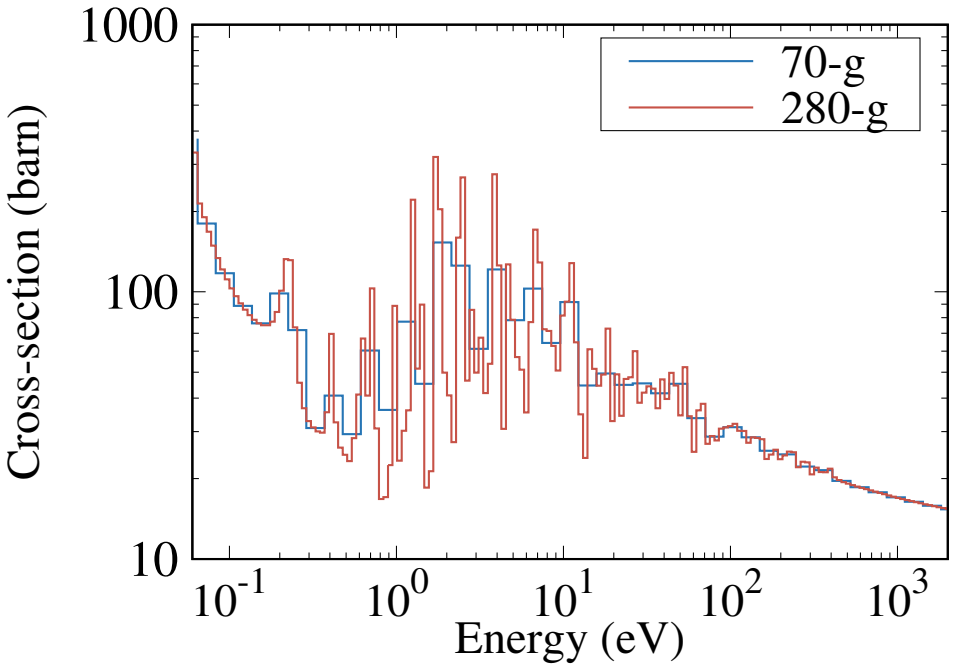

(b) Total cross-section of ^{235}U in a fast reactor inner-core region (enlarged)

Figure 2.1: Examples of energy group structure scheme.

2.2.2 Fuel assembly calculations to obtain homogeneous (homogenized) cross sections

Since all the fuel assemblies are treated as homogeneous in the whole-core calculations by FRBurner, spatial homogenization of the fuel assemblies is required prior to whole-core calculations. This is done at the assembly calculation step. In the assembly calculation of FRBurner, all assemblies, including blanket assemblies, are modeled with a single assembly with the reflective boundary conditions, and multi-group cross-section calculations (or resonance self-shielding calculations) and neutron flux spatial distribution calculations are conducted with this single assembly model.

Regarding the assembly model, three options can be chosen: the zero-dimensional model, the one-dimensional cylinder model, and the two-dimensional hexagonal model, as shown in **Figure 2.2**.

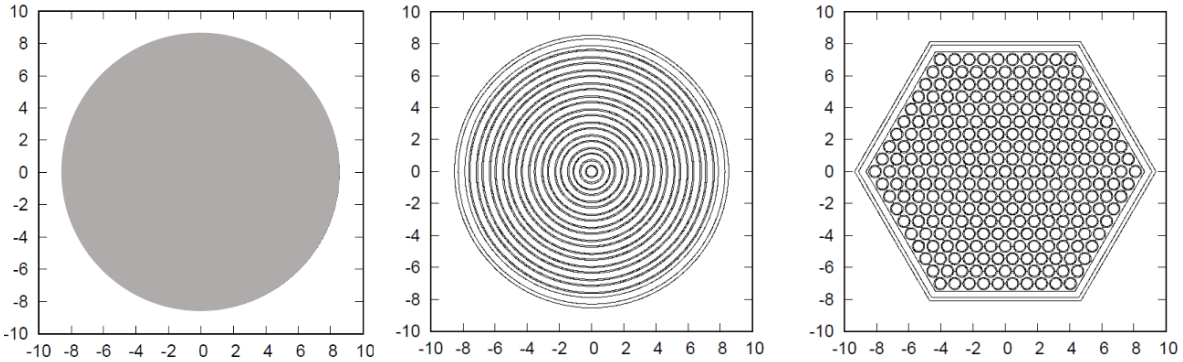

Figure 2.2: Three options of lattice model for assembly calculation: zero-dimensional, one-dimensional and two-dimensional (left to right).

In the zero-dimensional model, nuclide number densities are spatially averaged over a whole assembly with volume weight, and the resulting homogeneous mixture is treated. The background cross sections for resonance treatment are calculated with this mixture, and the multi-group cross sections of this mixture can be easily

calculated. In this case, no spatial neutron flux calculations are required, and the infinite neutron multiplication factor can be easily calculated by solving the one-point B_1 equation.

In the cylinder and hexagonal models, multi-group cross sections of each medium are calculated using the method proposed by Tone [24]. In Tone's method, the lattice heterogeneity effect is taken into account in background cross-section calculations via the collision probabilities. After multi-group cross sections of each medium are obtained, the multi-group neutron transport equation is solved by the collision probability method, and multi-group neutron flux spatial distributions are calculated. The leakage effect is accounted for by the pseudo absorption cross sections defined by the critical buckling. With the calculated neutron flux spatial distribution, spatial homogenization is carried out to obtain the homogenized multi-group cross sections. The homogenized multi-group cross sections are used in the subsequent whole-core calculations without any group collapsing (or condensation). The homogenized multi-group microscopic cross sections are calculated in the initial burnup cycle, and the homogenized macroscopic cross sections in the subsequent burnup cycles are calculated from these microscopic cross sections and nuclide number densities in the concerned burnup step.

2.2.3 Whole-core calculations to obtain eigenvalues and neutron flux distributions

Although several solvers for three-dimensional systems have been implemented in CBZ, the present version of FRBurner can only use the two-dimensional cylinder model; thus, users should construct a cylindrical core model from a three-dimensional

core configuration. The neutron diffusion or transport equation defined for the cylindrical core model can be solved, and the eigenvalue and the neutron flux spatial distribution over the whole core can be obtained. Another option for the core calculation, Simplified-P_3, will be discussed in an independent section. When the neutron diffusion equation is solved, a solver PLOS, which adopts the finite-volume spatial discretization, is used. When the neutron transport equation is solved, a solver SNRZ, which adopts the diamond-differencing spatial discretization scheme and the discrete ordinates angular discretization scheme, is used. The discrete ordinates angular discretization scheme is also known as the S_N method. The inner iterations are accelerated by the diffusion synthetic acceleration in SNRZ. Both solvers implement the coarse-mesh finite difference acceleration (CMFD acceleration) for the outer power iteration.

Calculations of the reactivity induced by the reduction in coolant density and the increase in the fuel temperature can be calculated by the exact perturbation theory in an arbitrary burnup cycle. The homogenized microscopic cross sections of the assemblies at these perturbed states are conducted in the initial burnup cycle. The effective delayed neutron fraction β_{eff} can be also calculated with the forward and adjoint neutron fluxes obtained by PLOS or SNRZ.

2.2.4 Fuel burnup calculations

With the neutron flux energy and spatial distribution obtained by the whole-core calculation, the nuclide-wise reaction rates can be calculated, and with these reaction rates, the changes in the nuclide number densities with time can be calculated. This nuclide transmutation process is simulated by fuel burnup calculations with a nuclide burnup chain.

In the nuclide burnup chain, 21 important actinides are considered generally. On fission products, the pseudo fission products are generally used in the fast reactor neutronic analyses since the variation in neutron capture cross sections of various fission products is not significant in fast reactors. When the pseudo fission products are introduced to a burnup chain, the number of nuclides in the burnup chain could be small, and the fuel burnup calculations can be done easily. On the other hand, the detailed information on the nuclide inventory included in the spent nuclear fuel is required for the works relevant to nuclear waste management or spent fuel reprocessing. In such cases, it is preferred that the fission products are explicitly treated in a burnup chain. This requires a relatively large computer memory since the information on nuclide inventories including a large number of fission products must be stored for all burnup media through whole-core burnup calculations. Such fuel burnup calculations with the detailed nuclide burnup chain treating fission products explicitly are also possible in FRBurner.

Nuclides transmutation is represented by the Bateman equation, and the solution to this equation is obtained by the matrix exponential method in FRBurner. There exists several methods to numerically calculate the matrix exponential in CBZ, and FRBurner adopts the mini-max polynomial approximation method [25, 26]. This can be adopted to the Bateman equation including the quite short half-lived nuclides, which should be considered in burnup calculations with the detailed nuclides burnup chain.

Fuel exchange during multiple burnup cycles can be simulated by FRBurner. Since a reactor core is modeled as a cylinder, the explicit representation of a reactor core consisting of fuel assemblies with different irradiation histories is impossible. In FRBurner, nuclide number densities are calculated for each assembly with its ir-

radiation history, but in the whole-core calculations, the macroscopic cross sections are obtained through the averaged number densities over a region which is involved in burnup calculation.

2.3 Verification work with the OECD/NEA benchmark

In this section, essential information about four fast reactor cores provided by the benchmark, the calculation methodology of FRBurner, and the reference results are introduced. Bias comparison and error analysis are discussed also in this section.

2.3.1 Core configuration

As mentioned in section 2.1, four fast reactor cores are described in the benchmark: MET-1000, MOX-1000, MOX-3600, and CAR-3600. The name of the cores indicates the fuel type and power level (core size), as listed in **Table 2.1**. Each core is modeled as multi-layer cylinder model, and the width of each layer is calculated from the sum of the hexagonal-cross-section assembly areas of corresponding layers. The layout of the MET-1000 multi-layer cylinder model is shown in **Figure 2.3** as one example, where the y-axis is the axial direction and the x-axis is the radial direction. Medium information is listed according to the medium number in the right of this figure.

The benchmark provides number density data at the beginning of equilibrium cycle (BOEC), and users calculate the number density data at the end of equilibrium cycle (EOEC) through the burnup calculations. The effective neutron multiplication factor k_{eff}, effective delayed neutron fraction β_{eff}, sodium void reactivity $\Delta\rho_{\text{void}}$ and Doppler reactivity $\Delta\rho_{\text{Doppler}}$ are four target parameters, and the reference results provided by a variety of institutes of these four parameters at BOEC and EOEC are given

Table 2.1: Fuel type and core size information of each benchmark core

Core name	Fuel type	Power level [MWe]
MET-1000	Metallic	1000
MOX-1000	MOX	1000
MOX-3600	MOX	3600
CAR-3600	Carbide	3600

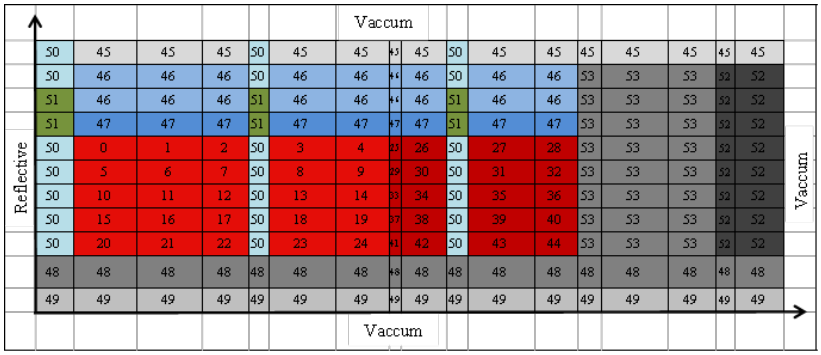

Number	Medium
0∼24	Inner-core
25∼44	Outer-core
45	Upper structure
46	Gas plenum
47	Replace sodium
48	Lower reflector
49	Lower structure
50	Empty duct
51	Control absorber
52	Shield rod
53	Radial reflector

Figure 2.3: Multi-layer cylinder model of MET-1000.

in the benchmark. The condition for calculating $\Delta\rho_{\text{void}}$ is that all sodium is voided. The condition for calculating $\Delta\rho_{\text{Doppler}}$ is that the temperature in the core regions are changed to twice those of the reference state.

The normalized forward and adjoint neutron fluxes at the center of each core calculated by the diffusion solver with the 70-group cross section are shown in **Figure 2.4** in order to exhibit the basic neutronic characteristics of these four reactors. It is obvious that MET-1000 consisting of metallic fuel has a harder neutron spectrum. Energy group-wise $\Delta\rho_{\text{void}}$ and $\Delta\rho_{\text{Doppler}}$, which are calculated by the diffusion solver with the 70-group cross section, are shown in **Figure 2.5**, and component-wise $\Delta\rho_{\text{void}}$ is shown in **Figure 2.6**. From Figure 2.5 it is noticed that all four cores have a significant $\Delta\rho_{\text{void}}$ peak around 0.8 MeV, which is caused by the sodium nuclide, and that $\Delta\rho_{\text{Doppler}}$ in an energy range higher than 10^5 eV is negligible. Then, Figure 2.6 reveals that $\Delta\rho_{\text{void}}$ is mostly caused by the scattering and leakage component reactivities.

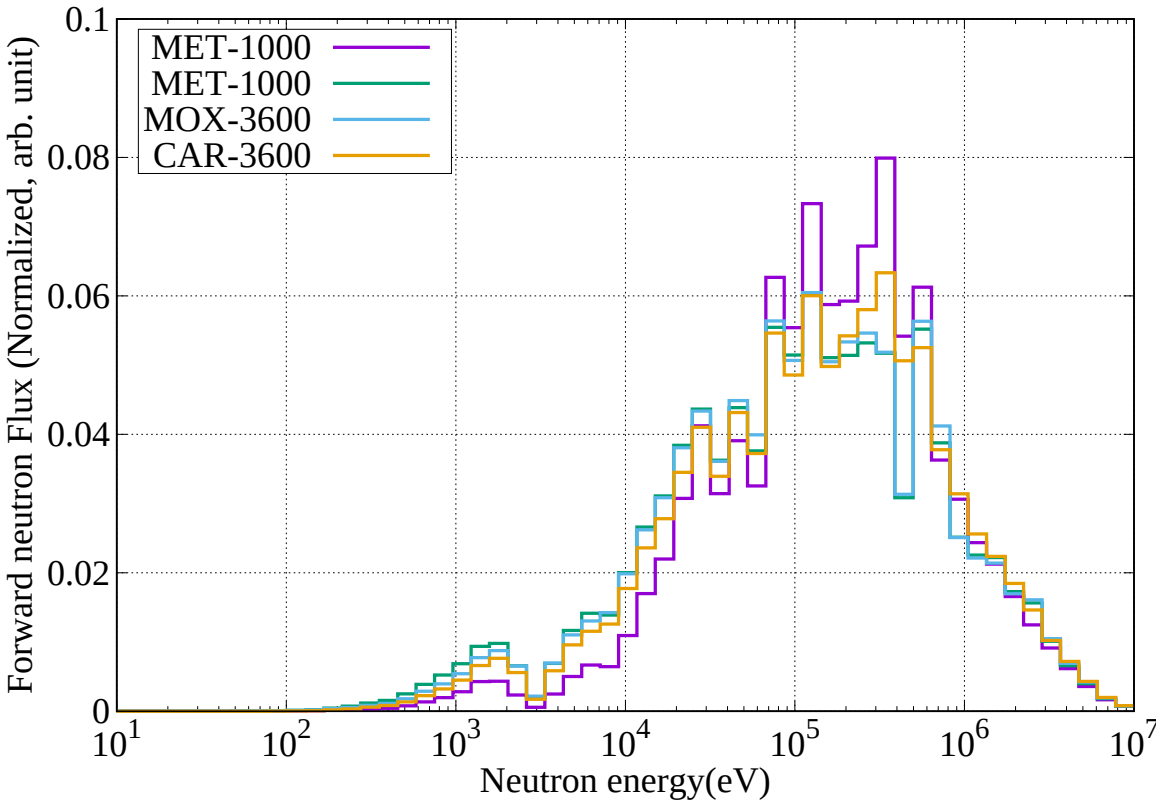

(a) Forward neutron flux.

Figure 2.4: Forward and adjoint neutron fluxes.

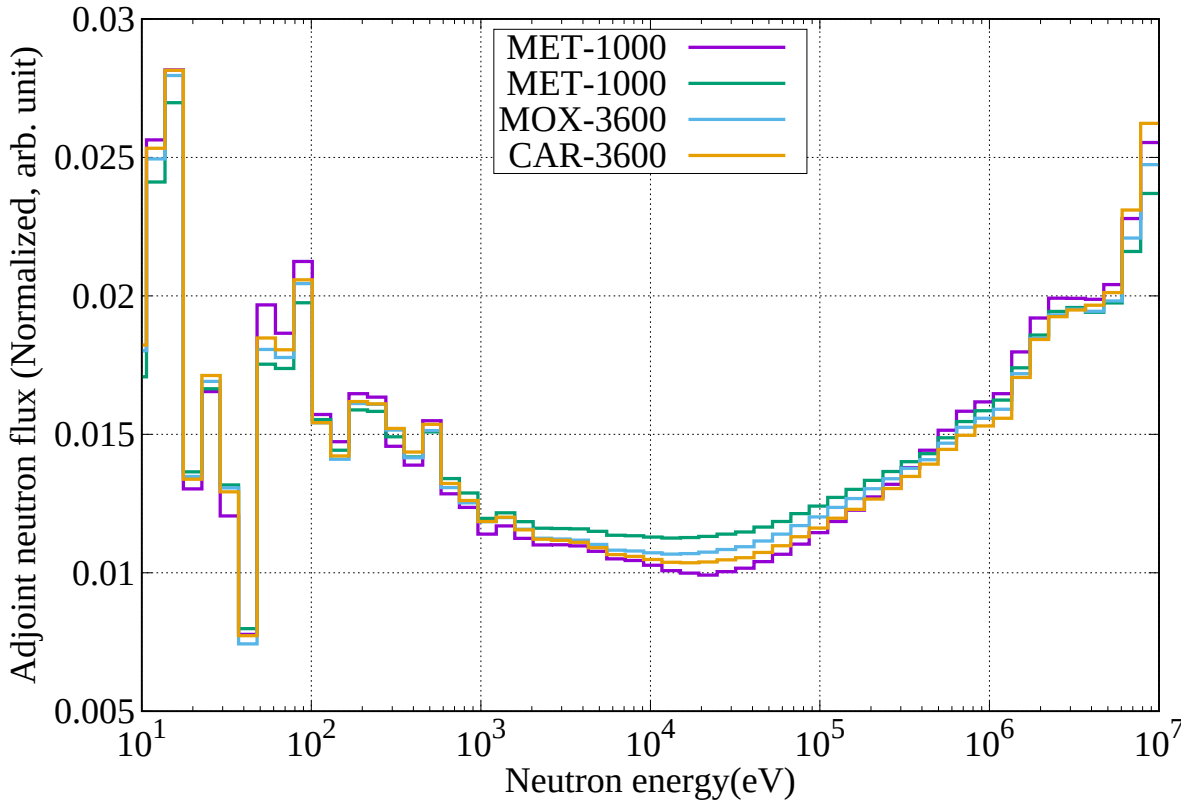

(b) Adjoint neutron flux.

Figure 2.4: (Cont.) Forward and adjoint neutron fluxes.

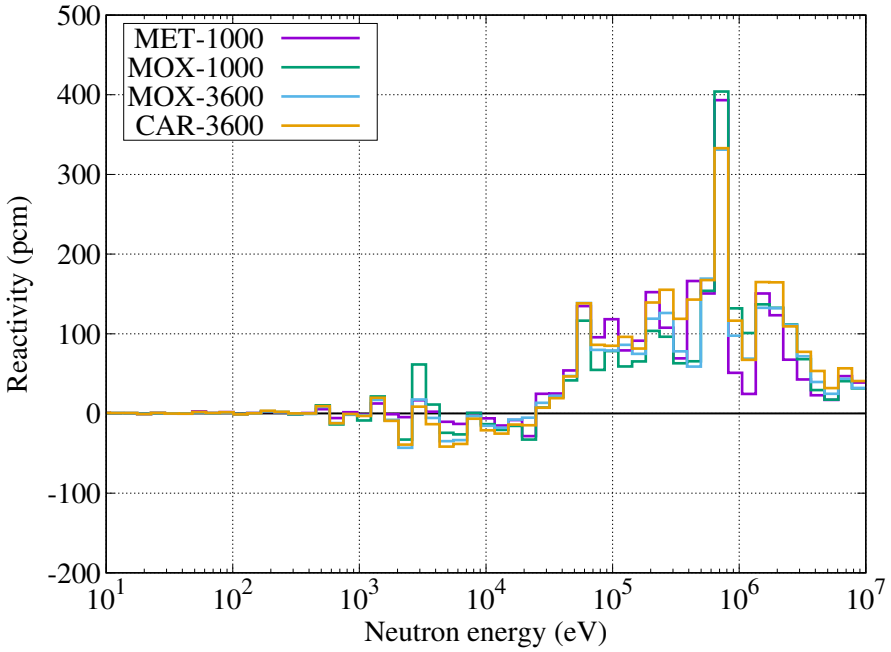

(a) Energy group-wise sodium void reactivity $\Delta\rho_{\text{void}}$.

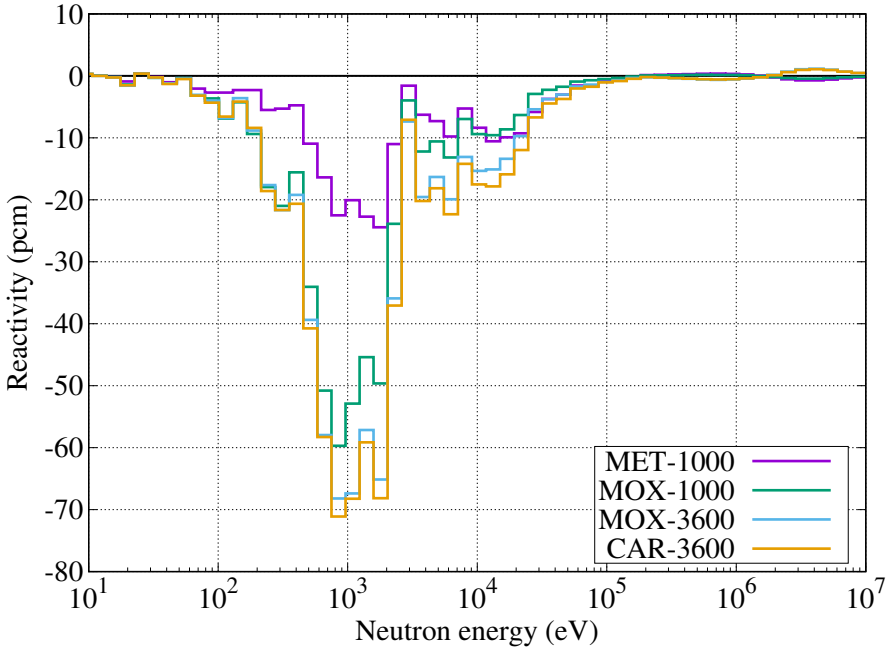

(b) Energy group-wise Doppler reactivity $\Delta\rho_{\text{Doppler}}$.

Figure 2.5: Energy group wise $\Delta\rho_{\text{void}}$ and $\Delta\rho_{\text{Doppler}}$.

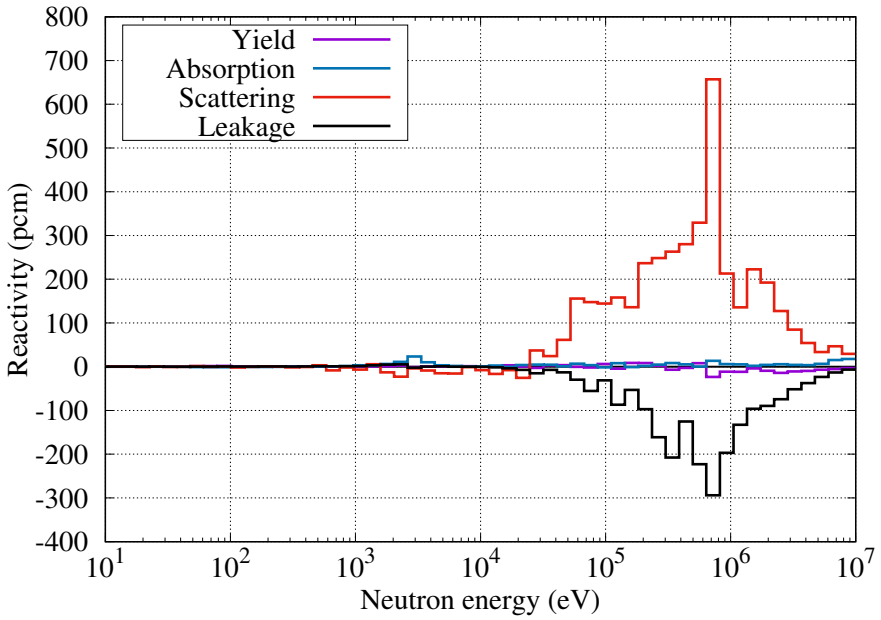

(a) MET-1000.

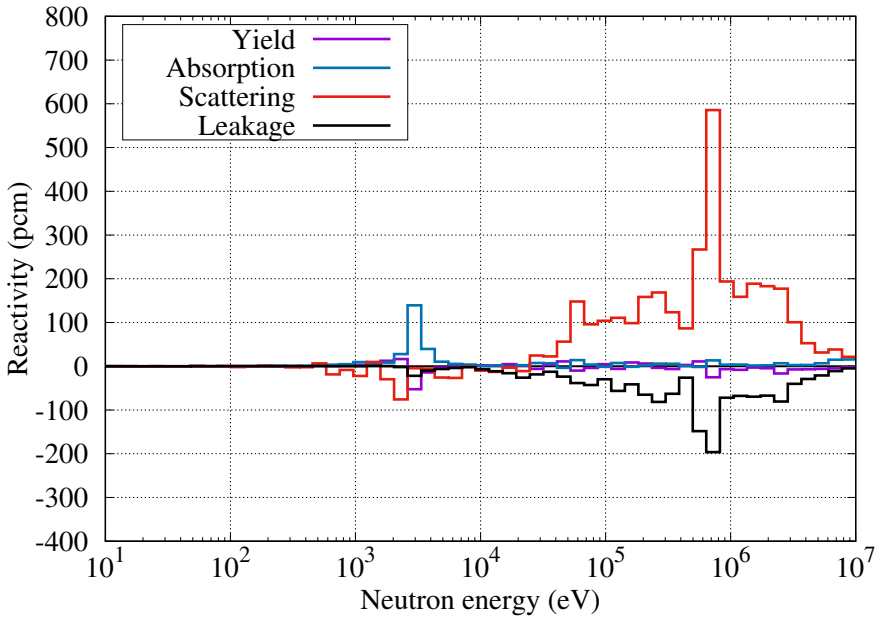

(b) MOX-1000.

*$\Delta\rho_{\text{void}}$ can be decomposed into non-leakage and leakage components. Non-leakage component consists of yield, absorption, and scattering components.

Figure 2.6: Component-wise $\Delta\rho_{\text{void}}{}^*$ of four cores.

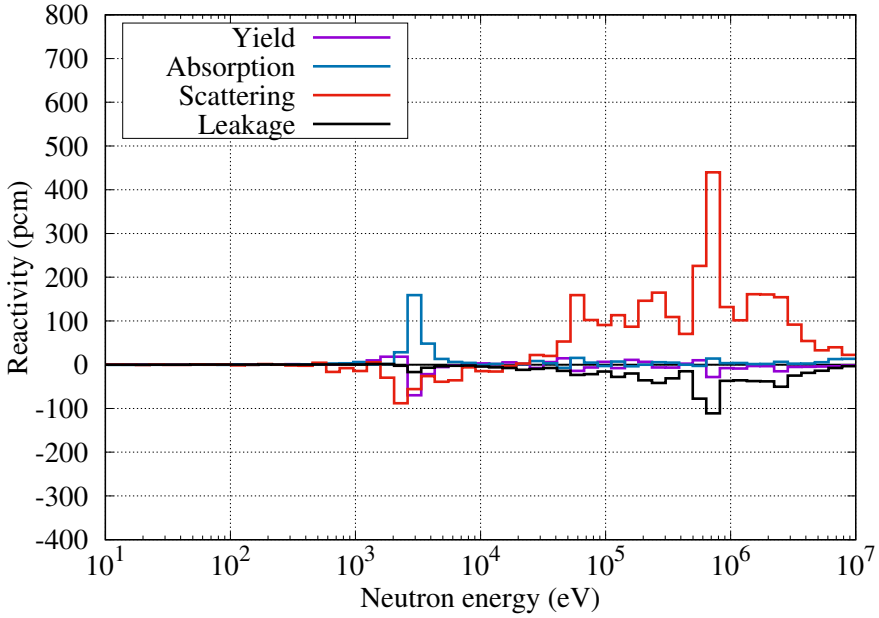

(c) MOX-3600.

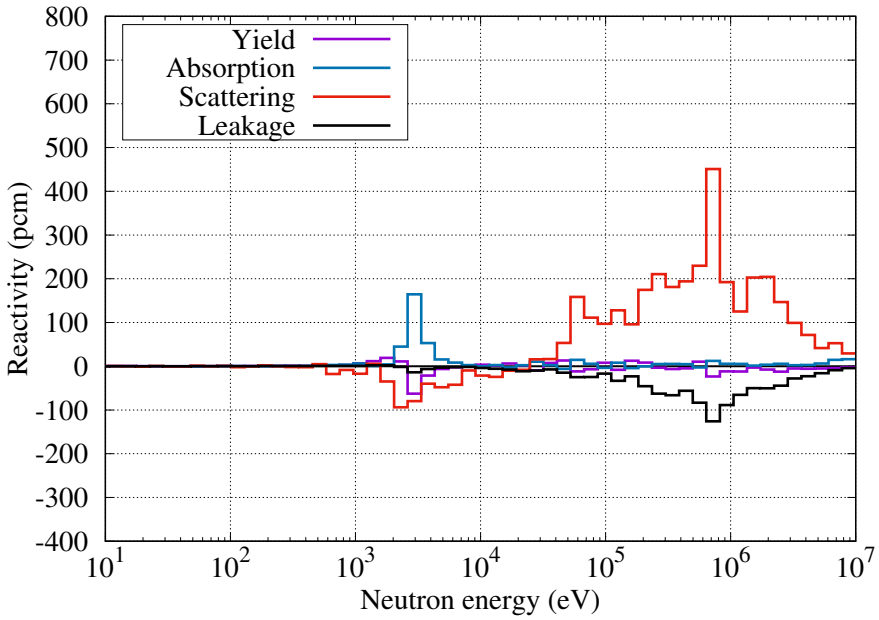

(d) CAR-3600.

*$\Delta\rho_{\text{void}}$ can be decomposed into non-leakage and leakage components. Non-leakage component consists of yield, absorption, and scattering components.

Figure 2.6: (Cont.) Component-wise $\Delta\rho_{\text{void}}{}^{*}$ of four cores.

2.3.2 Calculation methodology in the verification work

FRBurner applies the traditional two-step method to solve problems. Three lattice model options are available in the lattice calculation procedure: two-dimensional hexagonal rigorous model, one-dimensional cylinder model and zero-dimensional homogeneous model. The heterogeneity of the assembly structure cannot be considered in the whole-core calculation procedure since the whole core is completely homogenized as a two-dimensional multi-layer cylinder. Considering other options for theory, library and energy group structure, therefore, multiple combinations in FRBurner can be chosen for diverse problems according to purpose.

In the verification part, the most rigorous methodology, the two-dimensional lattice model in assembly calculation procedure with the transport theory-based solver SNRZ (P_1S_4, this is explained in the subsection 2.4.4) with 280-group CBZLIB, is used. The 280-group structure CBZLIB is based on the JAERI fast set-3 (JFS-3) structure proposed for sodium-cooled fast reactor analysis, and each group of this 70-group structure is divided into 4 groups. References provided by JAEA (Japan Atomic Energy Agency) and CEA (Commissariat à l'énergie atomique) were used for verification. The methodologies of these two chosen references are shown in **Table 2.2**. The suffix of the reference name in **Table 2.2** is to maintain consistency with the benchmark. It should be noted that these references use 3-dimensional models in the whole-core calculation step. Although these two institutes provided several references, only one reference from each institute is chosen. The JENDL-4.0 [27]-based CBZLIB and the JEFF-3.1.1 [28]-based CBZLIB were used for the present calculation for comparison with the JAEA-2 and CEA-1 reference results, respectively.

To verify the burnup function of FRBurner, the number density at EOEC was

calculated by FRBurner based on the BOEC number density which is given by the benchmark.

Table 2.2: Methodologies used for the references.

	JAEA-2	CEA-1
Library	JENDL-4.0	JEFF-3.1
Lattice code	MARBLE (SLAROM-UF)	ECCO
Core code	MARBLE (TRITAC)	ERANOS VARIANT8
Lattice geometry	Heterogeneous	Heterogeneous
Core geometry	Homogeneous	Homogeneous
Approximation	Diffusion (Transport correction)	Transport SP_3
Depletion chain	-	Pseudo FP
Fuel S/A	One-dimensional multi-ring	Two-dimensional hexagonal
Energy groups in lattice/core	70-group/70-group	1968-group/33-group

As this work was preliminary verification, the criteria of the FRBurner module calculation on k_{eff}, β_{eff}, $\Delta\rho_{\text{void}}$ and $\Delta\rho_{\text{Doppler}}$ were set at 0.5%, 3%, 10% and 10%, respectively.

2.3.3 Bias comparison with the JAEA reference result

The JAEA-2 reference only contains the results of MET-1000 and MOX-3600. The reference and the FRBurner calculation results are summarized in **Table 2.3**. Burnup reactivity $\Delta\rho_{\text{cycle}}$ which is the reactivity caused by fuel burnup is shown as well. A relative biases comparison is shown in **Figure 2.7**. The difference on k_{eff} is multiplied by 10 and expressed as $10(k_{\text{eff}})$ for a clear comparison in these figures, and this setting is accepted by other figures in this chapter.

Table 2.3: JAEA-2 reference and FRBurner results based on the JENDL-4.0 library.

	BOEC				EOEC				
	k_{eff}	β_{eff}	$\Delta\rho_{\text{void}}$	$\Delta\rho_{\text{Doppler}}$	k_{eff}	β_{eff}	$\Delta\rho_{\text{void}}$	$\Delta\rho_{\text{Doppler}}$	$\Delta\rho_{\text{cycle}}$
JAEA-2									
MET-1000	1.0289	339	2170	-375	1.0081	338	2256	-389	-2004
MOX-3600	1.0133	363	1948	-921	1.0193	355	1977	-881	581
FRBurner									
MET-1000	1.0291	336	2147	-352	1.0082	335	2239	-366	-2019
MOX-3600	1.0089	361	2002	-924	1.0160	353	2027	-878	696

* k_{eff} is unitless parameter, the unit of the others are per cent mille (pcm).

* $\Delta\rho_{\text{cycle}}$ value in benchmark is not calculated from k_{eff}. To keep consistency, $\Delta\rho_{\text{cycle}}$ calculated by k_{eff} is listed at here.

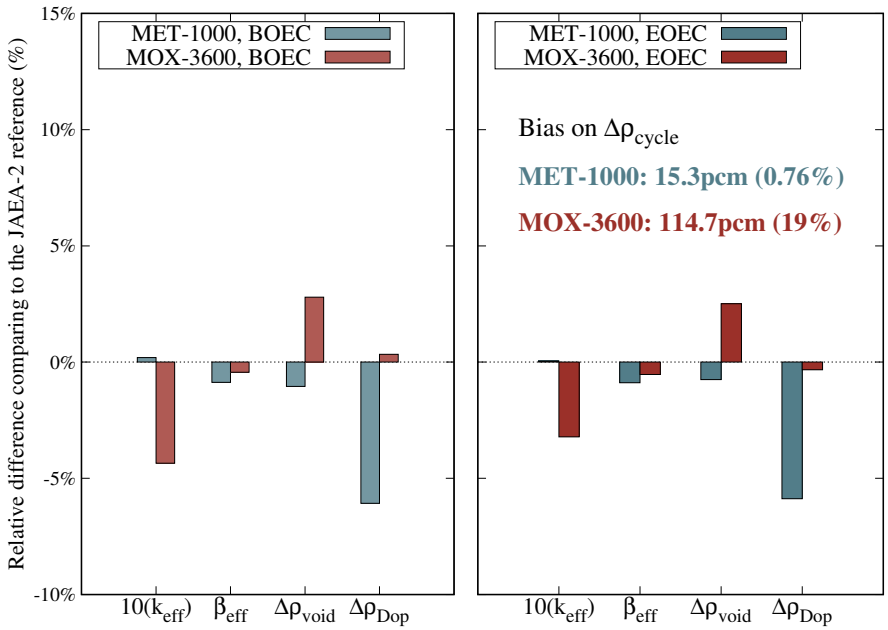

* The bias on k_{eff} is multiplied by 10 for a clear comparison in this figure.

Figure 2.7: Biases comparison between FRBurner and the JAEA-2 reference at BOEC and EOEC.

The maximum bias of each parameter is less than 0.5%, 1%, 3% and 7% respectively. Preferable results were obtained through comparison between the JENDL-4.0-based CBZLIB FRBurner calculation results and the JAEA-2 reference results. The biases at BOEC and EOEC were consistent with each other, suggesting perfect performance of the burnup calculation function.

2.3.4 Bias comparison with the CEA reference result

The CEA-1 reference was used as supplement due to methodology differences between CEA-1 and FRBurner although it provides results for all four cores. The CEA-1 reference and the FRBurner calculation results are summarized into **Table 2.4**. Relative biases of each parameter are summarized into **Figure 2.8**.

The maximum bias of each parameter is less than 1.0%, 4%, 12% and 8%, respectively. These results are regarded as acceptable regardless of the relatively large biases ($>$10%) on MET-1000 $\Delta\rho_{\mathrm{void}}$, since just this one case shows a large bias.

2.3.5 Bias analysis

Firstly, the comparison between the FRBurner calculation and the JAEA-2 reference suggested that FRBurner can give acceptable results on fast reactor analysis work, although consistent results are not obtained when compared with the CEA-1 reference. The reason for the discrepancy between FRBurner and CEA-1 is due to differences in calculation conditions. More importantly, the biases at BOEC and EOEC show obvious differences when compared with the CEA-1 reference. This is because the depletion calculation conditions between FRBurner and CEA-1 are different. According to the benchmark, the recommended depletion calculation uses molybdenum to

Table 2.4: CEA-1 reference and FRBurner result based on the JEFF-3.1.1 library.

	BOEC				EOEC				
	k_{eff}	β_{eff}	$\Delta\rho_{\text{void}}$	$\Delta\rho_{\text{Doppler}}$	k_{eff}	β_{eff}	$\Delta\rho_{\text{void}}$	$\Delta\rho_{\text{Doppler}}$	$\Delta\rho_{\text{cycle}}$
CEA-1									
MET-1000	1.0372	355	2190	-362	1.0100	354	2385	-357	-2596
MOX-1000	1.0316	345	1922	-789	1.0141	342	2060	-767	-1673
MOX-3600	1.0162	381	1931	-971	1.0136	-	2056	-887	-252
CAR-3600	1.0097	391	2122	-1048	1.0147	381	2233	-949	488
FRBurner									
MET-1000	1.0384	343	2012	-348	1.0155	342	2108	-364	-2165
MOX-1000	1.0379	334	1845	-731	1.0242	332	1881	-747	-1289
MOX-3600	1.0145	370	1856	-926	1.0188	362	1896	-884	413
CAR-3600	1.0090	380	2053	-970	1.0205	371	2162	-921	1114

* k_{eff} is unitless parameter, the unit of others are per cent mille (pcm).

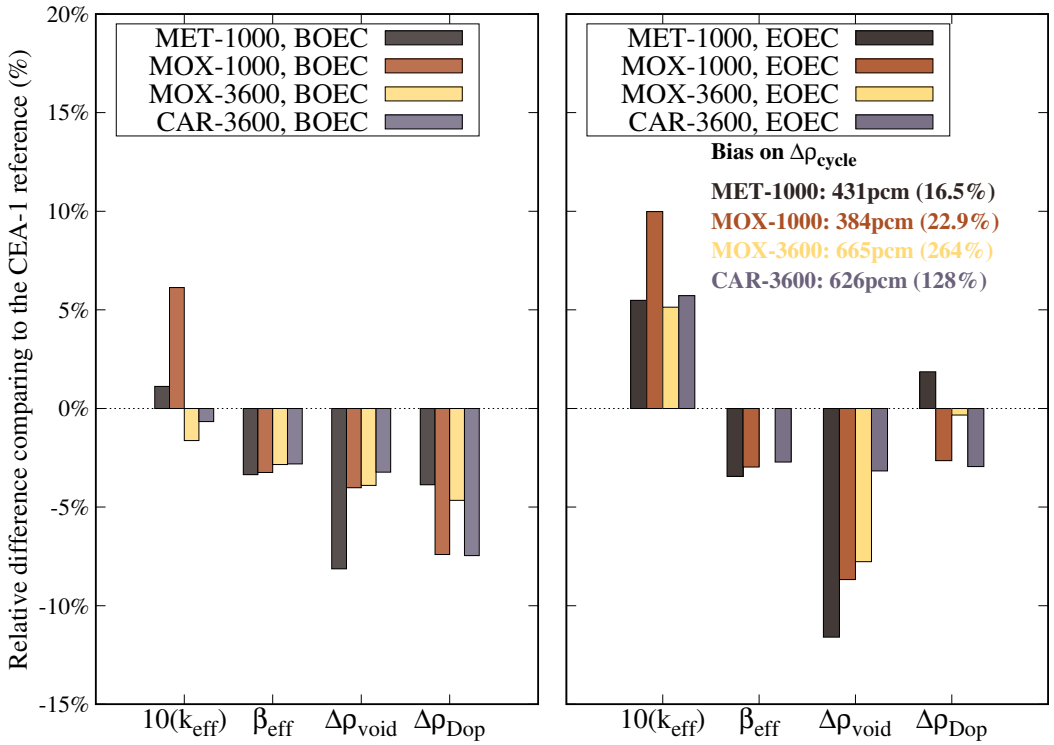

* The bias on k_{eff} is multiplied by 10 for a clear comparison in this figure.

Figure 2.8: Biases comparison between FRBurner and the CEA-1 reference at BOEC and EOEC.

substitute every fission product; therefore, the discrepancy caused by the depletion mode can be eliminated. The same depletion calculation condition as the JAEA-2 reference applies is chosen for keeping consistency. CEA-1, however, applies pseudo-FP treatment, which is different from the recommendation.

As the FRBurner module applies a two-dimensional cylindrical model in the whole-core calculation step, the biases found in the two comparisons should be caused by the difference in models in the whole-core calculation step. It is noteworthy that the impact of this difference in the whole-core calculation step would not be large since acceptable agreement was observed when compared with the JAEA reference result.

Additionally, as for the biases on β_{eff} found in comparison with the CEA-1 reference, the delayed neutron emission data are partly responsible for them. While energy-dependent delayed neutron yield, ν_{d}, is used in CBZ, energy-independent ν_{d} is adopted by CEA-1. As ν_{d} becomes smaller with increased incident energy, FRBurner tends to give smaller β_{eff} than the CEA-1 reference.

2.4 Impact of the methodology option on numerical result

In this section, the effects about applying different lattice models (the zero-dimensional, one-dimensional, or two-dimensional model), different theories (the diffusion or transport theory), and different nuclear data library (the coarse- or fine-energy group structure library) are investigated. The dependencies among these three aspects are also studied. The differences between two different order options of the transport theory solver ($P_N S_N$) are studied as well. Data used in this section is obtained only

from the JEFF-3.1.1-based CBZLIB calculations, because there is no correlation between ENDF library and the terms analyzed in this section. Accordingly, the JENDL-4.0-based calculation results are not discussed here. To investigate the differences, not only k_{eff}, β_{eff}, $\Delta\rho_{\text{void}}$ and $\Delta\rho_{\text{Doppler}}$ are focused, but also the components of $\Delta\rho_{\text{void}}$: the non-leakage and leakage components. To avoid redundancy, only the effects at BOEC are shown in tables and figures in this section since these effects have no relationship with the burnup calculation.

2.4.1 Three lattice models (model effect)

Three options for the lattice model in the first step of the traditional two-step method are provided in FRBurner. It is essential to recognize the degree of effect caused by the one-dimensional cylinder model or two-dimensional hexagonal model when compared with the zero-dimensional homogeneous model since the zero-dimensional model is applied particularly at the beginning of work, and researchers would like to adjust the core configuration based on this preliminary calculation result. It would be beneficial if users could estimate a more accurate value using the result of such a comparison.

Firstly, the two-dimensional lattice model effect (the difference between using 0-dimensional homogeneous and 2-dimensional heterogeneous lattice models) is shown in **Figure 2.9**, where the terms ”N-Leak” and ”Leak” in these figures mean the non-leakage component and leakage component sodium void reactivity, respectively. From Figure 2.9 the followings can be concluded.

1. The utilization of a two-dimensional lattice model leads to notable alterations in k_{eff}, $\Delta\rho_{\text{void}}$, and $\Delta\rho_{\text{Doppler}}$, resulting in an approximate increase of 0.4% to

0.6%, a decrease of -5% to -8%, and an increase of 5%, respectively, when comparing to the zero-dimensional lattice model.

2. The lattice model effect does not depend on the theory (diffusion/transport) and the energy group structure.

Secondly, direct comparison between the 2- and 1-dimensional lattice models is shown in **Figure 2.10**. According to Figure 2.10, it can be concluded that the one-dimensional lattice model causes almost identical changes on four parameters compared with the two-dimensional lattice model; namely, the one-dimensional lattice model represents the characteristics of the two-dimensional hexagonal assembly pretty well for standard fuel assemblies of fast reactors.

The increase in k_{eff} obtained from the heterogeneous lattice model is due to the spatial and energy self-shielding effects, which reduces the neutron absorption of the two/one-dimensional lattice model system compared with that in the zero-dimensional lattice. The decrease in $\Delta\rho_{\text{void}}$ is due to the decrease in the non-leakage component of $\Delta\rho_{\text{void}}$ which is positive. More accurately, the decrease in the non-leakage component of $\Delta\rho_{\text{void}}$ is due to the changes in yield, absorption, and scattering fractions (the main contribution being the scattering fraction). The signs of the yield, absorption, and scattering fractions are negative, positive, and positive, respectively, and the heterogeneous model enhances the yield fraction and decreases the absorption and scattering fractions. Thus, these total effects decrease $\Delta\rho_{\text{void}}$ when applying the heterogeneous model. The increase in $\Delta\rho_{\text{Doppler}}$ is due to the change in the background cross section Σ_b in resonance calculations. Σ_b in the homogeneous model is larger than that in the heterogeneous model. Therefore, the absorption cross section of ^{238}U and its change due to temperature increase in the homogeneous model are

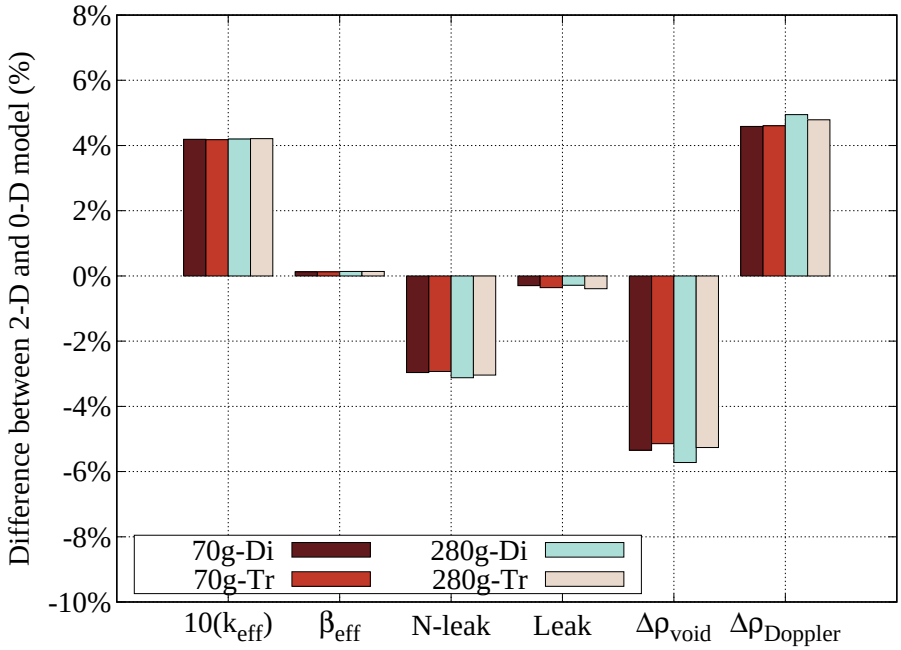

(a) MET-1000.

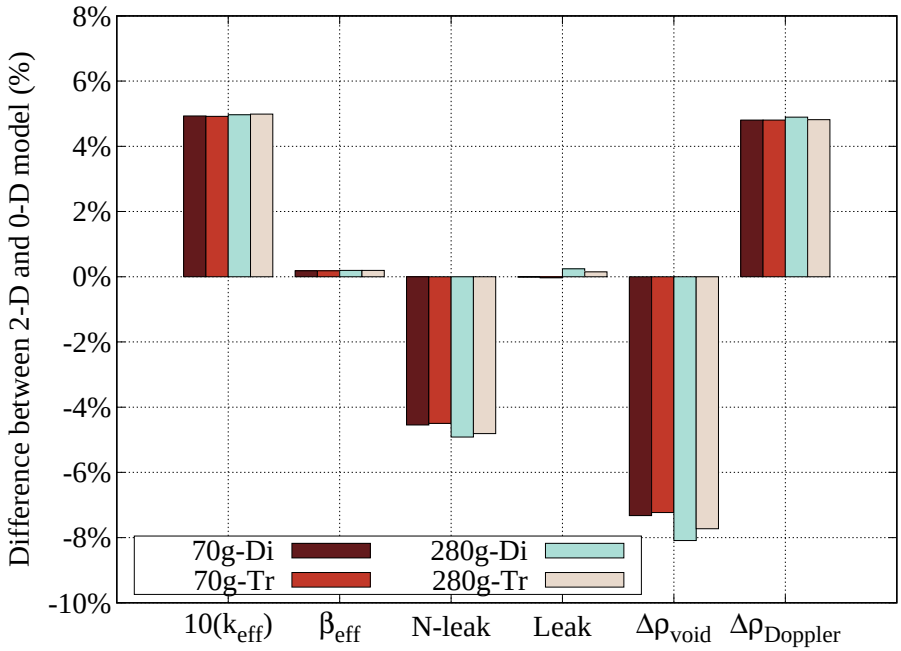

(b) MOX-1000.

Figure 2.9: Two-dimensional lattice model effects of multiple methodologies.

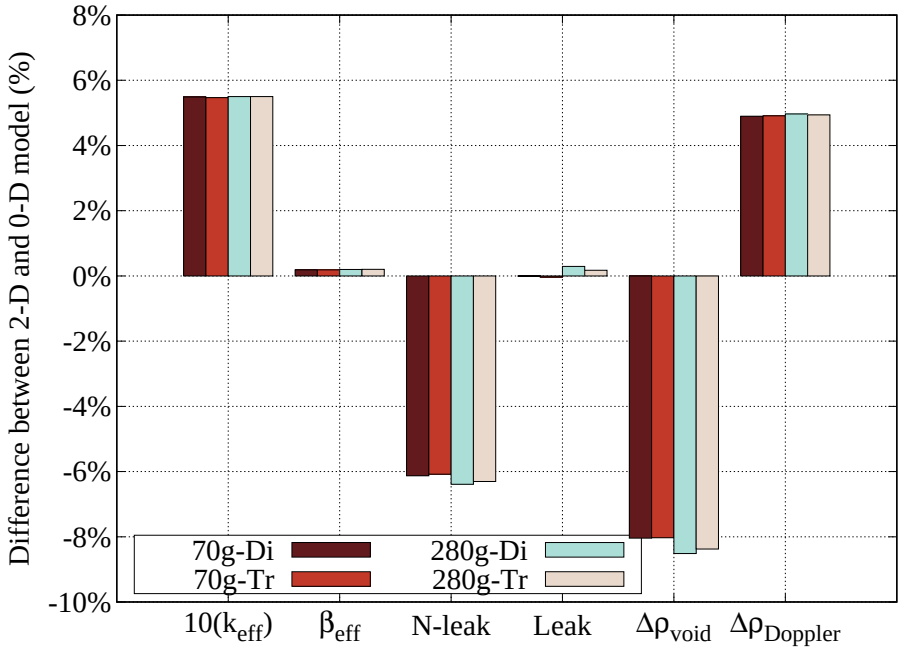

(c) MOX-3600.

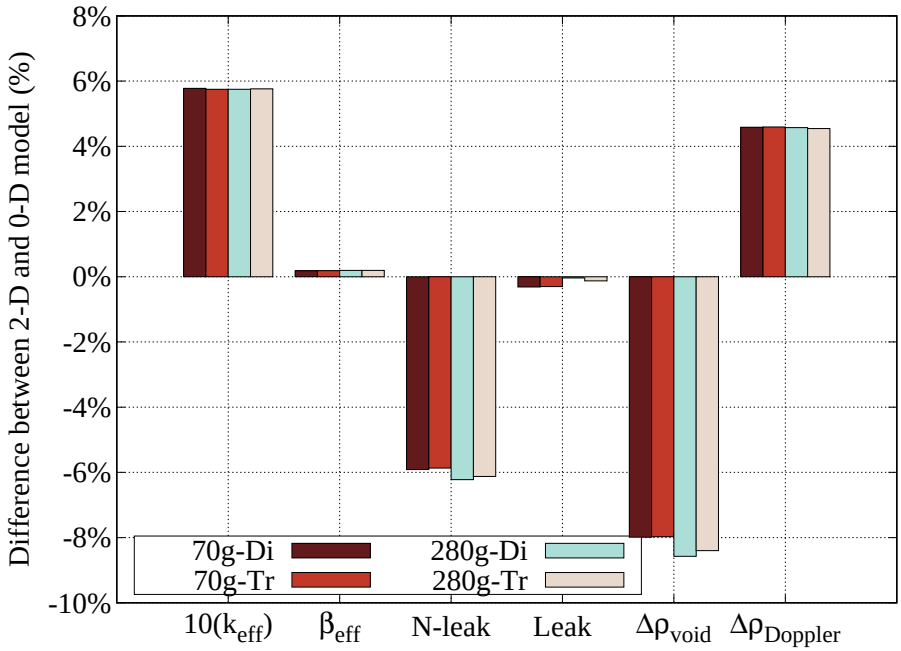

(d) CAR-3600.

Figure 2.9: (Cont.) Two-dimensional lattice model effects of multiple methodologies.

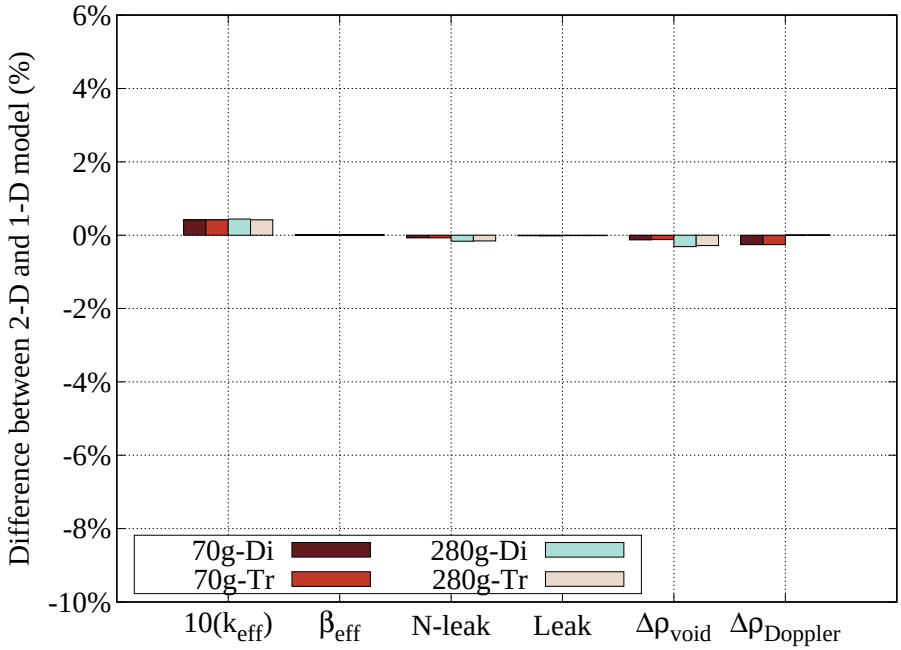

(a) MET-1000.

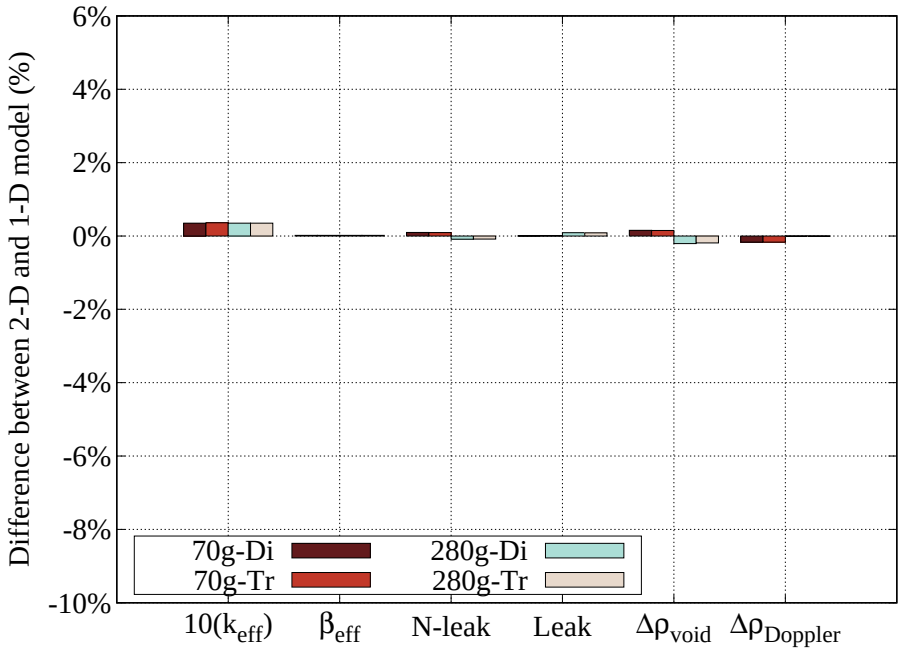

(b) MOX-1000.

Figure 2.10: Direct comparison between 2- and 1-dimensional lattice models.

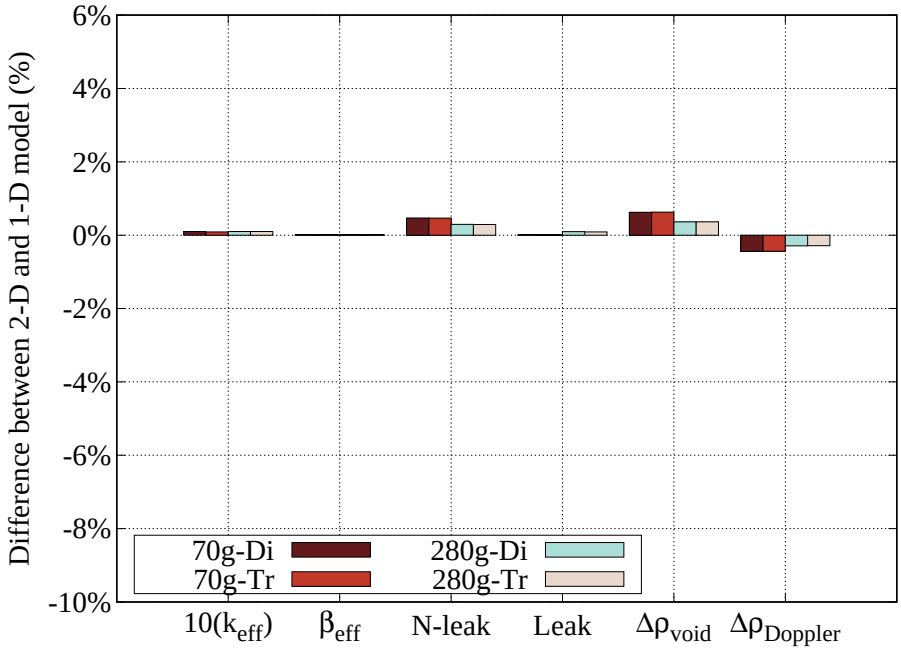

(c) MOX-3600.

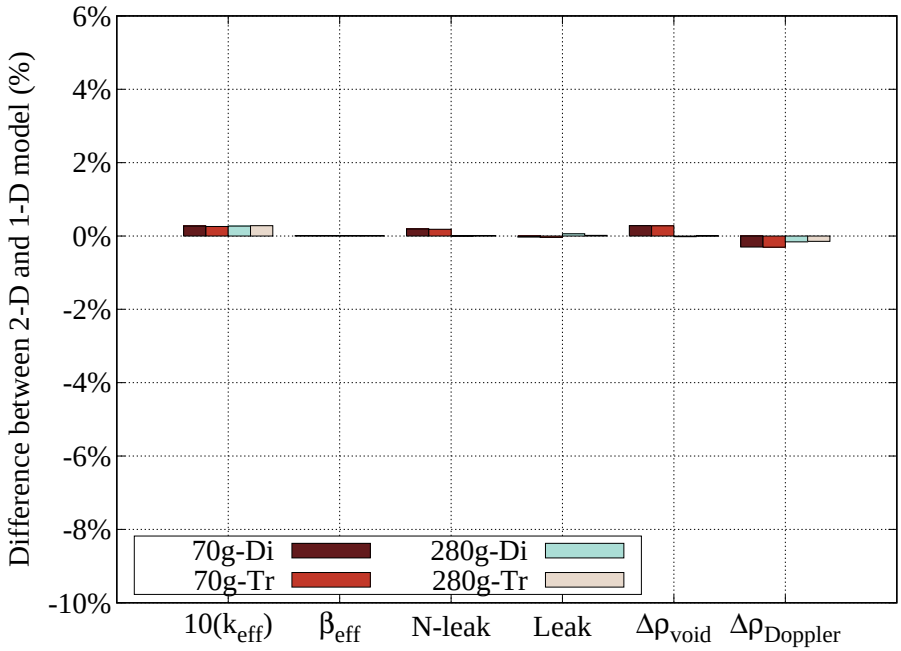

(d) CAR-3600.

Figure 2.10: (Cont.) Direct comparison between 2- and 1-dimensional lattice models.

larger than those in the heterogeneous model.

2.4.2 Two solvers (transport effect)

At present, FRBurner offers three available solvers which employ the diffusion theory, the transport theory and the SP_3 theory, respectively. In this work, only the diffusion and transport solvers are employed for verification and methodologies differences investigation. The differences between the transport and diffusion theory solvers under three lattice models with two energy group structures are studied in this subsection. **Figure 2.11** displays the transport effect obtained by this six methodologies.

1. The transport theory solver (transport effect) causes a significant increase in k_{eff}, about 0.4% for the 70-group calculation and 1.0% for the 280-group calculations.

2. Concerning $\Delta\rho_{\text{void}}$, the transport effect differs for different sized cores. The effect on the middle-sized cores is more obvious than that on the large-sized cores. The transport effect on $\Delta\rho_{\text{void}}$ of the large-sized cores is quite small.

3. The transport effect strongly relates to the energy group structure, and fine-energy group structure enhances the transport effect. However, the transport effect is independent of the lattice model.

In order to ascertain the root cause of the transport effect and determine why the fine-group structure amplifies this effect, the MET-1000 and MOX-3600 cores are selected as targets for investigation. Specifically, the neutron flux in various representative locations, the relative difference between the transport-solver-calculated

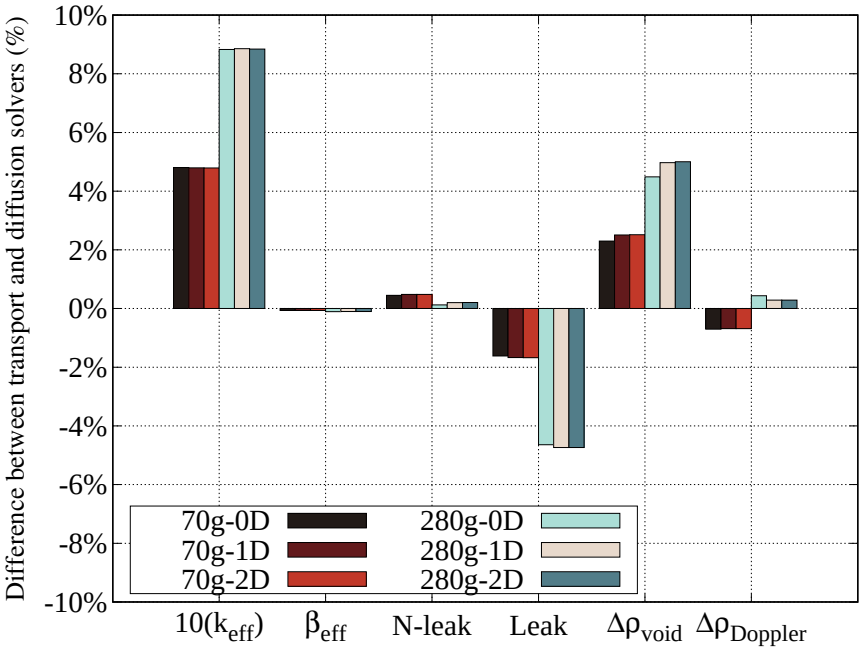

(a) MET-1000 core

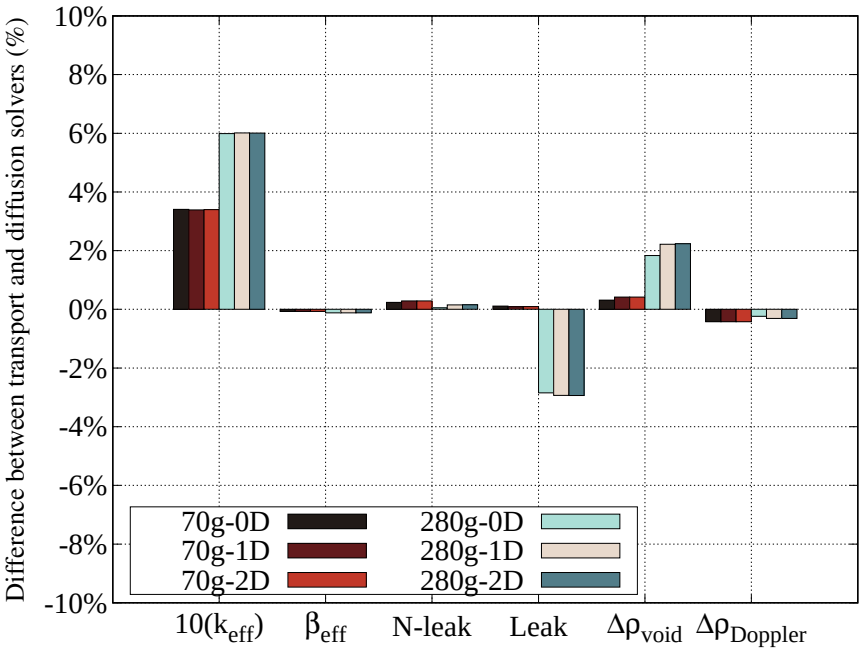

(b) MOX-1000 core

Figure 2.11: Transport effect obtained by multiple methodologies.

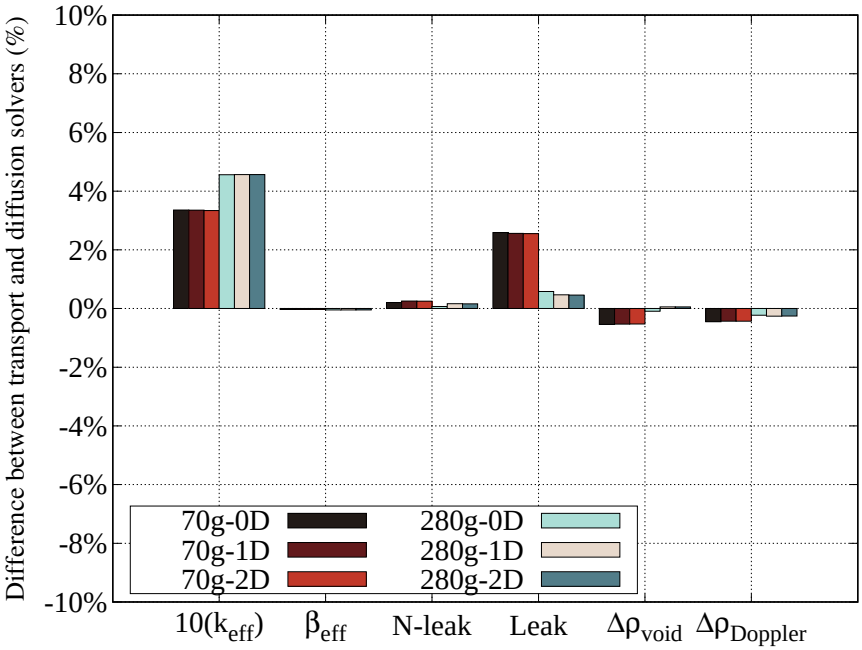

(c) MOX-3600 core

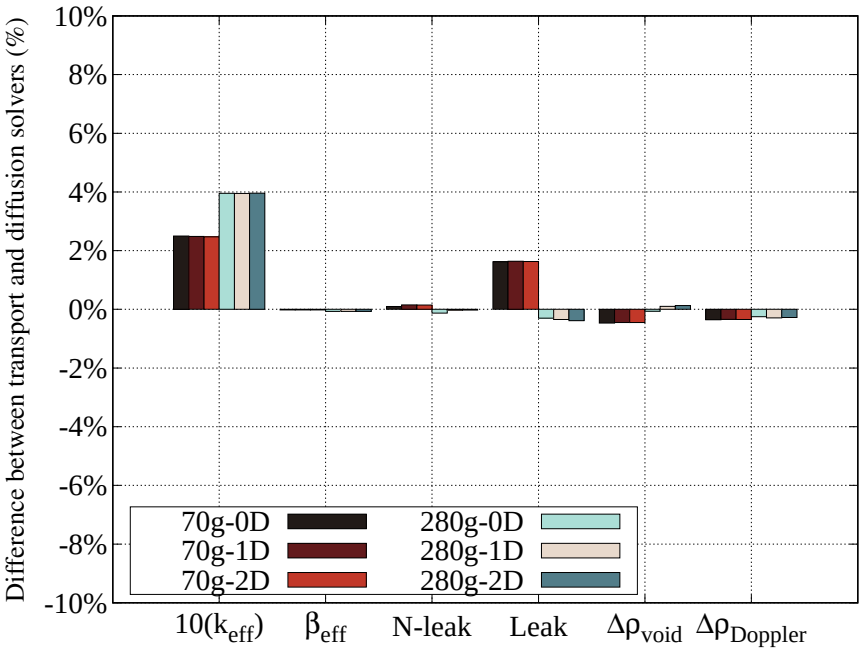

(d) CAR-3600 core

Figure 2.11: (Cont.) Transport effect obtained by multiple methodologies.

neutron flux ϕ_{Tr} and the diffusion-solver-calculated neutron flux ϕ_{Di} (transport effect on the neutron flux), the macroscopic total and scattering cross-sections, as well as the microscopic scattering cross-sections of Na and Fe are all examined. Figures 2.12 and 2.13 illustrate the energy-wise distribution of the transport effect on neutron flux. For MET-1000, medium 0, 10, and 20 are situated in the inner-core, while medium 27, 35, and 43 are located in the outer-core. Medium 0 and 27 are located at the top, while medium 20 and 43 are located at the bottom. Similarly, for MOX-3600, medium 0, 18, and 36 belong to the inner-core fuel assembly, while medium 47, 57, and 67 belong to the outer-core fuel assembly. Medium 0 and 47 are located at the top, while medium 36 and 67 are located at the bottom.

The following points can be concluded.

- Although the transport effect show negative impacts in certain regions and energy ranges, it ultimately has a positive effect on the target reactors.
- The transport effect in outer-core regions and near-reflector regions is more obvious.
- Fine-energy group structure enhances the transport effect across the entire energy range, mostly in the outer-core regions.

Besides, Figure 2.12 suggests that the transport effect has a correlation with scattering cross-section since there is a peak around 3 keV, and Na has an elastic-scattering cross-section peak around 3 keV (**Figure 2.14**).

The transport effect on neutron flux behaves differently in inner-core and outer-core regions, suggesting that it is a "spatially correlated" effect. The transport effect reduces the inner-core neutron flux level and increases the outer-core neutron flux level. Since the outer-core region has more fissile material, k_{eff} is increased eventu-

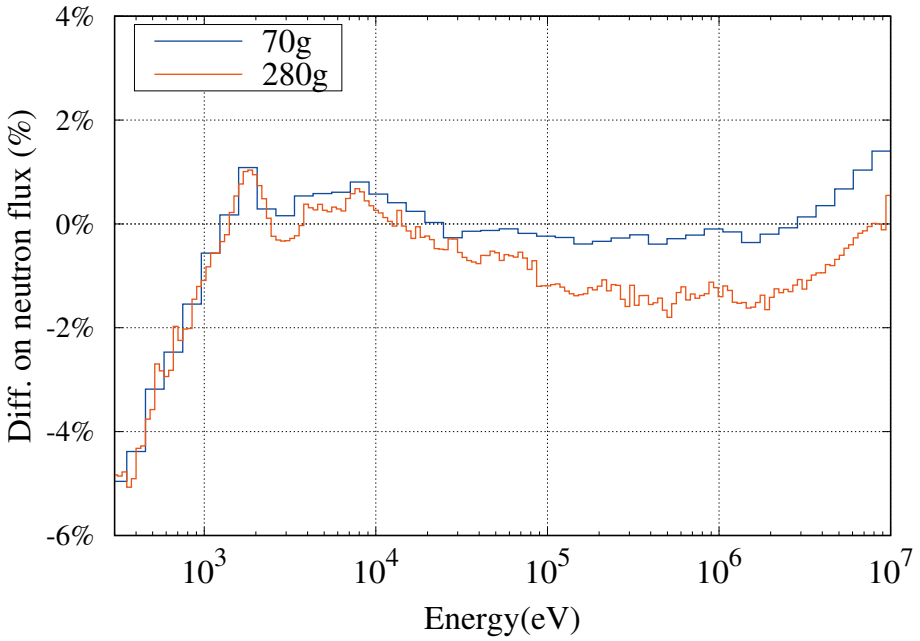

(a) Medium-0 (belongs to inner-core fuel assembly and locates at top).

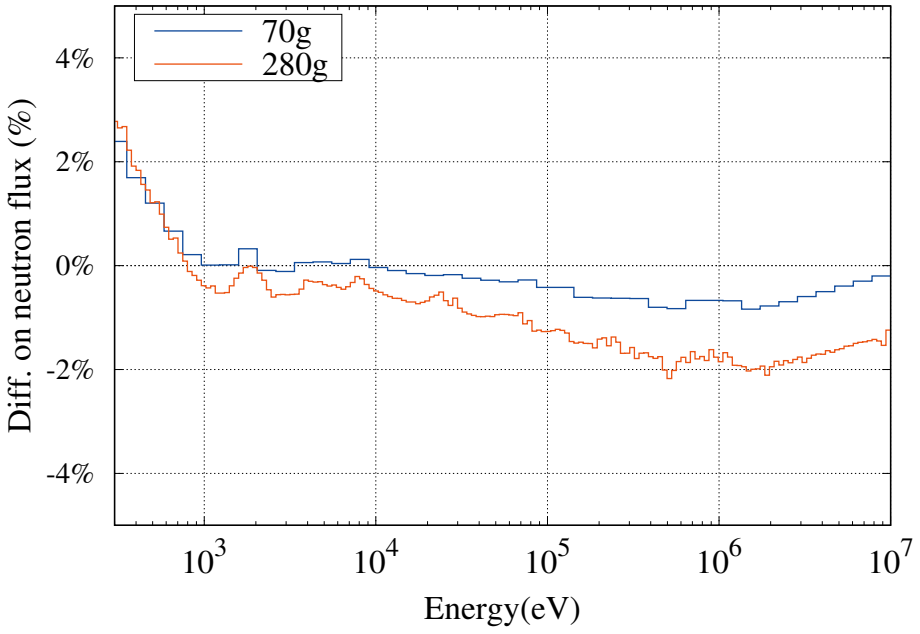

(b) medium-10 (belongs to inner-core fuel assembly and locates at middle).

Figure 2.12: Transport effect on neutron flux, MET-1000.

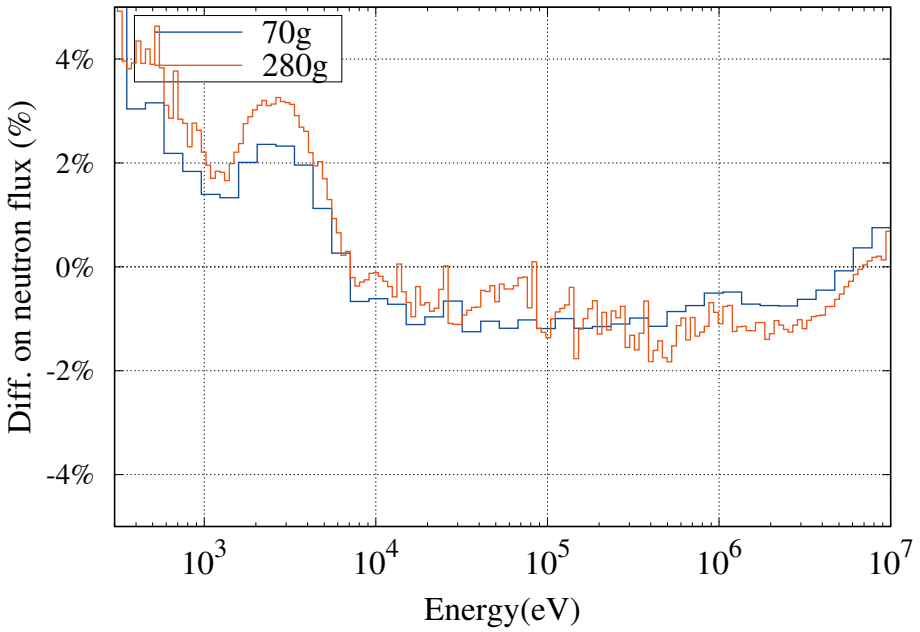

(c) Medium-20 (belongs to inner-core fuel assembly and locates at bottom).

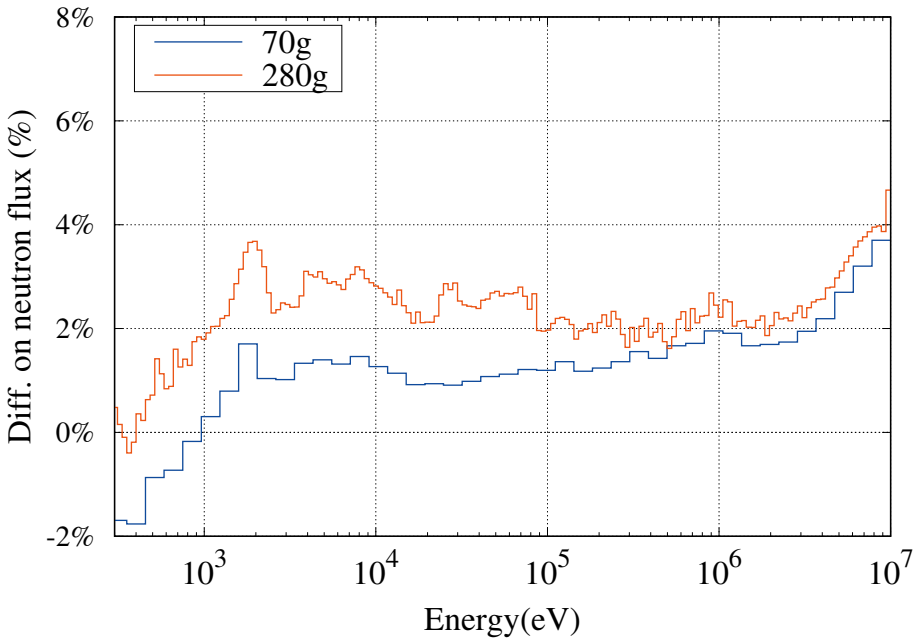

(d) Medium-27 (belongs to outer-core fuel assembly and locates at top).

Figure 2.12: (Cont.) Transport effect on neutron flux, MET-1000.

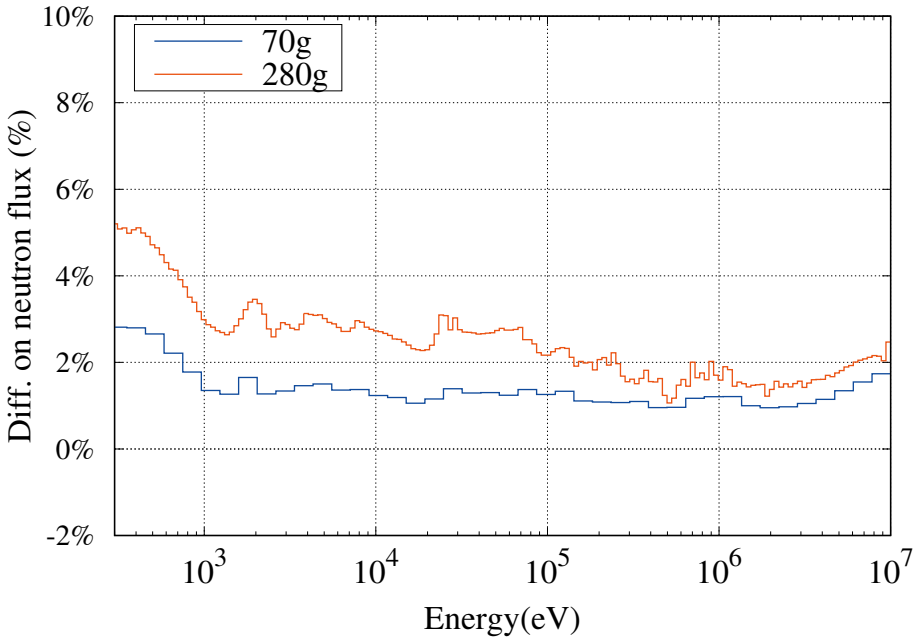

(e) Medium-35 (belongs to inner-core fuel assembly and locates at middle).

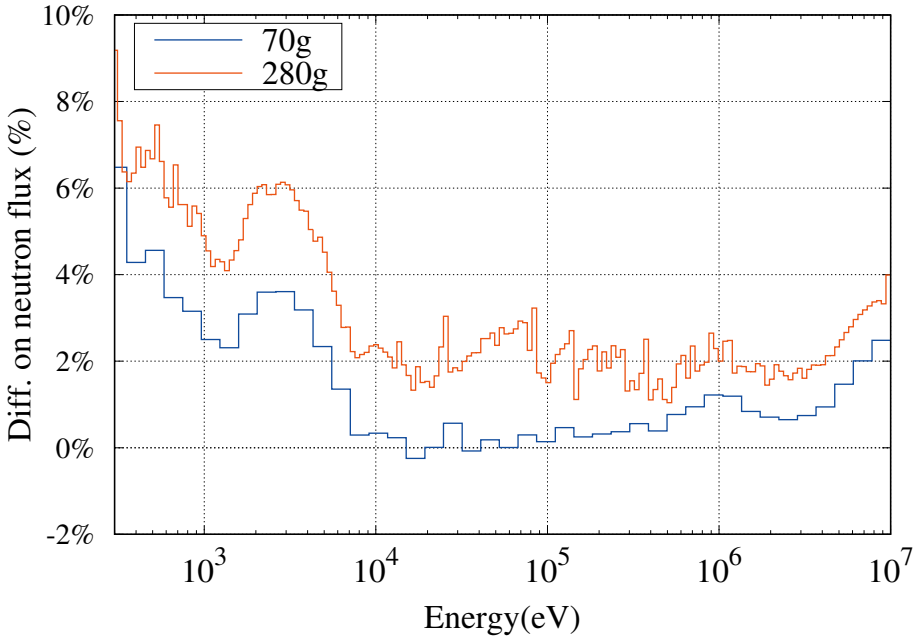

(f) Medium-43 (belongs to outer-core fuel assembly and locates at bottom).

Figure 2.12: (Cont.) Transport effect on neutron flux, MET-1000.

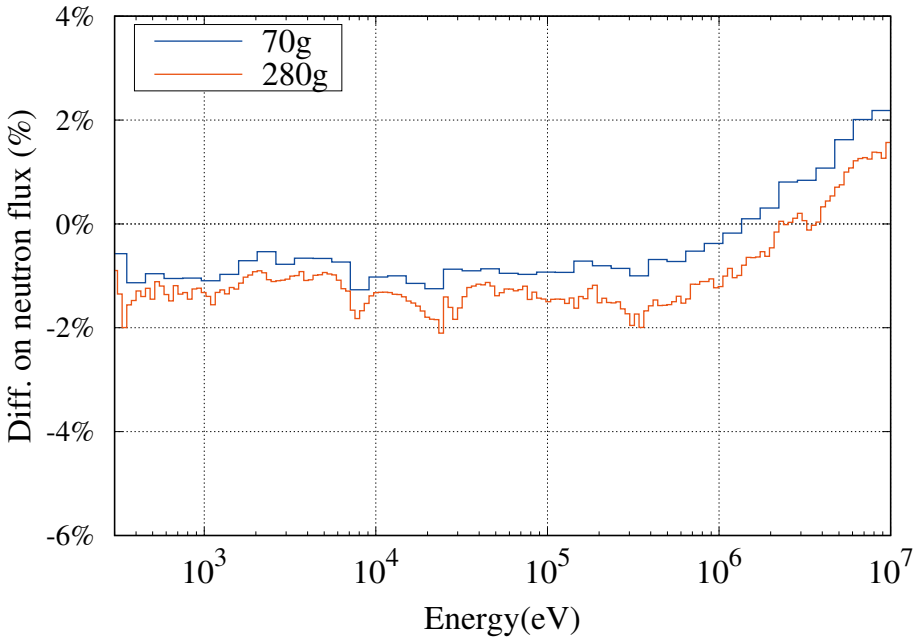

(a) Medium-0 (belongs to inner-core fuel assembly and locates at top).

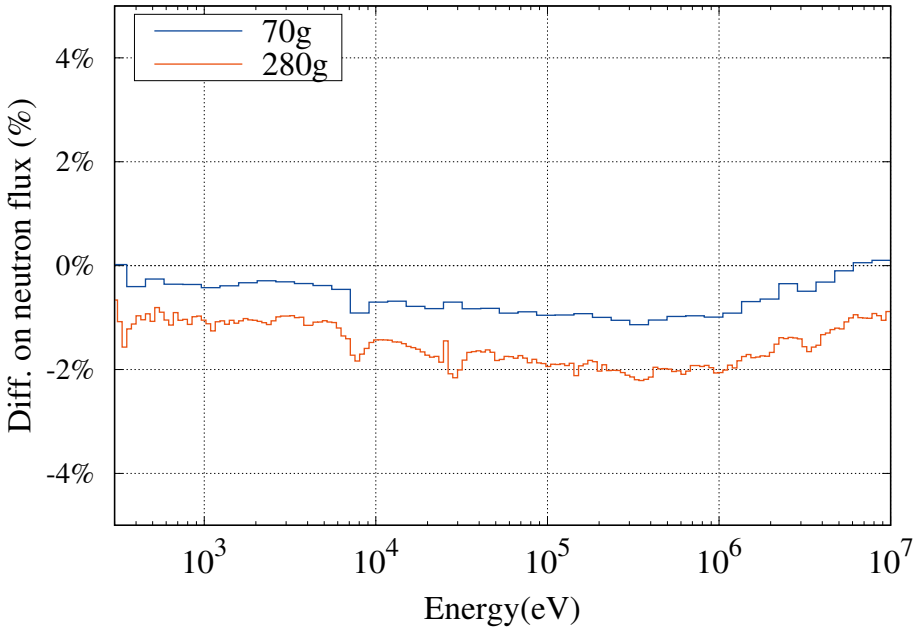

(b) Medium-18 (belongs to inner-core fuel assembly and locates at middle).

Figure 2.13: Transport effect on neutron flux, MOX-3600.

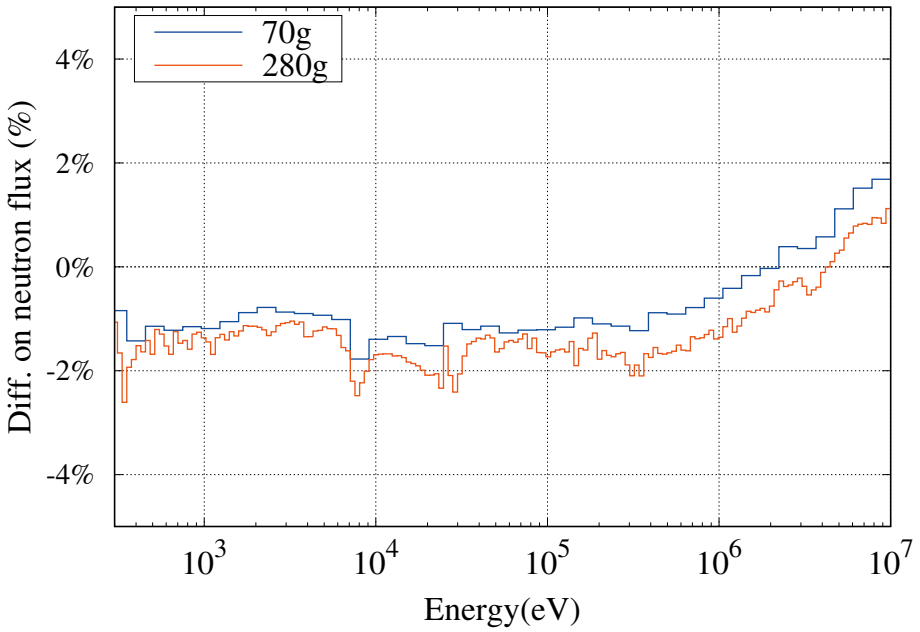

(c) Medium-36 (belongs to inner-core fuel assembly and locates at bottom).

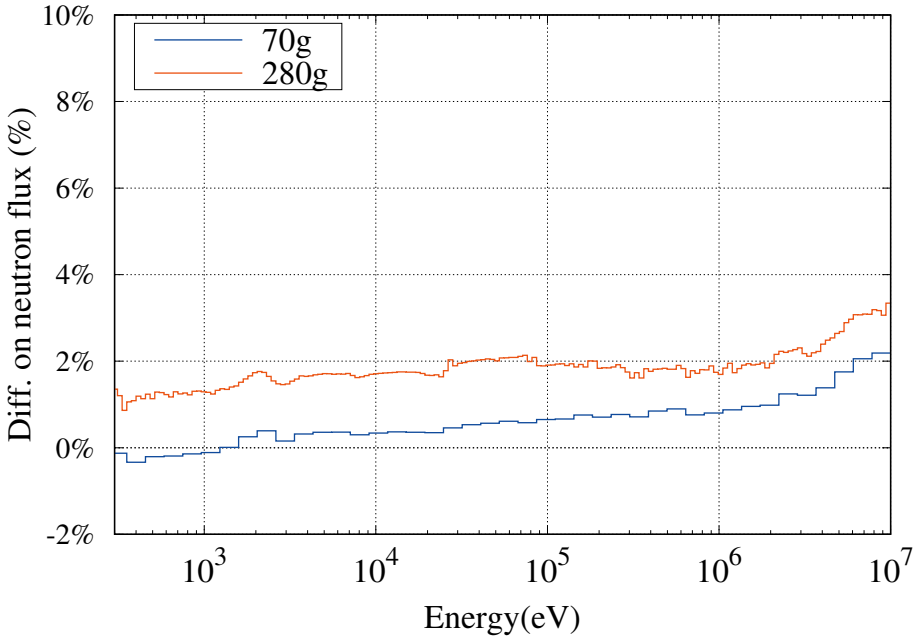

(d) Medium-47 (belongs to outer-core fuel assembly and locates at top).

Figure 2.13: (Cont.) Transport effect on neutron flux, MOX-3600.

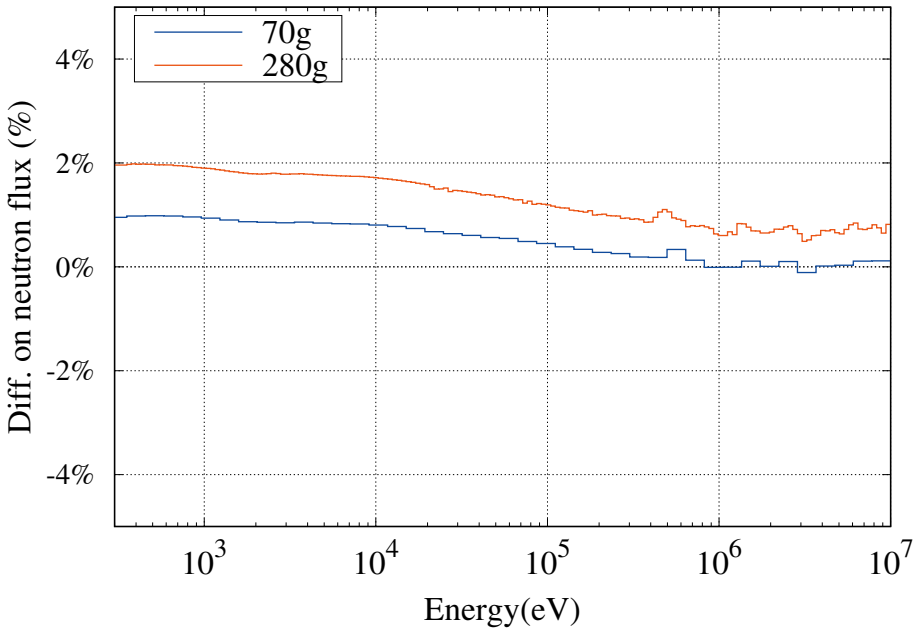

(e) Medium-57 (belongs to outer-core fuel assembly and locates at middle).

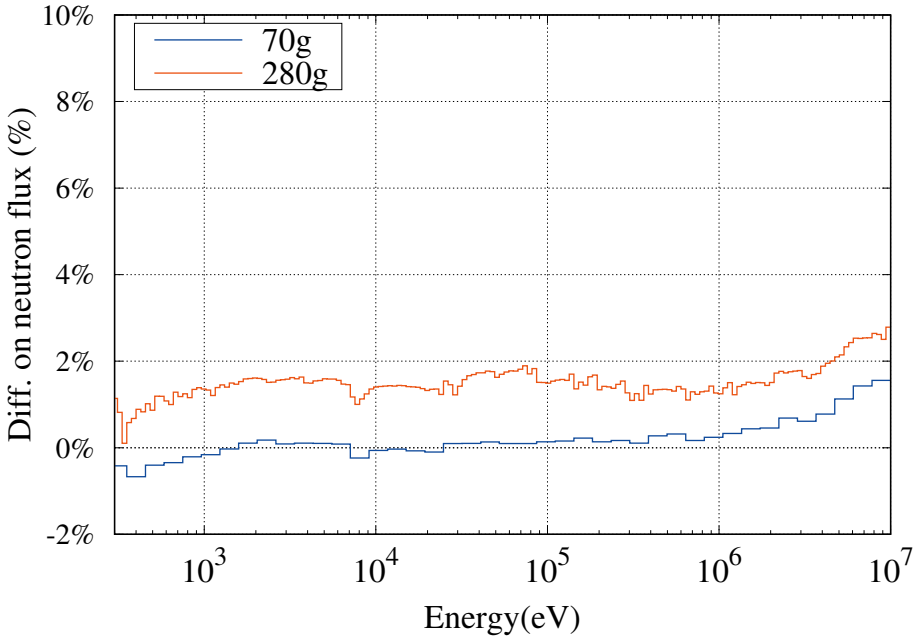

(f) Medium-67 (belongs to outer-core fuel assembly and locates at bottom).

Figure 2.13: (Cont.) Transport effect on neutron flux, MOX-3600.

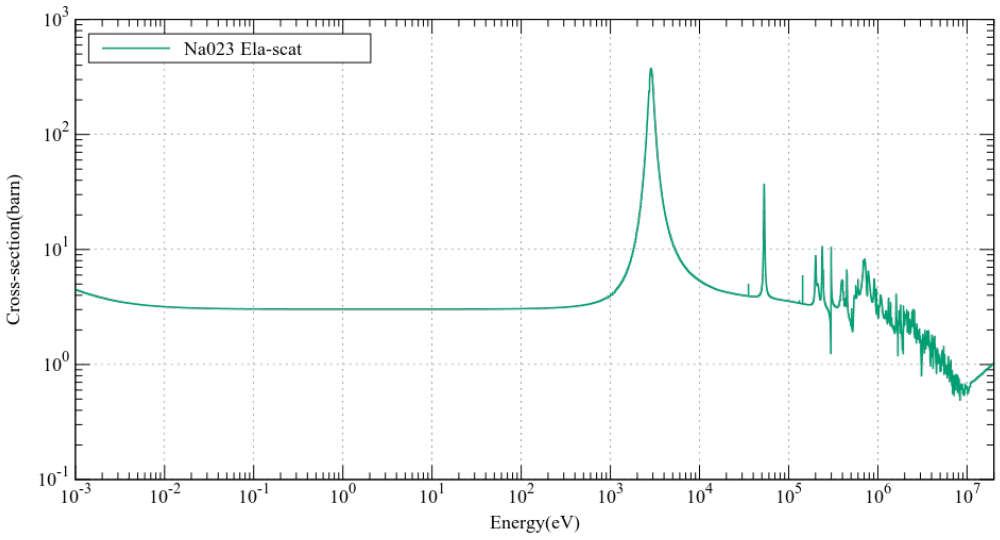

Figure 2.14: Na elastic scattering cross-section (from PENDF data).

ally. If considering the transport effect reversely, the nature of the transport effect is the error caused by the diffusion approximation. Therefore, these two figures indicate that the diffusion solver increases the neutron flux level in the inner-core and reduces the flux level in the outer-core. The gradient of neutron flux is increased by using the diffusion solver. Naturally, the neutron leakage is further overestimated due to the increased neutron flux gradient.

As for the detailed mechanism of fine-energy group structure that enhances the transport effect, it is difficult to give a quantified explanation since the system is complicated, so that further discussion is omitted here.

Above discussion also indicates one thing that the diffusion solver shall cause larger error for a sodium-cooled reactor, especially for reactor which has multiple regions (inner region and outer region). Such an analysis for this type of reactor system should not be conducted with the diffusion solvers. When neutronic analysis of such a type of reactor system is conducted by the diffusion theory, one should pay more attention to the bias caused by the diffusion approximation.

The reason for the increase in $\Delta\rho_{\text{void}}$ obtained by the transport solver for the

middle-sized cores is the same as that for the increase in k_{eff}. That is, correcting the neutron leakage overestimation would decrease the leakage component of $\Delta\rho_{\text{void}}$, as shown in Figure 2.11. Neutron leakage in large-sized cores, however, is less significant than that in middle-sized cores. Accordingly, correcting the overestimation of neutron leakage for large-sized core calculations does not result in significant differences when compared with the diffusion theory solver. It is believed that the different levels of neutron leakage for different-sized cores are responsible for the difference in this significant transport effect.

Additionally, the transport effect calculated for MET-1000 is larger than that for the others. This is due to the relatively harder neutron spectrum of the metallic fuel core than that of the other cores. For this reason, the overestimation of neutron leakage is more significant.

2.4.3 Coarse/fine energy group structure (fine-energy group effect)

Two energy group structures were applied in this work: the 70- and 280-group. There would be six methodologies for each core: two/one/zero/dimensional lattice model with diffusion/transport theory solver. **Figure 2.15** shows this fine-energy group effect and indicates that:

1. The fine-energy group calculation largely increases k_{eff}: around 0.2% for the diffusion theory solver calculations, and from 0.2% to 0.6% for the transport theory solver calculations.

2. The fine-energy group calculation has a negative effect on $\Delta\rho_{\text{void}}$. The negative effect is due to the decrease of the non-leakage component of $\Delta\rho_{\text{void}}$ (positive

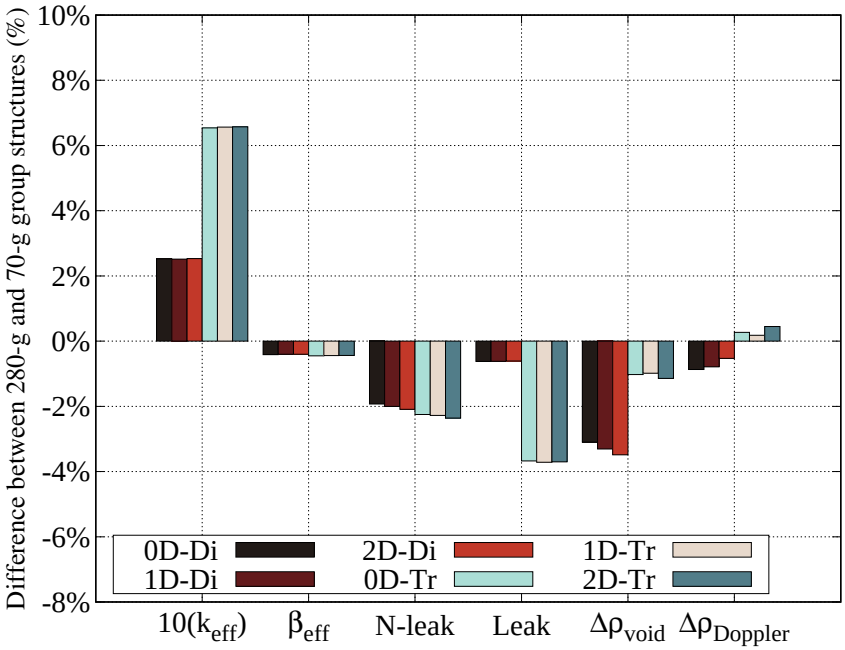

(a) MET-1000.

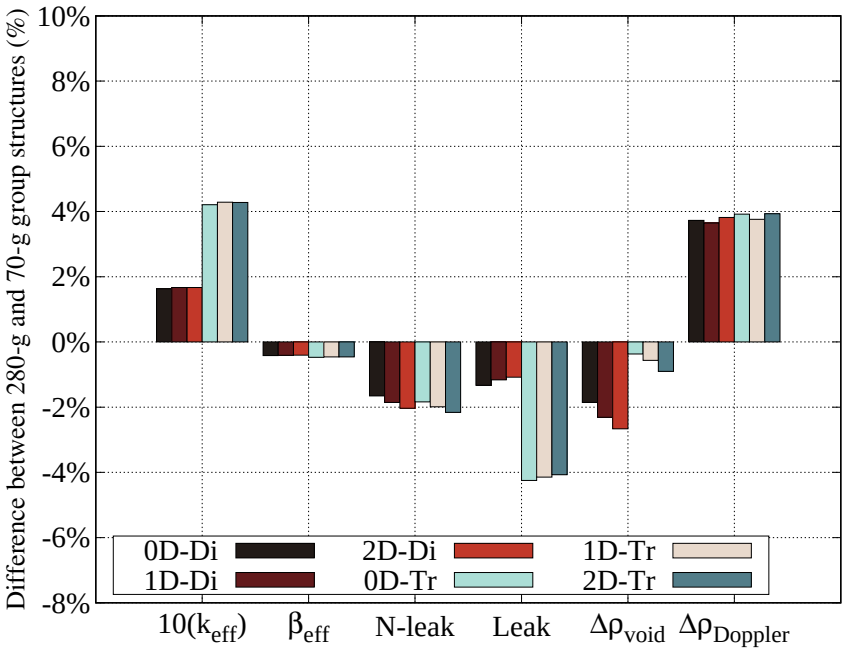

(b) MOX-1000.

Figure 2.15: Fine-energy group structure effects under multiple methodologies.

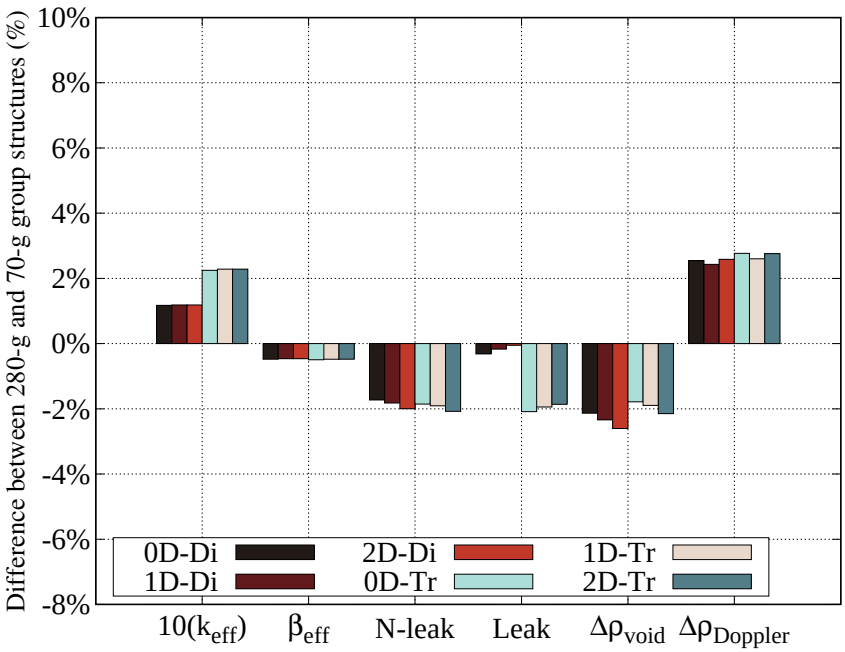

(c) MOX-3600.

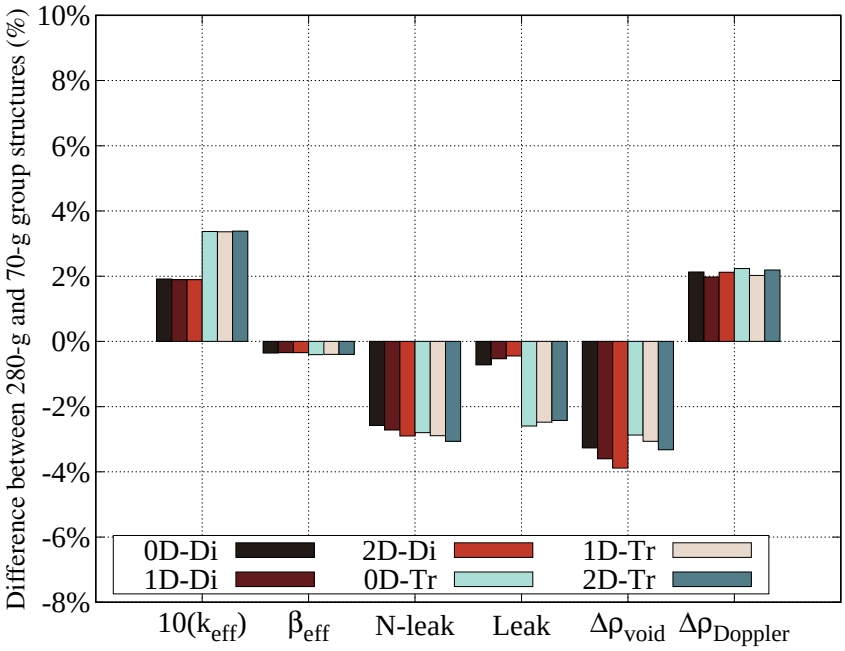

(d) CAR-3600.

Figure 2.15: (Cont.) Fine-energy group structure effects under multiple methodologies.

value) and the increase of leakage component of $\Delta\rho_{\text{void}}$ (negative value). Besides, the negative effects on $\Delta\rho_{\text{void}}$ differ between the middle-sized and large-sized cores. In the middle-sized cores, the negative effect is more intense in the diffusion theory solver calculations; however, in the large-sized cores, the negative effect is nearly identical.

3. The fine-energy group effect is independent on the lattice model, but it has a relationship with the calculation theory. For large-sized cores, the difference between theories becomes negligible.

There are several possible explanations for these fine-energy group effects. The first is the weighting function used to generate the multi-group constant. In this study, IWT = 8 weighting function was used. In the 70-group case, the IWT = 8 weighting function may have caused errors, but the errors would be reduced in the 280-group structure case. The second is the change in the resonance absorption cross sections of medium-mass nuclei such as Fe and Na. These two factors should contribute to the fine-energy group effect.

2.4.4 The order of transport solver

In FRBurner, the order of the transport solver is determined by two parameters: P_N and S_N, which are the maximum order of the Legendre polynomial for the anisotropic scattering cross-section expansion and the number of discrete points in a direction angle, respectively. It is notable that the P_N-order here is different from the famous *P_N method*. The P_N method is using spherical harmonic functions (or Legendre Polynomials) to expand the angular neutron flux. The *S_N method* is discrete ordinates method (DOM) in the reactor physics field, and it applies quadrature sets to choose

angles which need to be considered. The weights of directions are different according to geometry and the number of directions. The introduction of the S_N method can be found in many textbooks [4, page 821] [29, Page 171]. There are several different S_N quadrature sets and the commonly used is the level symmetric quadrature sets [30]. The order N decides the number of directions in space, and it must be even integer (≥ 2). **Figure 2.16** shows an example of the S_N level symmetric quadrature set when N = 6.

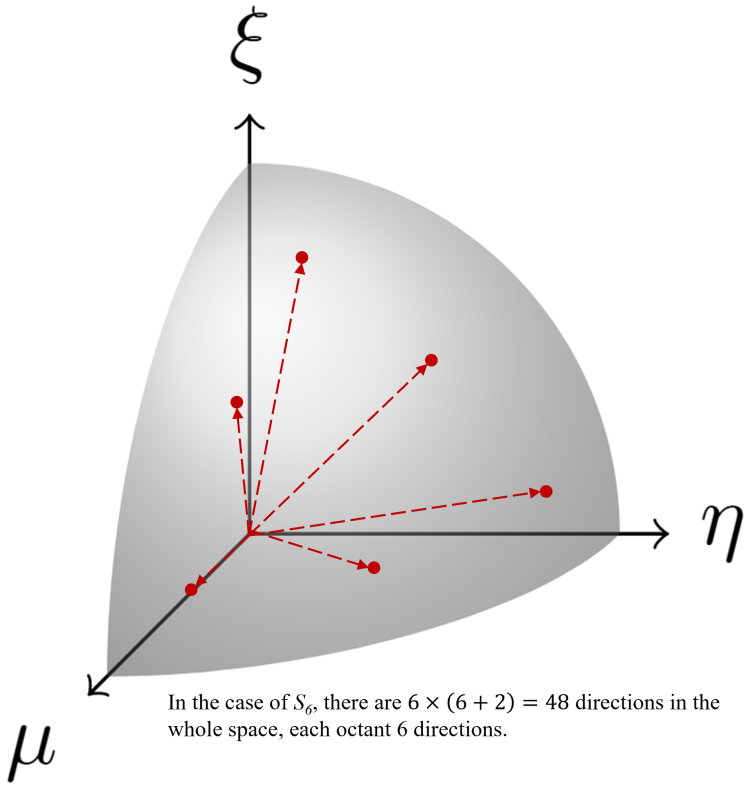

Figure 2.16: Example of S_N (N = 6) level symmetric quadrature sets.

Therefore, the order $P_N S_N$ in FRBurner indicates the order of scattering cross section expansion and level symmetric quadrature sets. Generally speaking, the option $P_1 S_4$ is applied. The option $P_3 S_8$ is known to be more accurate; however, it could be extremely time-consuming. **Figure 2.17** shows the differences between the $P_1 S_4$ and $P_3 S_8$ options in 70-group calculations.

According to Figure 2.17, one can know that the option P_1S_4 could provide preferable results with enough accuracy for problems such as preliminary or initial stage calculations that do not require high accuracy.

2.4.5 Dependency among three variables on methodology

The above investigations have thoroughly described the degree to which changes would be caused by different methodologies. The dependencies among the lattice model effect, the transport effect, and the fine-energy group effect are discussed in this subsection.

Firstly, from Figure 2.9 it is obvious that the lattice model effect has no relationship with the core calculation theory and the energy group structure. This independence indicates that users could freely choose any lattice model according to their demands. On the contrary, it is clear from Figure 2.11 that the transport effect depends on the energy group structure. As discussed above, it is not appropriate to apply the fine-energy group option with the diffusion theory. Accordingly, the fine-energy group effect has relationship with the calculation theory as well, as shown in Figure 2.15.

The dependency investigation suggests to users how to properly set the calculation methodology with the FRBurner module.

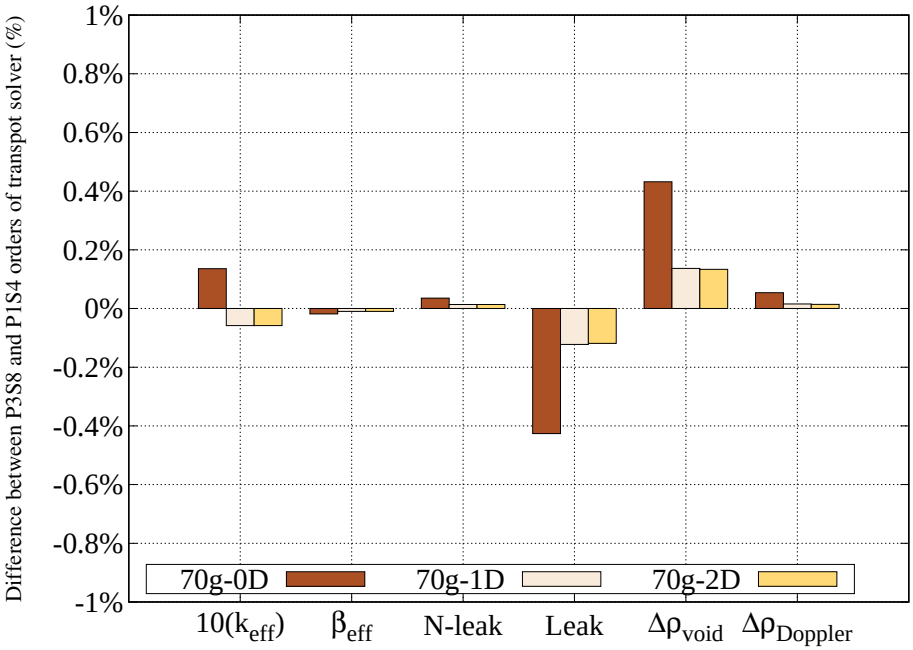

(a) MET-1000.

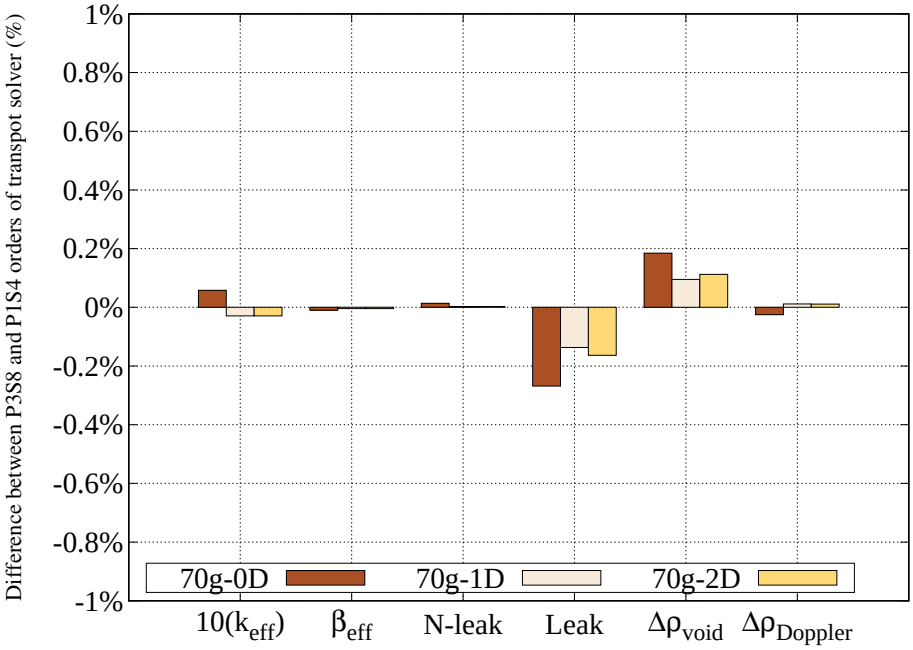

(b) MOX-1000.

Figure 2.17: Differences between P_1S_4 and P_3S_8 options for transport solver.

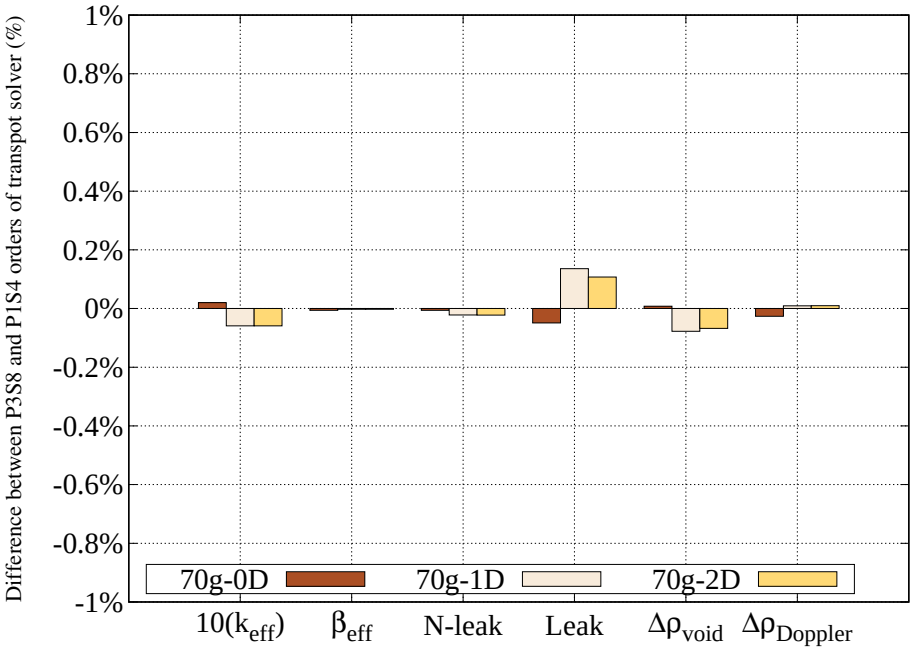

(c) MOX-3600.

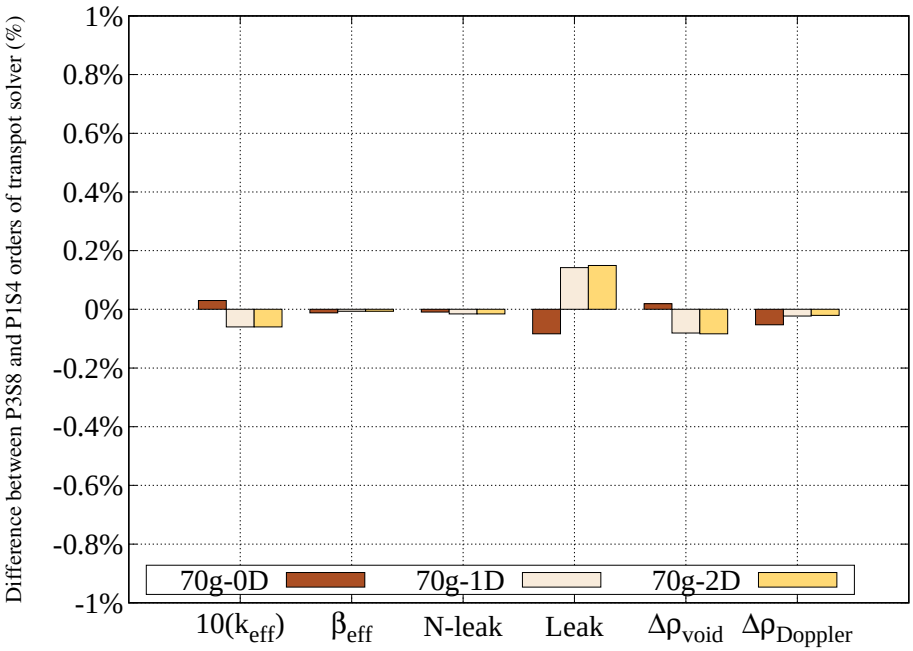

(d) CAR-3600.

Figure 2.17: (Cont.) Differences between P_1S_4 and P_3S_8 options for transport solver.

2.5 SP_3 calculation capability

There is another solver, the Simplified-P_3 (SP_3), available for the core calculation step in FRBurner. The Simplified-P_N (SP_N) theory was initially proposed by Gelbard [31] in 1960. As concluded by Larsen [32], although a solid theory basis was not constructed in the very beginning, the SP_N theory was proved valid though applications. In this section, the SP_3 core calculation function is compared with the diffusion and transport solvers to show the feature on fast reactor analysis.

The SP_3 calculation function also needs to be verified in a similar manner since this function has not been verified officially. As the transport calculation function has been verified in section 2.3, the most rigorous calculation methodology option, that the 2-D hexagonal lattice model S_N (P_3S_8) calculation with fine energy-group structure library (280-g), is used to provide reference results. Meanwhile, results given by the diffusion solver calculation options are compared to the S_N and SP_3 calculation options results, intending to exhibit the feature of the SP_3 method in fast reactor analysis. The k_{eff} is focused here. The prediction accuracy and computing time both are taken into account. On the computing time, a CMFD-acceleration factor is applied to evaluate the SP_3 solver computing time since the CMFD-acceleration has not been implemented to the SP_3 solver yet. This CMFD-acceleration factor is obtained by comparing the computing time of the diffusion solver with and without the CMFD-acceleration. As the computing time strongly relates to the performance of computer, each computational task is assigned an independent core to perform the calculation. The maximum memory requirement (around 20 GB in the case of S_N solver P_3S_8 2-dimensional lattice model with 280-g library) is still much smaller than the total memory of the computer (around 600 GB in total), therefore, comput-

ing time is not affected by the competition on memory resource.

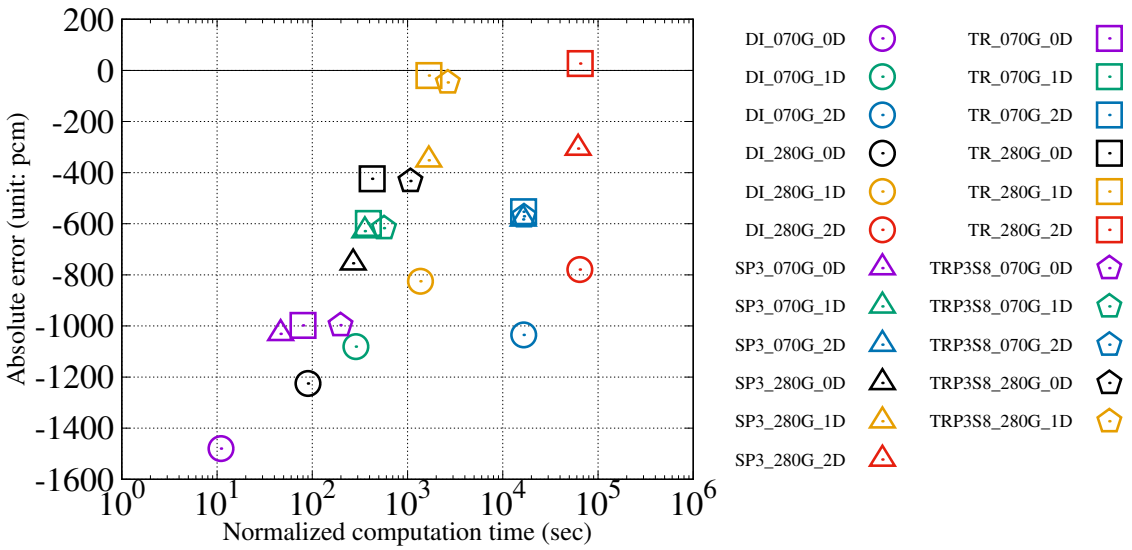

Figure 2.18: Comparison between diffusion, SP_3 and transport solvers on MET-1000 k_{eff} calculation.

There is a trend that the SP_3 solvers can give more accurate results comparing to the diffusion solvers while the computing time is less than the S_N solvers. **Figures 2.18** and **2.19** can be used to help users choose appropriate calculation method according to real calculation demand. For instance, methods locates at the left bottom can be used for preliminary stage work, methods at the center can be used for intermediate stage work, and methods locates at the top right are suitable for final stage work.

It would be clear to check the advantage of the SP_3 method through comparing the errors on power distribution as well. Errors on power of each spatial mesh of fuel assembly given by the SP_3 and diffusion solvers are summarized into **Figures 2.20** and **2.21**. In these two figures, the x-axis is the position of the spatial mesh along the radial-direction in the 2-dimensional multi-layer cylinder model of reactor, the y-axis is the position of the spatial mesh in the axial-direction, and the z-axis is the

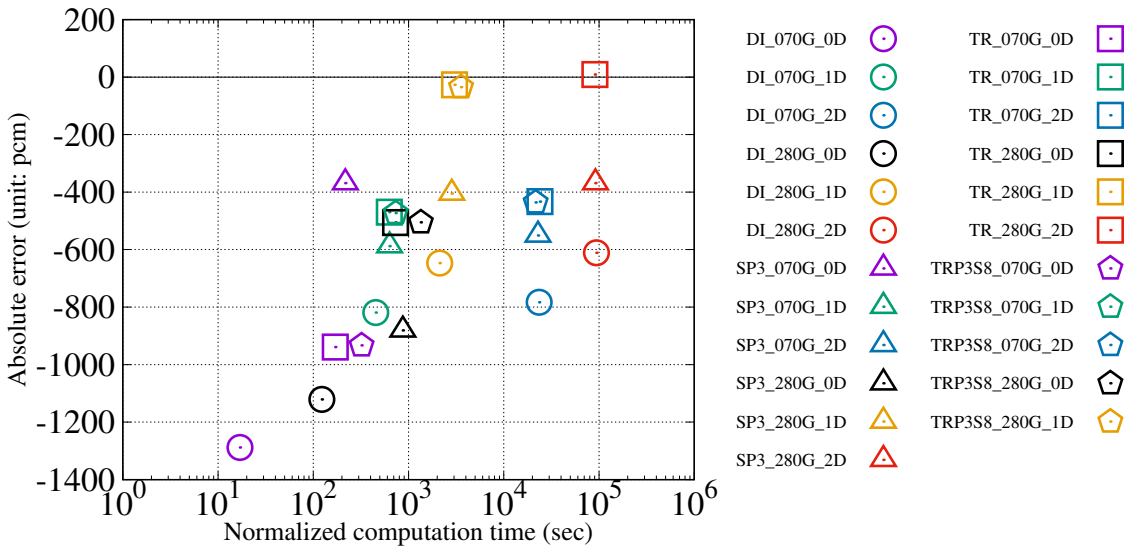

Figure 2.19: Comparison between diffusion, SP_3 and transport solvers on MOX-1000 k_{eff} calculation.

relative error on power comparing to the reference given by the S_N solver. Since the fuel region is further divided into several spatial meshes in FRBurner intending to improve the calculation accuracy, the numbers on the x-axis only indicate the spatial meshes potion (for instance, the 9-layer fuel region of MET-1000 is further divided into 36 spatial meshes).

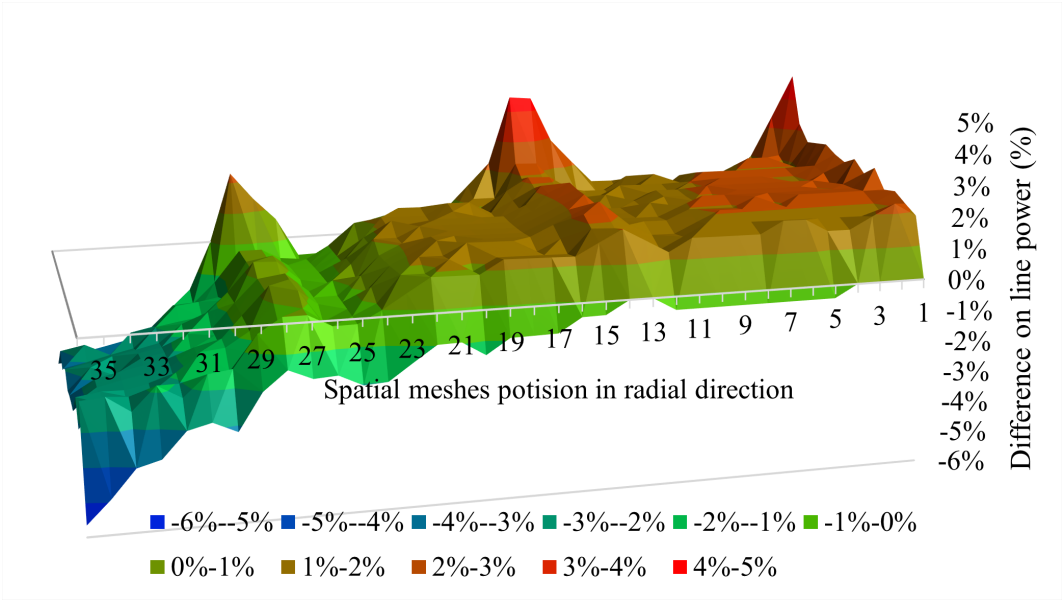

(a) Diffusion solver.

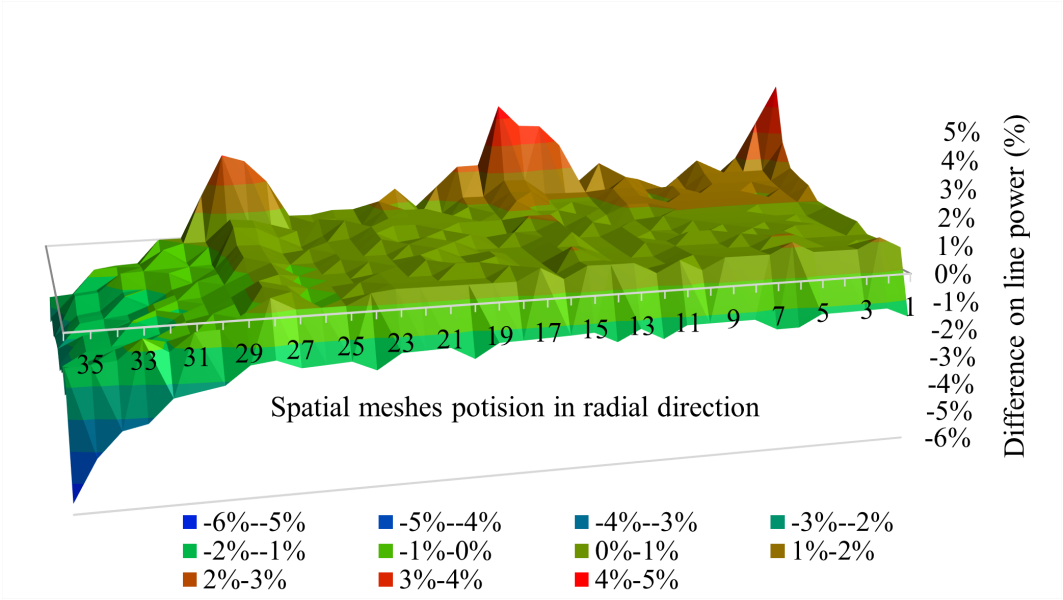

(b) SP_3 solver.

Figure 2.20: SP_3 and diffusion solvers calculation error on power distribution, MET-1000.

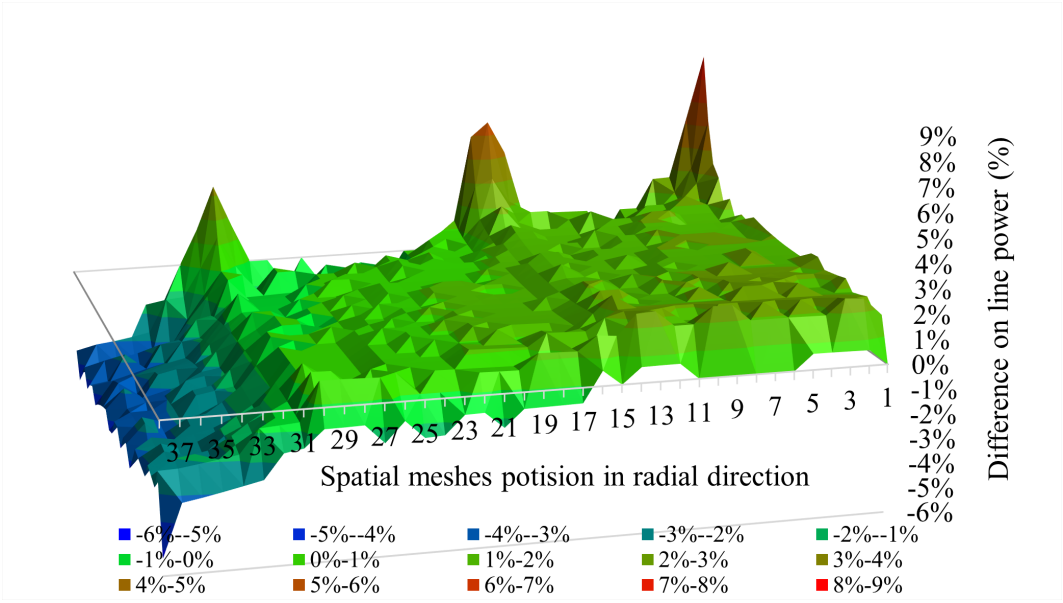

(a) Diffusion solver.

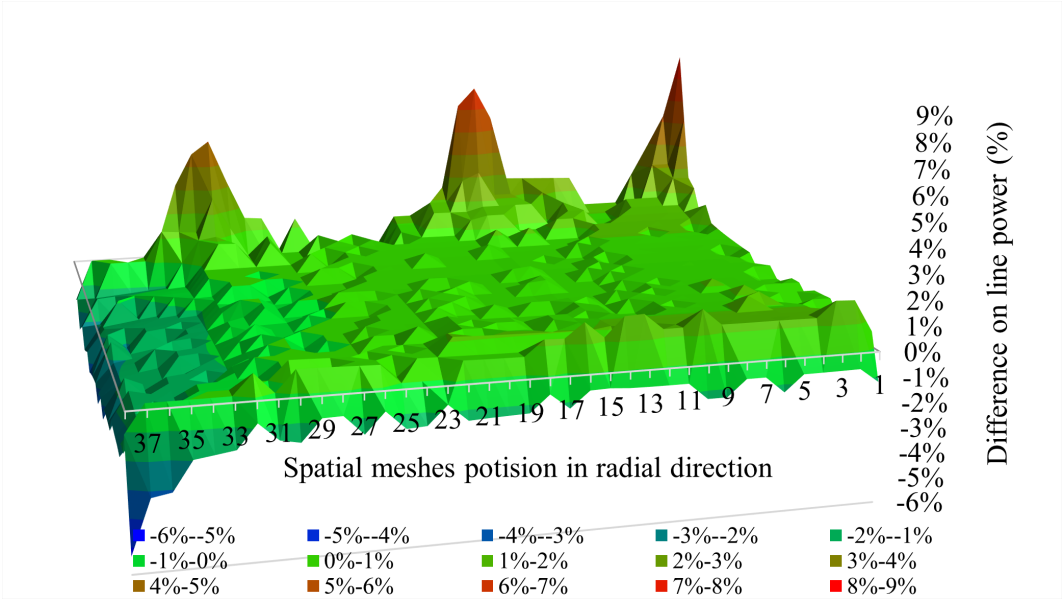

(b) SP_3 solver.

Figure 2.21: SP_3 and diffusion solvers calculation error on power distribution, MOX-1000.

Although both the SP_3 and diffusion solvers give relatively large error on the positions near the neutron absorber (error peaks at top position), the SP_3 solver gives more accurate results over all the core. More importantly, there are obvious error increases in the regions near the control rod assembly, and such error increase is not shown in SP_3 solver calculations.

It can be said that the SP_3 method can be regarded as an intermediate point between the diffusion and transport methods. According to this conclusion, a new reactivity calculation method based on the SP_3 theory has been developed with CBZ, and this new method is going to be discussed in the next chapter.

2.6 Conclusion

FRBurner, which is a recently developed fast reactor neutronic calculation module of the CBZ code system, has been verified through the calculation of four fast reactor core problems and compared with two references provided by two institutes. Four key reactor physics parameters were focused on in this verification: k_{eff}, β_{eff}, $\Delta\rho_{\text{void}}$ and $\Delta\rho_{\text{Doppler}}$. The maximum biases obtained from the JENDL-4.0-based CBZLIB and the JEFF-3.1.1-based CBZLIB were less than 0.5%, 1%, 3% and 10%, and 1.0%, 4%, 12% and 8%, respectively. This verification work indicated that FRBurner could provide an accurate prediction on k_{eff}, β_{eff}, $\Delta\rho_{\text{void}}$ and $\Delta\rho_{\text{Doppler}}$ for general-type fast reactor systems since the four fast reactor cores used for verification cover typical fuel types and core sizes proposed as fast reactor concepts.

Secondly, the differences between methodologies available in FRBurner are investigated. The investigation of the lattice model effect suggested that the heterogeneous model is crucial for calculation but that the one-dimensional lattice model is sufficiently accurate to estimate the neutronic properties. As the heterogeneous models have large influence on k_{eff}, $\Delta\rho_{\text{void}}$ and $\Delta\rho_{\text{Doppler}}$, it is essential to take into account the effect when studying these three parameters with the 0-dimensional homogeneous lattice model.

The transport-effect study indicated that the transport solver has a large impact on k_{eff} and $\Delta\rho_{\text{void}}$ (only for the middle-sized cores). A large transport effect on k_{eff} for the fine-energy group calculations means that the diffusion theory solver should not be applied with the fine-energy group library. Thus, the use of methodology options in combination with the fine-energy group library and the diffusion theory solver should be avoided. The transport effect investigation also indicates that the diffusion

approximation may cause a large bias for sodium-cooled fast reactors, especially in systems with multiple core regions. Therefore, when the diffusion theory is used in sodium-coolant fast reactor analysis, more attention should be paid to bias. In addition, the study on the P_NS_N order of the transport solver revealed that the P_1S_4 option is sufficiently accurate to represent P_3S_8 for a problem that does not require a highly accurate calculation in the preliminary/initial stage.

The fine-energy group effect investigation suggests that the fine-energy group structure calculation is necessary for reasonably accurate analysis of k_{eff}. Considering the magnitude of biases, it is not necessary to apply the fine-energy group calculation for reasonably accurate analysis of β_{eff}, $\Delta\rho_{\text{void}}$ and $\Delta\rho_{\text{Doppler}}$.

A comprehensive investigation of the above-mentioned effects while applying diverse methodologies may be useful in choosing an appropriate methodology for work with a different purpose.

More importantly, the feature of the SP_3 method on fast reactor analysis is discussed through comparing with the diffusion and transport solvers. Therefore, the novelty of the work in this chapter is that various methods differ from the calculation theory (whole-core calculation step), the dimension of lattice model (lattice calculation step), the burnup chain model, and the library. These four aspects are comprehensively compared in the field of fast reactors. It is noteworthy that a series calculation methods based on the SP_3 theory is used for fast reactor analysis in this chapter. Utilization of the SP_3 theory in fast reactors analysis is limited in the past. People have started to use the SP_3 theory in fast reactor analysis very recently. Therefore, the accumulated data is insufficient, and the work summarized in this chapter fills the blank from the point of view of application.

Future work on the FRBurner module includes implementing the capability for

three-dimensional core calculations, generating libraries based on recent libraries such as JENDL-5.0 [33], ENDF/B-VIII.0 [34], and JEFF-3.3 [35], and implementing the advanced leakage theory [36].

Chapter 3

A New Method for Reactivity Calculation

3.1 Introduction

The Simplified-P_N (SP_N) theory was initially proposed by Gelbard [31] in 1960. As concluded by Larsen [32], although a solid theoretical basis was not constructed in the very beginning, the SP_N theory was proven effective through applications. The SP_N theory can be regarded as an intermediate point between the transport theory and the diffusion theory. From the perspective of practice, the SP_3 method has an obvious advantage since it could give more accurate results than the diffusion method does and with less computation burden than methods based on the transport theory, such as the spherical harmonic (P_N) method, the discrete ordinates (S_N) method, and the method of characteristic. In the following decades, theoretical basis of SP_N was gradually filled, and the field of the SP_3 utilization has been expanded to analyzing radioactive cooling process of glass, crystal growth, photon radiative transfer

in biological tissues, plasma spectroscopy, etc. [16]. Recently, a new and rigorous SP_N theory with rigorous interface and boundary conditions was built by Chao [37] in 2016. However, the conventional SP_N theory is still attractive to the nuclear energy research community from the perspective of engineering practice. The research themes vary from GPU acceleration for reactor physics analysis [38] [39], pin-wise homogenization treatment [40], variance reduction [41] and so on.

The perturbation theory, which origins from the quantum science, was developed to evaluate the impact of perturbation (small disturbances) on systems. In the field of reactor engineering, there is great concern about the impact of perturbations on a reactor system. Therefore, the perturbation theory has been widely used in reactor reactivity analyses. We all know that the reactivity can be calculated using two effective neutron multiplication factor (k_{eff}) values before and after the perturbation, and this is known as *direct calculation*. This way, however, cannot reveal the nature of reactivity, i.e., the causes of reactivity. On the contrary, through the perturbation theory we could acknowledge how much reactivity is contributed by each of the different physical quantities. In the field of fast spectrum reactor analysis, the reactivity can be categorized into different components: yield, absorption, scattering, and leakage components. The sum of yield, absorption, and scattering components is referred to as the non-leakage component. Component-wise reactivity information is crucial for fast reactor analysis due to the physical processes that it can reveal.

In this chapter, a novel SP_3-Perturbation (SP_3P) method is developed for fast reactor reactivity analysis based on the SP_3 and perturbation theories. A physical meaning unclear term is discussed since it brings difficulty on its reactivity categorization. This difficulty is solved through using the perturbation equations under the P_3 theory. The P_3-Perturbation equations (P_3P) suggest that the physical meaning unclear

term in the SP_3P equations comes from math manipulation. The author innovatively uses a form-changed SP_3 equations set which is different from the widely used form to give the perturbation expression under the SP_3 theory. To distinguish these two SP_3P methods, they are named as SP_3P and Original-SP_3-Perturbation (OSP_3P) methods, respectively. The word *original* represents the SP_3 equations which are not manipulated to form diffusion-like equations. The method of OSP_3P can be regarded as a second version of SP_3P actually. Then, both methods are implemented into CBZ, which is a general-purpose deterministic reactor physics analysis code system. The verification of the new method is carried out with an OECD/NEA fast reactor benchmark [18] used in the preceding chapter.

3.2 Theory and implementation

3.2.1 Perturbation theory and component-wise reactivity

Reactivity (coefficient) calculation is a crucial part of work for reactor physics analysis from the perspective of reactor transient safety and control. There is a need of decomposing the reactivity to acknowledge the inside physical processes. A classical way is using the perturbation theory to conduct reactivity calculation. Therefore, the perturbation theory and reactivity categorization are introduced in this section at first.

The discretized neutron transport equation (and its approximation form) can be expressed into a matrix form,

$$\boldsymbol{A}\phi = \frac{1}{k_{\text{eff}}}\boldsymbol{F}\phi, \tag{3.1}$$

in which

$\boldsymbol{A}$: operator for neutron loss,

$\boldsymbol{F}$: operator for neutron generation by fission reaction, and

ϕ : vector representing neutron flux.

The adjoint neutron transport equations can be obtained through transposing the operators simply. The perturbation theory requires the adjoint matrix $\boldsymbol{A}^{\dagger}$ (which could also be written as $\boldsymbol{A}^{H}$ or $\boldsymbol{A}^{*}$, representing the Hermite transform), and it is the conjugate transposition matrix of $\boldsymbol{A}$ in actuality. The conjugate transposition matrix of $\boldsymbol{A}$ is identical to its transposition matrix $\boldsymbol{A}^{T}$ in reactor physics calculations since all parameters are real numbers.

The reactivity $\Delta\rho$ can be calculated with the following equation according to the perturbation theory,

$$\Delta\rho = \frac{\frac{1}{k}\left\langle \phi^{\dagger}, \Delta\boldsymbol{F}\phi' \right\rangle - \left\langle \phi^{\dagger}, \Delta\boldsymbol{A}\phi' \right\rangle}{\left\langle \phi^{\dagger}, \boldsymbol{F}'\phi' \right\rangle}, \tag{3.2}$$

in which

ϕ' : neutron flux after perturbation,

$\phi^{\dagger}$: adjoint neutron flux,

$\langle , \rangle$: integrating for all phase space,

$\Delta\boldsymbol{F}, \Delta\boldsymbol{A}$: changing on operators A and F after the perturbation, and

$\boldsymbol{A}'$,$\boldsymbol{F}'$: operators A and F after the perturbation.

Typically, the reactivity can be decomposed into four parts: yield, absorption, scattering, and leakage components, in which the sum of yield, absorption, and scattering components is regarded as a non-leakage component. This categorization is general for reactivity analysis. Given that the problem under study is the coolant (sodium) loss reactivity in fast spectrum reactors, another categorization

that is specified for the fast reactor reactivity analysis is introduced here. Four phenomena [42] contribute to the overall sodium void reactivity; they are (1) spectral hardening, (2) increased leakage, (3) elimination of sodium capture, and (4) change in self-shielding. They can be a categorization of the sodium void reactivity. The correspondence between these two categorization ways will be explained as follows.

In the first categorization way, which is the general way, the $\nu\Sigma_f$-perturbation reactivity and the χ-perturbation reactivity are regarded as yield component; the Σ_a-perturbation reactivity is categorized as absorption component reactivity; the $\Sigma_{s,g\to g'}$-perturbation reactivity is categorized as scattering component; and the diffusion coefficient D-perturbation reactivity (in the case of theories with the diffusion approximation) is categorized as leakage component. Note that the notations here are classical.

Table 3.1 lists the general way of sodium void reactivity categorization with expression example in component-wise. The actual categorization corresponding to the SP_3P method in the section of numerical calculation result is slightly different from this table since there are two neutron fluxes and two adjoint neutron fluxes in the SP_3P equations. The ϕ^2 is the second-order Legendre expansion moment of angular neutron flux. Higher-order Legendre moments of angular fluxes are considered to be related to neutron leakage. Therefore, the reactivity described by both $\phi^{2\dagger}$ and ϕ^2 is categorized as leakage component in the present work.

Here, it is necessary to emphasize that there is a clear corresponding relationship between the two categorization ways mentioned above. The spectral hardening component is exactly the scattering component; the increased leakage component is the leakage component; the elimination of sodium capture and change in self-shielding components together are the absorption and yield components [42]. Out of the clear

Table 3.1: Information about reactivity categorization in present work.

Component	Causes	Expression example
Yield	$\nu\Sigma_f$ and χ	$\left\langle \phi^\dagger, \Delta\Sigma_f \phi' \right\rangle$
Absorption	Σ_a	$\left\langle \phi^\dagger, \Delta\Sigma_a \phi' \right\rangle$
Scattering	$\Sigma_{s,g\to g'}$	$\left\langle (\phi^\dagger_{g'} - \phi^\dagger_g), \Delta\Sigma_{s,g'\to g}\phi'_{g'} \right\rangle$
Leakage	Diffusion coefficient D (i.e., on flux gradient)	$\left\langle \nabla\phi^\dagger, \Delta D \nabla\phi' \right\rangle$

corresponding relationship, therefore, the general categorization way is accepted in the present work.

3.2.2 Derivation of SP$_3$-Perturbation (SPP) equation

This work starts with derivation of perturbation equations of the SP$_3$ theory. The SP$_3$ equations with isotropic scattering source can be expressed as below, according to the works of Larsen [32], Tatsumi and Yamamoto [43].

$$-D_g\nabla^2\left(\phi_g^0+2\phi_g^2\right)+\Sigma_{r,g}\left(\phi_g^0+2\phi_g^2\right)=\frac{\chi_g}{k_{\text{eff}}}\sum_{g'=1}^{G}\nu\Sigma_{f,g'}\phi_{g'}^0+\sum_{g'\neq g}^{G}\Sigma_{s,g'\to g}^0\phi_{g'}^0+2\Sigma_{r,g}\phi_g^2, \tag{3.3}$$

$$-\frac{27}{35}D_g\nabla^2\phi_g^2+\Sigma_{t,g}\phi_g^2=\frac{2}{5}\left\{\Sigma_{r,g}\phi_g^0-\left(\frac{\chi_g}{k_{\text{eff}}}\sum_{g'=1}^{G}\nu\Sigma_{f,g'}\phi_{g'}^0+\sum_{g'\neq g}^{G}\Sigma_{s,g'\to g}^0\phi_{g'}^0\right)\right\}, \tag{3.4}$$

where

D_g : diffusion coefficient of group g,

∇^2 : Laplace operator,

ϕ_g^l : neutron flux of the l-th order in group g,

$\Sigma_{r,g}$: removal cross-section in group g;

χ_g : neutron fission spectrum in group g,

$\Sigma^l_{s,g'\to g}$: the l-th order macroscopic scattering cross-section from group g' to g.

G : the number of energy groups.

Then, writing the SP_3 equations set into operator form and obtaining the adjoint SP_3 equations set,

$$-D_g\nabla^2\phi_g^{0\dagger}+\Sigma_{r,g}(\phi_g^{0\dagger}-\frac{2}{5}\phi_g^{2\dagger})-\sum_{g'\neq g}^{G}\left[\Sigma^0_{s,g\to g'}(\phi_{g'}^{0\dagger}-\frac{2}{5}\phi_{g'}^{2\dagger})\right]=\frac{1}{k}\nu\Sigma_{f,g}\sum_{g'=1}^{G}\chi_{g'}(\phi_{g'}^{0\dagger}-\frac{2}{5}\phi_{g'}^{2\dagger}), \tag{3.5}$$

$$-D_g\nabla^2(2\phi_g^{0\dagger}+\frac{27}{35}\phi_g^{2\dagger})+\Sigma_{t,g}\phi_g^{2\dagger}=0, \tag{3.6}$$

in which $\phi_g^{l\dagger}$ is l-th order adjoint neutron flux.

The adjoint neutron flux $\phi^\dagger$ is used as weighting in reactivity calculations. Splitting Eq. (3.2), and writing out the specific expression of $\langle\phi^\dagger,\Delta\boldsymbol{A}\phi'\rangle$ and $\langle\phi^\dagger,\Delta\boldsymbol{F}\phi'\rangle$, as shown with Eqs. (3.7) and (3.8). Although the math manipulation of $\langle,\rangle$ has been defined as integrating for all phase space, only energy group (one phase space) is assumed in these equations here for simplicity. Therefore, the integral for material zones (another phase space) is omitted in these equations. Please also note that assuming the fission spectrum χ is not affected by perturbation for simplification here. If taking the perturbation on χ into account, we can add $\Delta\chi_g$ term into Eq. (3.8).

$$\begin{aligned}\langle\phi^\dagger,\Delta A\phi\rangle=\sum_{g=1}^{G}\Bigg\{&\phi_g^{0\dagger}\left[(-\Delta D_g\nabla^2+\Delta\Sigma_{r,g})\phi_g^{'0}-2\Delta D_g\nabla^2\phi_g^{'2}-\sum_{g'\neq g}^{G}\Delta\Sigma^0_{s,g'\to g}\phi_{g'}^{'0}\right]\\&+\phi_g^{2\dagger}\left[-\frac{2}{5}\Delta\Sigma_{r,g}\phi_g^{'0}-(\frac{27}{35}\Delta D_g\nabla^2-\Delta\Sigma_{t,g})\phi_g^{'2}+\frac{2}{5}\sum_{g'\neq g}^{G}\Delta\Sigma^0_{s,g'\to g}\phi_{g'}^{'0}\right]\Bigg\},\end{aligned} \tag{3.7}$$

$$\langle\phi^\dagger,\Delta F\phi'\rangle=\sum_{g=1}^{G}\left(\phi_g^{0\dagger}\chi_g\sum_{g'=1}^{G}\Delta\nu\Sigma_{f,g'}\phi_{g'}^{'0}\right). \tag{3.8}$$

The form of Eq.(3.7) can be modified according to the definition of component-wise reactivity. Among them, the most important one is the scattering component reactivity since the expression for considering the removal cross-section is

$$\Sigma_{r,g} = \Sigma_{a,g} + \sum_{g' \neq g}^{G} \Delta\Sigma_{s,g\to g'} - \Sigma_{n2n,g}. \tag{3.9}$$

The scattering component reactivity in the SP_3P method can be expressed as Eq. (3.10) based on the general way of categorization,

$$\left\langle \phi^{\dagger}, \Delta A \phi' \right\rangle_{scat} = \sum_{g=1}^{G}\sum_{g'=1}^{G} (\phi_{g'}^{0\dagger} - \phi_{g}^{0\dagger})\Delta\Sigma_{s,g'\to g}^{0}\phi_{g'}^{\prime 0} - \frac{2}{5}\sum_{g=1}^{G} + \sum_{g'=1}^{G} (\phi_{g'}^{2\dagger} - \phi_{g}^{2\dagger})\Delta\Sigma_{s,g'\to g}^{0}\phi_{g'}^{\prime 0}. \tag{3.10}$$

It is notable that the physical meaning of the second term on the right-hand-side of Eq. (3.10), $\left\langle -\frac{2}{5}(\phi_{g'}^{2\dagger} - \phi_{g}^{2\dagger})\Delta\Sigma_{s,g'\to g}^{0}\phi_{g'}^{\prime 0} \right\rangle$, is not as clear as the first term. The reasons for clarifying the physical meaning are (a) that it helps us categorize the different components of reactivity, which is important from the viewpoint of safety design, and (b) that such information could help people on nuclear data sensitivity analysis research. The physical interpretation of $\phi^{2\dagger}$ is clear since ϕ^2 comes from the Legendre polynomials expansion of the angular neutron flux in the transport equation and $\phi^{2\dagger}$ represents the weight of ϕ^2. The higher-order Legendre expansion moment is considered to be related to neutron leakage, as mentioned previously. A straightforward interpretation about the physical meaning of this term is that $\phi^{2\dagger}$ is used as a weight function to evaluate the reactivity caused by perturbation on Σ_r. However, here comes a difficulty in categorizing this term.

From the perspective of angular neutron flux $\phi^{2\dagger}$, the $\left\langle -\frac{2}{5}(\phi_{g'}^{2\dagger} - \phi_{g}^{2\dagger})\Delta\Sigma_{s,g'\to g}\phi_{g'}^{\prime 0} \right\rangle$ term shall be categorized as the leakage component. According to the calculation result shown in Section 3.3, however, this term is reasonable to be considered as scattering component reactivity. This confusing fact leads us trace the source of this

part of reactivity through comparing to the P_3-perturbation equations. This part of work is summarized in the next section.

3.2.3 Derivation of OSP$_3$-Perturbation method

The SP_3P method is implemented in the CBZ code system. The numerical calculation result implies a fact that the $\left\langle -\frac{2}{5}(\phi_{g'}^{2\dagger} - \phi_g^{2\dagger})\Delta\Sigma_{s,g'\to g}\phi_{g'}^{\prime 0} \right\rangle$ term belongs to the scattering component since the result on the scattering component given by the SP_3P method is more accurate if this term is counted (*Table 3.2*). To give theoretical explanation, further investigation is carried out through using the P_N-perturbation since the SP_N theory origins from the P_N theory.

The P_3 equations set of a one-dimensional planar system is

$$\frac{d}{dx}\phi_g^1 + \Sigma_{r,g}\phi_g^0 - \sum_{g'\neq g}^{G}\Sigma_{s,g'\to g}^0\phi_{g'}^0 = \frac{\chi_g}{k_{\text{eff}}}\sum_{g'=1}^{G}\nu\Sigma_{f,g'}\phi_{g'}^0, \tag{3.11}$$

$$\frac{1}{3}\frac{d}{dx}\phi_g^0 + \frac{2}{3}\frac{d}{dx}\phi_g^2 + \Sigma_{t,g}\phi_g^1 - \sum_{g'=1}^{G}\Sigma_{s,g'\to g}^1\phi_{g'}^1 = 0, \tag{3.12}$$

$$\frac{2}{5}\frac{d}{dx}\phi_g^1 + \frac{3}{5}\frac{d}{dx}\phi_g^3 + \Sigma_{t,g}\phi_g^2 - \sum_{g'=1}^{G}\Sigma_{s,g'\to g}^2\phi_{g'}^2 = 0, \tag{3.13}$$

$$\frac{3}{7}\frac{d}{dx}\phi_g^2 + \Sigma_{t,g}\phi_g^3 - \sum_{g'=1}^{G}\Sigma_{s,g'\to g}^3\phi_{g'}^3 = 0. \tag{3.14}$$

In Gelbard's work [31], the SP_3 equations are derived through replacing the one-dimensional operator with multi-dimensional operator ∇. The subsequent derivations included in this dissertation will use the same expression to keep consistency. Besides, the higher-order scattering moment than the second-order is ignored generally, i.e., $\Sigma_s^l \approx 0, (l \geq 2)$. The higher-order scattering terms in Eqs. (3.13) and (3.14) are retained for consistency with the other equations. Then, introducing the widely used *out-scatter approximation* for the odd-order moment, which is used to get the

transport cross-section [44],

$$\sum_{g'=1}^{G} \Sigma^N_{s,g'\to g}\phi^N_{g'} \approx \sum_{g'=1}^{G} \Sigma^N_{s,g\to g'}\phi^N_{g}, (N = 1, 3, 5, ...), \tag{3.15}$$

and after straightforward derivation, a form-changed SP_3 equations set can be obtained as

$$-D_g\nabla^2(\phi^0_g + 2\phi^2_g) + \Sigma_{r,g}\phi^0_g - \sum_{g'\neq g}^{G} \Sigma^0_{s,g'\to g}\phi^0_{g'} = \frac{\chi_g}{k_{\text{eff}}} \sum_{g'=1}^{G} \nu\Sigma_{f,g'}\phi^0_{g'}, \tag{3.16}$$

$$-\frac{2}{5}D_g\nabla^2(\phi^0_g + 2\phi^2_g) - \frac{3}{5}D^3_g\nabla^2\phi^2_g + \Sigma_{t,g}\phi^2_g - \sum_{g'=1}^{G} \Sigma^2_{s,g'\to g}\phi^2_{g'} = 0. \tag{3.17}$$

in which

$$D_g = \frac{1}{3(\Sigma_{t,g} - \sum\limits_{g'=1}^{G} \Sigma^1_{s,g\to g'})}, \tag{3.18}$$

$$D^3_g = \frac{3}{7(\Sigma_{t,g} - \sum\limits_{g'=1}^{G} \Sigma^3_{s,g\to g'})}. \tag{3.19}$$

This form-changed SP_3 equations is named as original-SP_3 (OSP_3) equations since they are derived from the P_3 equations straightforwardly.

The expression of Eq.(3.19) is not as common as Eq.(3.18) which is the definition of the diffusion coefficient. Assuming the third-order Legendre coefficient of scattering cross-section is approximately equal to the first-order Legendre coefficient of scattering cross-section, which can be described by $\sum\limits_{g'=1}^{G} \Sigma^1_{s,g\to g'} = \sum\limits_{g'=1}^{G} \Sigma^3_{s,g\to g'}$, the following relation holds,

$$D^3_g = \frac{3\cdot 3}{7\cdot 3(\Sigma_{t,g} - \sum\limits_{g'=1}^{G} \Sigma^3_{s,g\to g'})} \approx \frac{9}{7}D_g.$$

Then, the OSP_3 equations can be written as the exactly same form as the SP_3 equations with assuming that $\sum\limits_{g'=1}^{G} \Sigma^2_{s,g'\to g}\phi^2_{g'} \approx 0$.

With the approximations mentioned above, Eqs. (3.16) and (3.17) are equivalent to Eqs. (3.3) and (3.4) completely. Their adjoint equations, however, are not equivalent. This means that although the neutron fluxes ϕ^0 and ϕ^2 described by SP_3 and OSP_3 are identical, their adjoint neutron fluxes, $\phi^{0\dagger}$ and $\phi^{2\dagger}$, are not identical. As described in Section 3.2.1, the adjoint equations are obtained through transposing the operators A and F. Equations (3.5) and (3.6) are adjoint equations for SP_3. For OSP_3, the adjoint equations are

$$-D_g^1\nabla^2\phi_g^{0\dagger}-\frac{2}{5}D_g^1\nabla^2\phi_g^{2\dagger}+\Sigma_{r,g}\phi_g^{0\dagger}-\sum_{g'\neq g}^{G}\Sigma_{s,g\to g'}^0\phi_{g'}^{0\dagger}=\frac{1}{k}\nu\Sigma_{f,g}\sum_{g'=1}^{G}\chi_{g'}\phi_{g'}^{0\dagger}, \tag{3.20}$$

$$-2D_g^1\nabla^2\left(\phi_g^{0\dagger}+\frac{2}{5}\phi_g^{2\dagger}\right)-\frac{3}{5}D_g^3\nabla^2\phi_g^{2\dagger}+\Sigma_{t,g}\phi_g^{2\dagger}-\sum_{g'\neq g}^{G}\Sigma_{s,g\to g'}^2\phi_{g'}^{2\dagger}=0. \tag{3.21}$$

Following the same derivation process, one can obtain the perturbation equations based on OSP_3 for reactivity calculation. The specific expression of the OSP_3-perturbation is shown here, in the same style as Eqs. (3.7) and (3.8),

$$\begin{aligned}\left\langle\phi^\dagger,\Delta A\phi'\right\rangle=\sum_{g=1}^{G}\Bigg\{&\phi_g^{0\dagger}\left[(-\Delta D_g\nabla^2+\Delta\Sigma_{r,g})\phi_g^{0'}-2\Delta D_g\nabla^2\phi_g^{2'}-\sum_{g'\neq g}^{G}\Delta\Sigma_{s,g'\to g}^0\phi_{g'}^{0'}\right]\\&+\phi_g^{2\dagger}\left[-\frac{2}{5}\Delta D_g\nabla^2\phi_g^{0'}+(\Delta\Sigma_{r,g}-\frac{4}{5}\Delta D_g\nabla^2-\frac{3}{5}\Delta D_g^3\nabla^2)\phi_g^{2'}\right]\Bigg\},\end{aligned} \tag{3.22}$$

$$\left\langle\phi^\dagger,\Delta F\phi'\right\rangle=\sum_{g=1}^{G}\left(\phi_g^{0\dagger}\chi_g\sum_{g'=1}^{G}\Delta\nu\Sigma_{f,g'}\phi_{g'}^{\prime 0}\right). \tag{3.23}$$

An important fact that can be observed from Eq.(3.22) is that there is no such $\left\langle(\phi_{g'}^{2\dagger}-\phi_g^{2\dagger}),\Delta\Sigma_{s,g'\to g}^0\phi_{g'}^0\right\rangle$ term. The scattering component reactivity in the OSP_3P method only has

$$\left\langle\phi^\dagger,\Delta A\phi'\right\rangle_{scat}=\sum_{g=1}^{G}\sum_{g'=1}^{G}(\phi_{g'}^{0\dagger}-\phi_g^{0\dagger})\Delta\Sigma_{s,g'\to g}^0\phi_{g'}^{\prime 0}. \tag{3.24}$$

This discovery indicates the physical meaning unclear term in the SP_3P method occurs due to math manipulation. Using OSP_3P can avoid the difficulty on categorizing reactivity since each term in OSP_3P implies certain physical meaning.

3.2.4 Implementation into the CBZ code system

The work to achieve the SP_3P and OSP_3P functions includes two parts,

(a) implementation of adjoint neutron flux $\phi^{\dagger}$ calculation functions, and

(b) implementation of perturbation calculation function according to the corresponding equations.

The first part of this work is to get the forward neutron flux, adjoint neutron flux, and eigenvalue. The forward neutron flux given by the SP_3 and OSP_3 equations are identical since these two equation sets are equivalent. Therefore, the SP_3 forward calculation function can be used for the OSP_3P calculation, and this means it is not necessary to implement the OSP_3 forward calculation function. The form of equations implemented into CBZ should be changed into diffusion-like form,

$$-D\nabla^2 f + \Sigma f = S.$$

This is because the diffusion-like form is a numerically solvable form, and the diffusion-like form equation can be implemented with an existing diffusion solver module. The diffusion-like form of the SP_3 forward equations set is

$$\begin{aligned} -D_g\nabla^2\left(\phi_g^0 + 2\phi_g^2\right) + &\Sigma_{r,g}\left(\phi_g^0 + 2\phi_g^2\right) = \\ &\frac{\chi_g}{k_{\text{eff}}}\sum_{g'=1}^{G}\nu\Sigma_{f,g'}\phi_{g'}^0 + \sum_{g'\neq g}^{G}\Sigma_{s,g'\to g}\phi_{g'}^0 + 2\Sigma_{r,g}\phi_g^2, \end{aligned} \tag{3.25}$$

$$-\frac{27}{35}D_g\nabla^2\phi_g^2+(\Sigma_{t,g}+\frac{4}{5}\Sigma_{r,g})\phi_g^2 = \frac{2}{5}\left\{\Sigma_{r,g}(\phi_g^0+2\phi_g^2)-\left(\frac{\chi_g}{k_{\text{eff}}}\sum_{g'=1}^{G}\nu\Sigma_{f,g'}\phi_{g'}^0+\sum_{g'\neq g}^{G}\Sigma_{s,g'\to g}\phi_{g'}^0\right)\right\}. \tag{3.26}$$

The diffusion-like form of the SP_3 adjoint equations set is

$$-D_g\nabla^2(\phi_g^{0\dagger}+\phi_g^{2\dagger})+\Sigma_{r,g}(\phi_g^{0\dagger}+\phi_g^{2\dagger}) = \frac{1}{k_{\text{eff}}}\nu\Sigma_{f,g}\sum_{g'=1}^{G}\chi_{g'}(\phi_{g'}^{0\dagger}+\phi_{g'}^{2\dagger})+\sum_{g'\neq g}^{G}\left[\Sigma_{s,g\to g'}(\phi_{g'}^{0\dagger}+\phi_{g'}^{2\dagger})\right]-2D_g\nabla^2\phi_g^{2\dagger}, \tag{3.27}$$

$$-\frac{27}{35}D_g\nabla^2(-\frac{28}{27}\phi_g^{0\dagger}+\phi_g^{2\dagger})+\Sigma_{t,g}\left(-\frac{28}{27}\phi_g^{0\dagger}+\phi_g^{2\dagger}\right)=-\frac{28}{27}\Sigma_{t,g}\phi_g^{0\dagger}. \tag{3.28}$$

The diffusion-like form of the OSP_3 adjoint equations set is

$$-D_g\nabla^2\left(\phi_g^{0\dagger}+\frac{2}{5}\phi_g^{2\dagger}\right)+\Sigma_{r,g}\left(\phi_g^{0\dagger}+\frac{2}{5}\phi_g^{2\dagger}\right) = \frac{1}{k_{\text{eff}}}\nu\Sigma_{f,g}\sum_{g'=1}^{G}\chi_{g'}\phi_{g'}^{0\dagger}+\sum_{g'\neq g}^{G}\Sigma_{s,g\to g'}^{0}\phi_{g'}^{0\dagger}+\frac{2}{5}\Sigma_{r,g}\phi_g^{2\dagger}, \tag{3.29}$$

$$-2D_g\nabla^2\left(\phi_g^{0\dagger}+\frac{7}{10}\phi_g^{2\dagger}\right)+\frac{10}{3}\Sigma_{t,g}\left(\phi_g^{0\dagger}+\frac{7}{10}\phi_g^{2\dagger}\right)=\frac{10}{3}\Sigma_{t,g}\left(\phi_g^{0\dagger}+\frac{2}{5}\phi_g^{2\dagger}\right). \tag{3.30}$$

After the calculation functions of these three coupled equation sets are implemented in CBZ, the perturbation reactivity calculation function is implemented separately for the yield, absorption, scattering, and leakage components, respectively. Due to the high similarity of the SP_3P and OSP_3P equations, the implementation of OSP_3P can be done with minor modifications based on the SP_3P method.

3.3 Numerical calculation and result analysis

3.3.1 Numerical calculation information

CBZ applies the classic *two-step method* in reactor physics calculation and multiple methodologies are available. The calculation methodology chosen for this work

is the two-dimensional lattice model (in the lattice calculation step) with a 70-group structure. The multi-group constant is generated by CBZ based on the JENDL-4.0 library. As for the whole-core calculation step, the core is modeled as a two-dimensional multi-layer cylinder. The perturbation setting (void patterns) for sodium void reactivity calculation is based on the assumption that (1) all sodium in the core is lost and (2) sodium in some regions is lost. The second void pattern is called the *local void pattern* in this work.

The result given by a transport solver (S_N method) in CBZ is regarded as a reference in the current work, and it is compared with the SP_3P and OSP_3P methods calculation in the next section.

Since the result given by perturbation calculation must be identical to the direct calculation result theoretically, it is necessary to compare the perturbation calculation result with the direct calculation result to confirm the validity. Reactivity evaluated by direct calculation is given by two k_{eff} values before and after the perturbation,

$$\Delta\rho = \frac{1}{k_{\text{eff}}} - \frac{1}{k'_{\text{eff}}}. \tag{3.31}$$

The reactivity value should be unique no matter what method is applied.

3.3.2 Whole-core void pattern

At first, the whole-core void pattern is discussed. This void pattern is also discussed in the benchmark [18]. All sodium in the core is voided (bond sodium insides fuel is kept). **Tables 3.2** to **3.5** exhibit the component-wise reactivity results given by S_NP, OSP_3P ,OSP_3P and diffusion-perturbation (DP) methods for the four reactors, respectively. The relative percent difference (RPD) of the results given by the OSP_3P,

SP_3P and DP methods comparing with the S_NP method result is also listed in these tables. The direct calculation results of the SP_3 and OSP_3 solvers in CBZ are included to prove the validity. For the S_NP method, the yield, absorption, scattering, non-leakage and leakage component reactivities, and net reactivity are shown in these tables. In particular, the scattering component is separated into two parts: $\phi^{0\dagger}$ and $\phi^{2\dagger}$ parts for the SP_3P method.

Table 3.2: Verification and comparison of OSP_3P and OSP_3P functions for reactivity calculation (unti: pcm), MET-1000.

	Yield	Absorp.	Scat.			Non-leak	Leak	Net	
S_NP	-14	221	3922			4129	-1812	2317	
	Yield	Absorp.	Scat.	$\phi^{0\dagger}$ Scat.	$\phi^{2\dagger}$ Scat.	Non-leak	Leak	Net	Direct
OSP_3P	-14	222	3922	3922	-	4129	-1734	2396	2395
SP_3P	-14	222	3922	3816	105	4129	-1734	2396	2395
DP	-14	222	3902	-	-	4111	-1843	2268	-
RPD_OSP_3P	-0.70%	0.29%	-0.01%			0.01%	-4.33%	3.40%	
RPD_SP_3P	-0.70%	0.29%	-0.01%			0.01%	-4.33%	3.40%	
RPD_DP	1.89%	0.53%	-0.49%			-0.45%	1.68%	-2.11%	

* Net value and direct calculation result for OSP_3P/SP_3P method are 2395.6 and 2395.3, respectively.

Firstly, we could confirm that the development of SP_3P and OSP_3P are successful since the direct calculation results are exactly identical to the perturbation calculation in all four reactors calculation. The validity of SP_3P and OSP_3P calculation function in CBZ can be proved.

Secondly, the sum of $\phi^{0\dagger}$-scattering and $\phi^{2\dagger}$-scattering components given by the

Table 3.3: Verification and comparison of OSP_3P and OSP_3P functions for reactivity calculation (unti: pcm), MOX-1000.

	Yield	Absorp.	Scat.			Non-leak	Leak	Net	
S_NP	-25	434	2970			3380	-1215	2165	
	Yield	Absorp.	Scat.	$\phi^{0\dagger}$ Scat.	$\phi^{2\dagger}$ Scat.	Non-leak	Leak	Net	Direct
OSP_3P	-25	440	2965	2965	-	3381	-1166	2215	2215
SP_3P	-25	440	2965	2907	58	3381	-1166	2215	2215
DP	-25	441	2954	-	-	3370	-1214	2156	-
RPD_OSP_3P	0.04%	1.25%	-0.15%			0.03%	-4.08%	2.34%	
RPD_SP_3P	0.04%	1.25%	-0.15%			0.03%	-4.08%	2.34%	
RPD_DP	1.58%	1.47%	-0.54%			-0.30%	-0.08%	-0.42%	

Table 3.4: Verification and comparison of OSP_3P and OSP_3P functions for reactivity calculation (unti: pcm), MOX-3600.

	Yield	Absorp.	Scat.			Non-leak	Leak	Net	
S_NP	-19	439	2441			2861	-662	2199	
	Yield	Absorp.	Scat.	$\phi^{0\dagger}$ Scat.	$\phi^{2\dagger}$ Scat.	Non-leak	Leak	Net	Direct
OSP_3P	-19	445	2435	2435	-	2861	-626	2235	2235
SP_3P	-19	445	2435	2399	36	2861	-626	2235	2235
DP	-20	445	2428	-	-	2853	-646	2207	-
RPD_OSP_3P	-0.37%	1.33%	-0.25%			0.00%	-5.40%	1.62%	
RPD_SP_3P	-0.37%	1.33%	-0.25%			0.00%	-5.40%	1.62%	
RPD_DP	4.71%	1.40%	-0.55%			-0.29%	-2.43%	0.36%	

Table 3.5: Verification and comparison of OSP_3P and OSP_3P functions for reactivity calculation (unti: pcm), CAR-3600.

	Yield	Absorp	Scat			Non-leak	Leak	Net	
S_NP	-21	499	2867			3345	-871	2473	
	Yield	Absorp	Scatt	$\phi^{0\dagger}$ Scat	$\phi^{2\dagger}$ Scat	Non-leak	Leak	Net	Direct
OSP3	-21	509	2855	2855	-	3343	-831	2513	2513
SP3	-21	509	2855	2807	48	3343	-831	2513	2513
Diffusion	-21	510	2849	-	-	3338	-858	2481	-
RPD_OSP3	0.96%	2.10%	-0.40%			-0.03%	-4.63%	1.59%	
RPD_SP3	0.96%	2.10%	-0.40%			-0.03%	-4.63%	1.59%	
RPD_Di	1.31%	2.30%	-0.60%			-0.18%	-1.55%	0.30%	

SP_3P method equal to the $\phi^{0\dagger}$-scattering component reactivity given by the OSP_3P method. This suggests that reactivity defined by the physical meaning unclear term belongs to scattering-component reactivity. This term can be eliminated by mathematical manipulation. So that the OSP_3P method is better than the SP_3P method from the perspective of physical interpretation.

Thirdly, there is slight advantage of the SP_3P/OSP_3P method with Tables 3.2 to 3.5. These two methods show more accurate non-leakage component calculation capability than the DP method. Besides, the computing time is significantly reduced comparing to the S_NP method. These results demonstrate the advantages of using SP_3 to calculate reactivity because this new method could provide more accurate results with shorter computing time. Additionally, the advantage of the new methods is more obvious in the middle-sized cores. The biases on non-leakage component reactivity in middle-sized core calculations are less than those in the large-sized

cores. Due to the core size, the middle-sized core has stronger neutron leakage. Furthermore, the difference on biases between SP_3P/OSP_3P and DP methods in the MET-1000 problem calculation is larger than that in the MOX-1000 problem. This is because MET-1000 applies metallic fuel, so the MET-1000 core has a harder neutron spectrum than the MOX-1000 core (also harder than two large-sized cores).

The advantage of the SP_3P method can be further exhibited through the spatial mesh-wise reactivity error distribution by taking the MET-1000 and MOX-1000 reactors as examples. The prediction errors on sodium void reactivity of SP_3P and diffusion-perturbation methods in every media of fuel region (**Figure 3.4** shows how a reactor core is modeled with FRBurner and indicates the core layout pf MET-1000) are shown in **Figures 3.1**, **3.2**, and **3.3**.

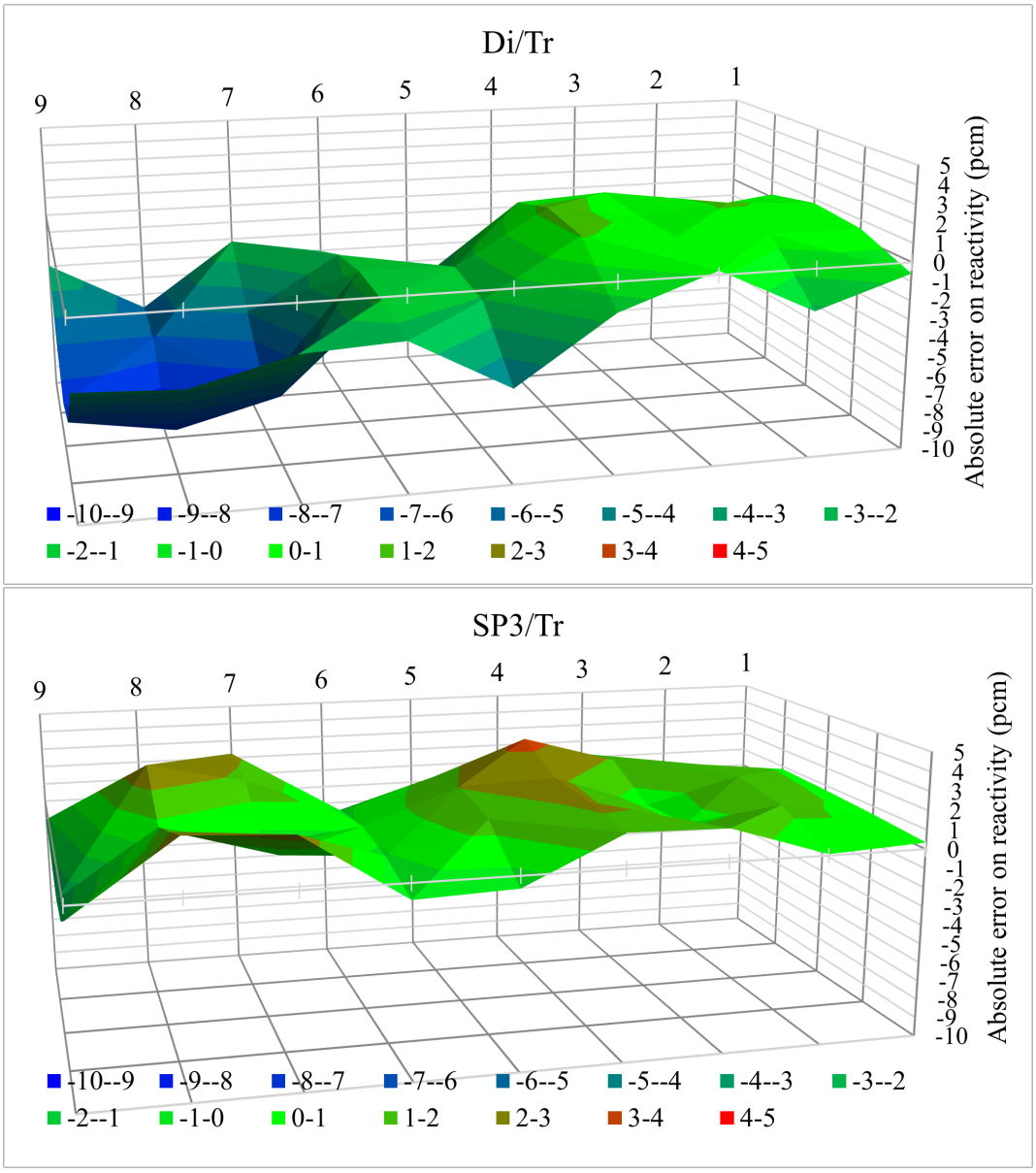

Figure 3.1: Error on cell wise net sodium void reactivity, MET-1000.

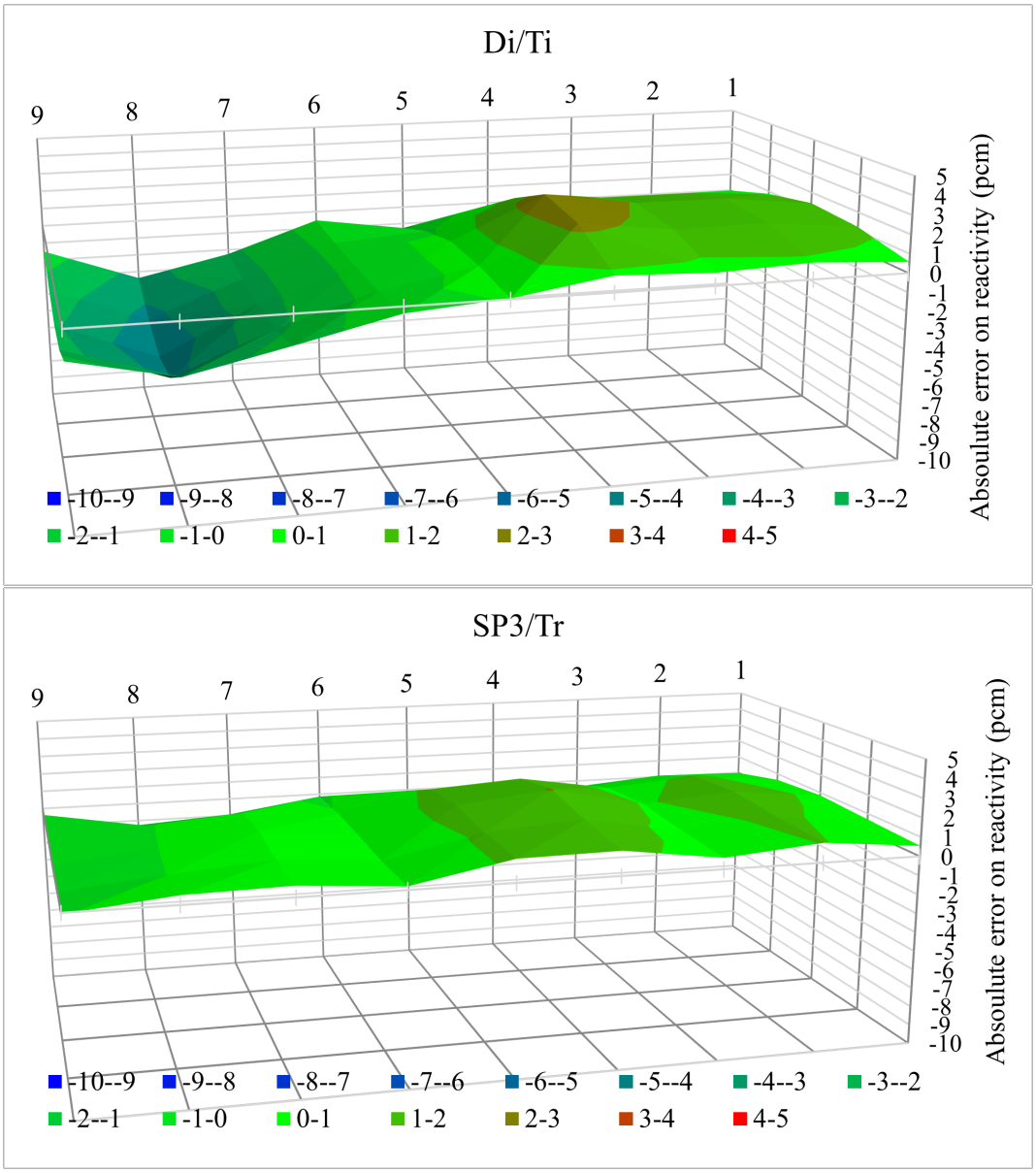

Figure 3.2: Error on cell wise scattering component sodium void reactivity, MET-1000.

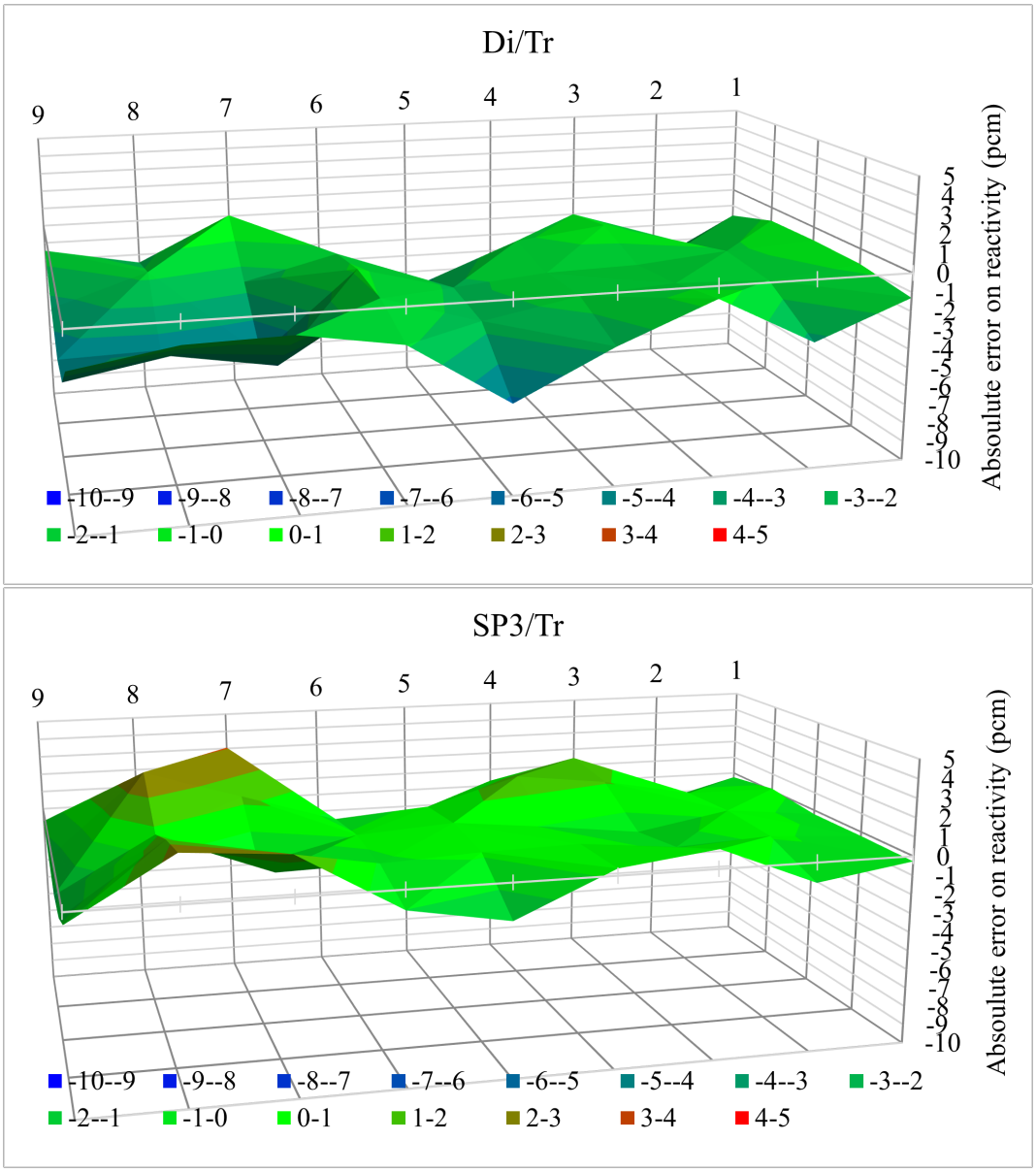

Figure 3.3: Error on cell wise leakage component sodium void reactivity, MET-1000.

The advantage of the SP_3P method on net and scattering component reactivities is obvious. As for the leakage component reactivity prediction, the SP_3P method does not exhibit clear advantage.

At present, the SP_3P and OSP_3P methods underestimate the leakage component reactivity by about $4\sim 5\%$, which makes the net reactivity overestimated. One possible reason for this underestimation on leakage component reactivity may relate to the treatment of interface and boundary conditions. The current SP_3P/OSP_3P method is developed based on the conventional SP_3 theory which was built up with ad-hoc interface and boundary conditions. Very recently, the interface and boundary conditions have been systematically discussed by Y. Chao [37] in the rigorous SP_N theory. Chao's work finally yields to the Generalized SP_N theory ($GSP_N^{(K)}$). Although the author wants to implement the rigorous SP_N into CBZ, the difficulty on numerical solution [45] and code implementation made the author postponed this idea as a future plan.

3.3.3 Local void pattern

The problem brought by the physical meaning unclear term and verification of the new methods have been discussed in the last section. Then, applicable scenarios of the new methods are going to be discussed with a local void pattern problem.

As introduced at the beginning of Section 3.1, the reactor is modeled as a two-dimensional multi-layer cylinder in FRBurner. **Figure 3.4** depicts how MET-1000 reactor is modeled in FRBurner as an example. The y-direction is axial direction, and the x-direction is radial direction. The width of each layer is calculated from the number of assemblies of each layer. Medium information corresponding to each region with number are listed in the right of the figure. Each layer consists of eleven

media, and five of them are fuel mediums for fuel layers (fuel assemblies). The local void pattern which is going to be discussed contains three cases: (1) the first plate (all fuel regions locate at the same position in z-axis together are regarded as a plate) is voided, (2) the third plate is voided, and (3) the axial-center region is voided. Since it is known that SP_3P gives exactly the same result as OSP_3P, only the result of OSP_3P will be discussed in this section.

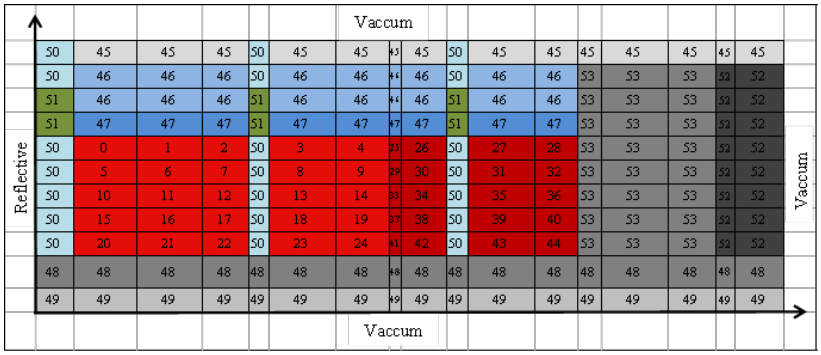

Number	Medium
0∼24	Inner core
25∼44	Outer core
45	Upper structure
46	Gas plenum
47	Replace sodium
48	Lower reflector
49	Lower structure
50	Empty duct
51	Control absorber
52	Shield rod
53	Radial reflector

Figure 3.4: Multi-layer cylinder model of MET-1000.

Figure 3.5 can represent the model of the core if further simplifying the schematic. The colored part represents voided region, therefore, coolant void in (a) the regions $0 \sim 4$ and 25∼28 are regarded as the first plate void pattern, (b) the regions $10 \sim 14$ and $33 \sim 36$ are regarded as the third plate void pattern, and (c) the regions 0, 5, 10, 15, and 20 are regarded as axial-center void pattern. The dominant neutron leakage for these three void patterns is quite different since the gradient of neutron flux in

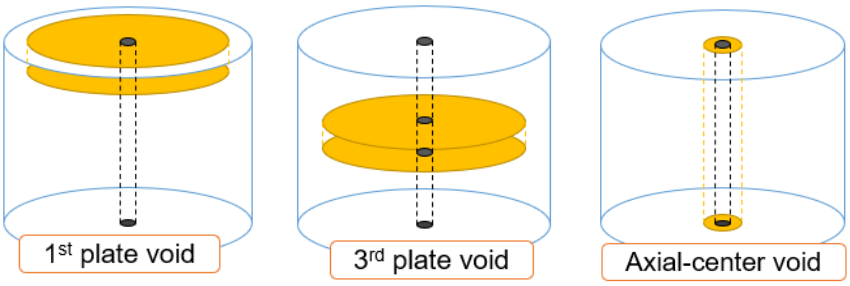

Figure 3.5: Local void pattern schema.

these voided regions is different. In the first-plate void pattern case, neutron leakage in axial- and radial-directions both are dominant. In the third-plate void pattern, the axial-direction neutron leakage is suppressed. In the axial-center void pattern, the axial-direction neutron leakage must be the dominant component. Therefore, we can investigate for which void pattern the OSP_3P method is more advantageous through these local void pattern problems, which have different dominant leakage component.

The net, scattering, and leakage component reactivity given by the OSP_3P and DP methods are compared to the results given by the S_NP method. The comparisons are summarized into **Figures 3.6** to **3.8**, and the corresponding data are summarized into **Tables 3.6 to 3.8**.

Table 3.6: Net reactivity perturbation calculation of local void pattern. [unit: pcm]

	1^{st}-void			3^{rd}-void			Axial-void		
	OSP_3P	DP	S_NP	OSP_3P	DP	S_NP	OSP_3P	DP	S_NP
MET-1000	-78.7	-89.8	-106.1	910.8	883.4	907.8	165.9	163.2	164.8
MOX-1000	-26.6	-40.3	-33.3	842.0	828.1	841.3	141.1	140.9	139.8
MOX-3600	89.5	81.8	76.7	785.1	778.9	789.2	58.4	57.5	57.0
CAR-3600	99.1	89.3	85.1	884.7	877.5	888.2	5.9	5.9	6.0

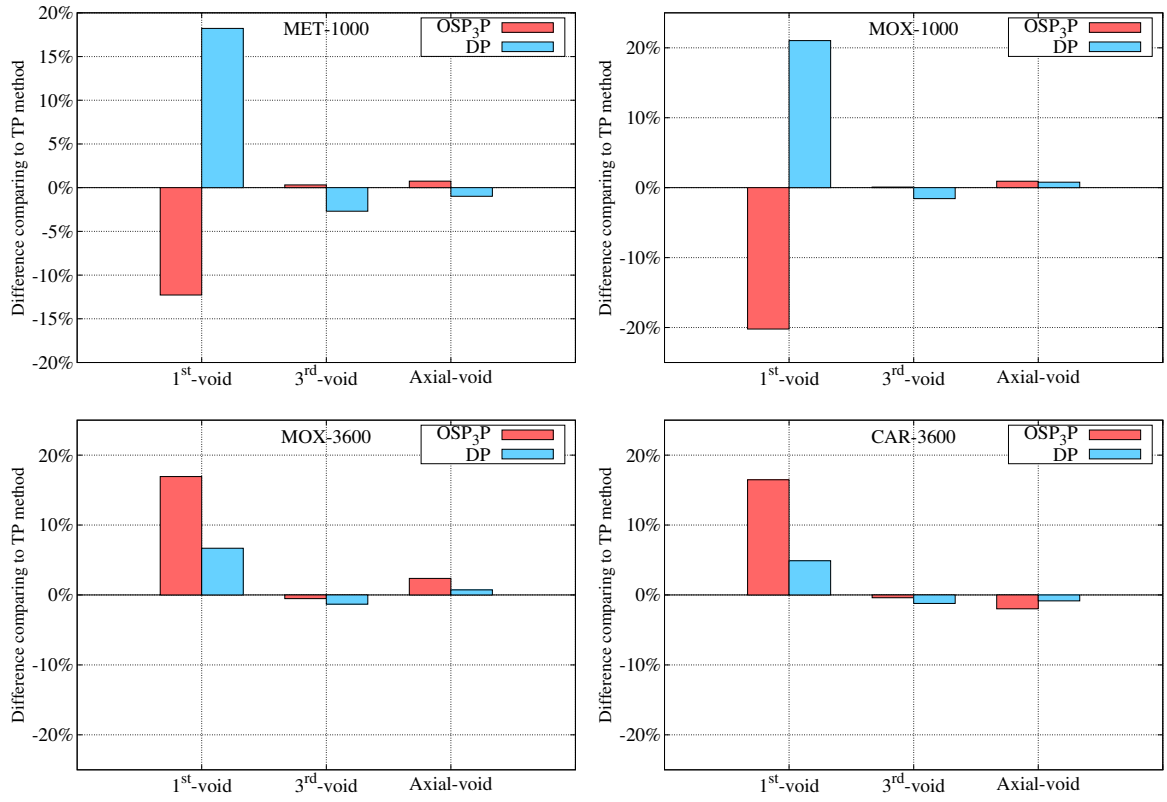

Figure 3.6: Net reactivity perturbation calculation of local void pattern.

Firstly, it seems that the SP_3P (OSP_3P as well) method does not show any advantage on the net reactivity calculation (Figure 3.6). This is caused, however, by error cancellation with the DP method. The symbols of non-leakage and leakage component reactivities are opposite. Therefore, there is error cancellation on net reactivity calculation, and this is one aspect of why reactivity decomposition is needed. Naturally, the component-wise reactivity calculation should be paid more attention to.

Secondly, the following points can be summarized.

1. The SP_3P method shows advantage on the scattering and leakage component reactivity calculations overall. This point can be explained with the characteristic of these two components of reactivity.

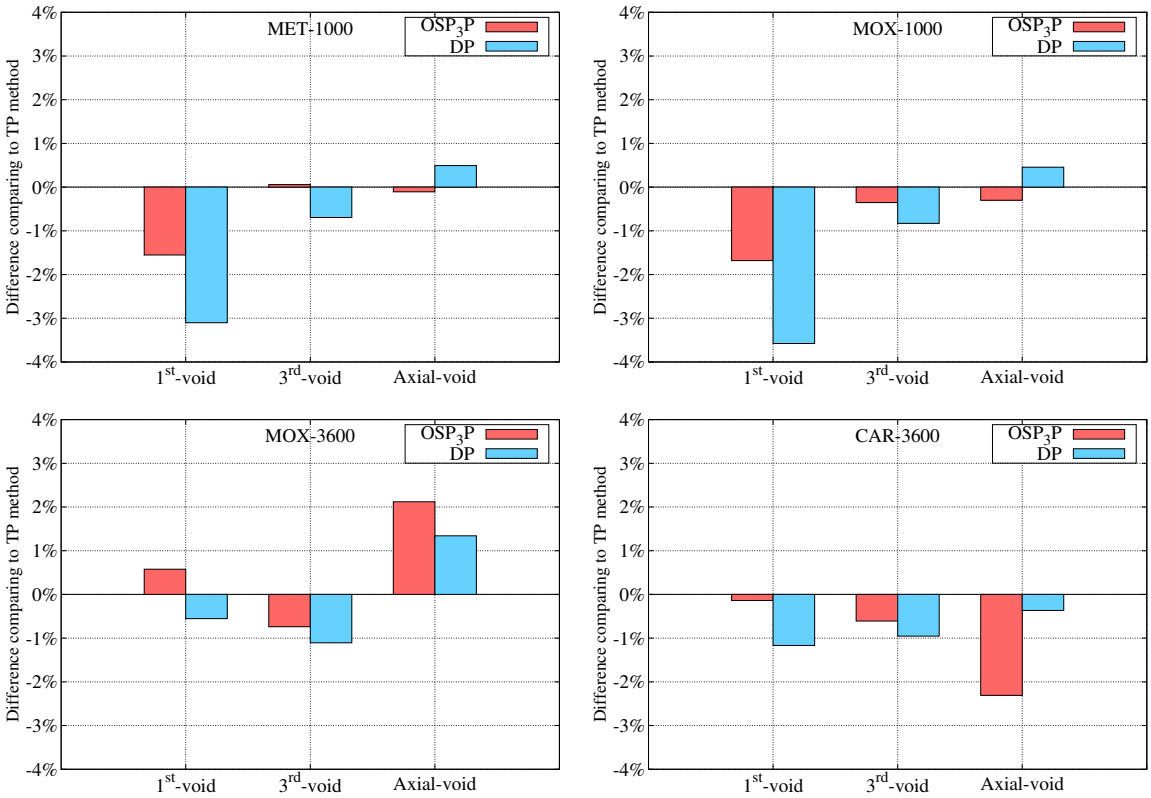

Figure 3.7: Scattering component reactivity perturbation calculation of local void pattern.

Table 3.7: Scattering component reactivity perturbation calculation of local void pattern. [unit: pcm]

	1st-void			3rd-void			Axial-void		
	OSP_3P	DP	S_NP	OSP_3P	DP	S_NP	OSP_3P	DP	S_NP
MET-1000	396.4	390.2	402.7	1052.1	1044.2	1051.5	212.7	214.0	213.0
MOX-1000	242.1	237.5	246.3	884.0	879.7	887.1	152.8	154.0	153.3
MOX-3600	240.1	237.4	238.7	722.1	719.4	727.5	59.8	59.3	58.6
CAR-3600	296.8	293.8	297.2	830.0	827.1	835.1	6.1	6.2	6.2

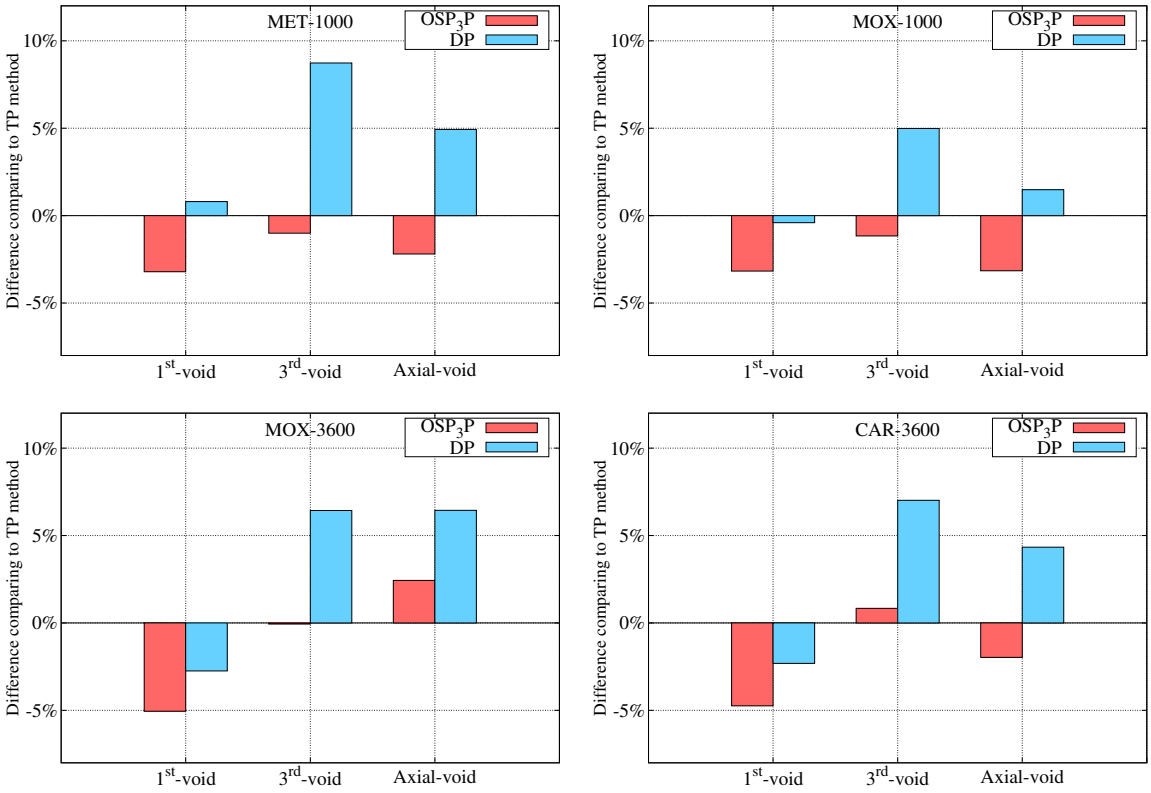

Figure 3.8: Leakage component reactivity perturbation calculation of local void pattern problem.

Table 3.8: Leakage component reactivity perturbation calculation of local void pattern problem. [unit: pcm]

	1st-void			3rd-void			Axial-void		
	OSP_3P	DP	S_NP	OSP_3P	DP	S_NP	OSP_3P	DP	S_NP
MET-1000	-497.9	-518.5	-514.4	-200.2	-219.9	-202.3	-59.6	-64.0	-61.0
MOX-1000	-299.6	-308.1	-309.4	-160.8	-170.8	-162.7	-34.7	-36.4	-35.9
MOX-3600	-190.5	-195.1	-200.6	-52.3	-55.7	-52.3	-12.1	-12.6	-11.8
CAR-3600	-247.2	-253.5	-259.5	-76.4	-81.1	-75.8	-1.2	-1.3	-1.3

2. About the scattering component, it is defined with both forward and adjoint neutron fluxes. The peak of both fluxes is in the center of reactor. Consequently, the third-plate void pattern has the largest scattering component reactivity. Although scattering component reactivity has no direct relationship with the neutron flux gradient, the correlation between them can be revealed through comparing the first- and third-plate void patterns. There are two reasons which make a larger neutron flux gradient for the first plate, one is the proximity to the edge, and the other is the presence of strong neutron absorber.

3. As for the leakage component, it is defined with the changes on diffusion coefficient and the gradient of neutron flux. Comparing the first- and third-plate void patterns, the SP_3P method predicts the leakage component reactivity well for the regions in which the neutron leakage is not obvious.

4. On the whole, the biases of new method results are less than that of DP method result.

It is necessary to point out that the center assemblies of the MET-1000, MOX-1000, MOX-3600, and CAR-3600 cores are the secondary control assembly, the secondary control assembly, the center reflector, and the fuel assembly, respectively. For the secondary control assembly, the control absorber material is located beyond the active fuel region, as shown in the benchmark report [18]. This is the reason that the axial-center void pattern calculation behaves quite differently on the MOX-3600 and CAR-3600 cores.

Thirdly, the energy wise reactivity information would be helpful. Regarding the discussion above, only the scattering and leakage component reactivities of MET-1000 calculation are summarized into **Figure 3.9**. The Figures 3.9 (a), (c), (e) are

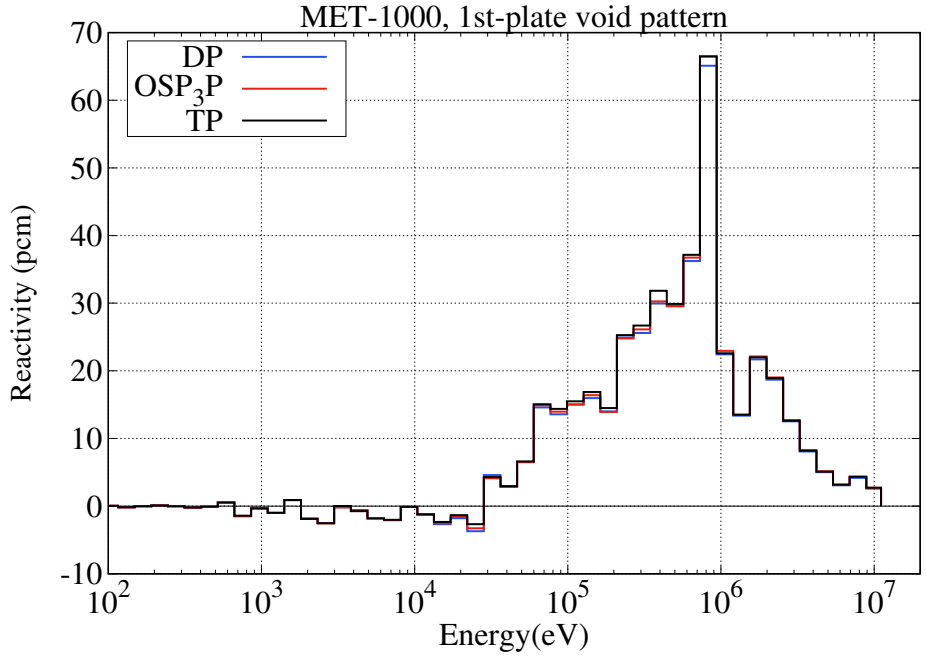

(a) Scattering component void reactivity.

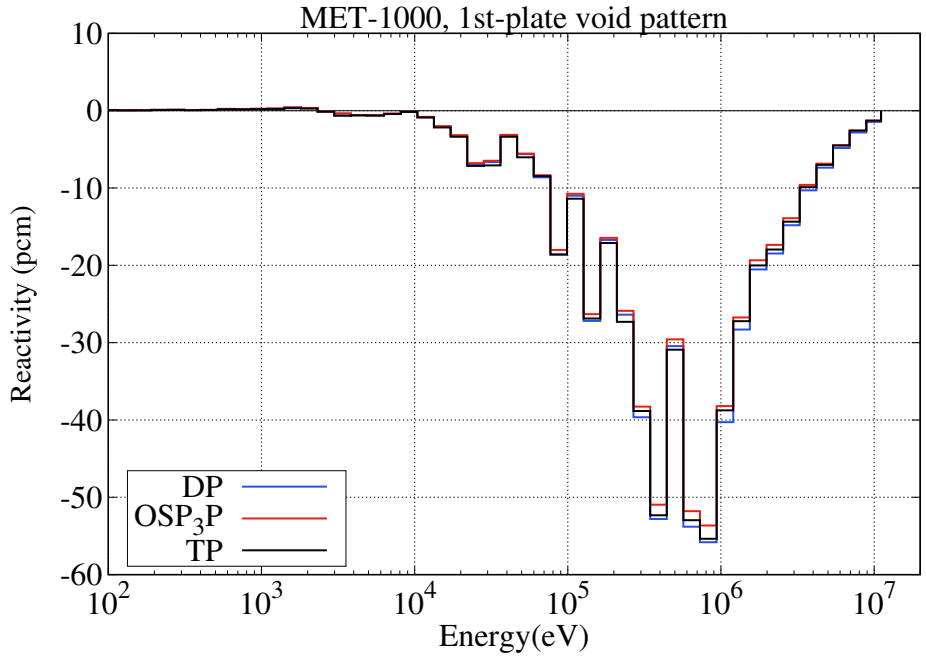

(b) Leakage component void reactivity.

Figure 3.9: MET-1000 core local void pattern energy-wise reactivity comparison.

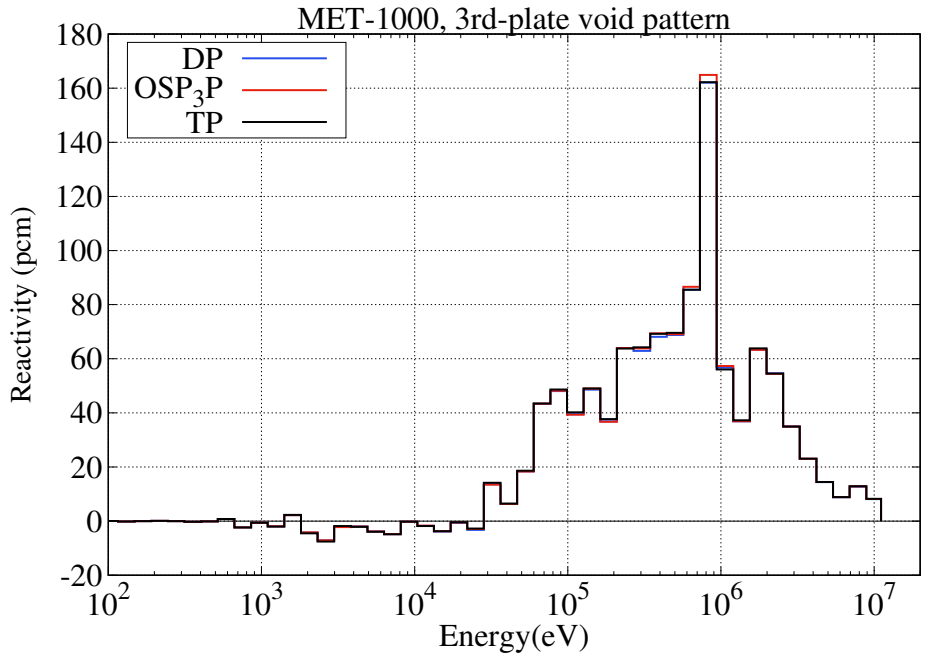

(c) Scattering component void reactivity.

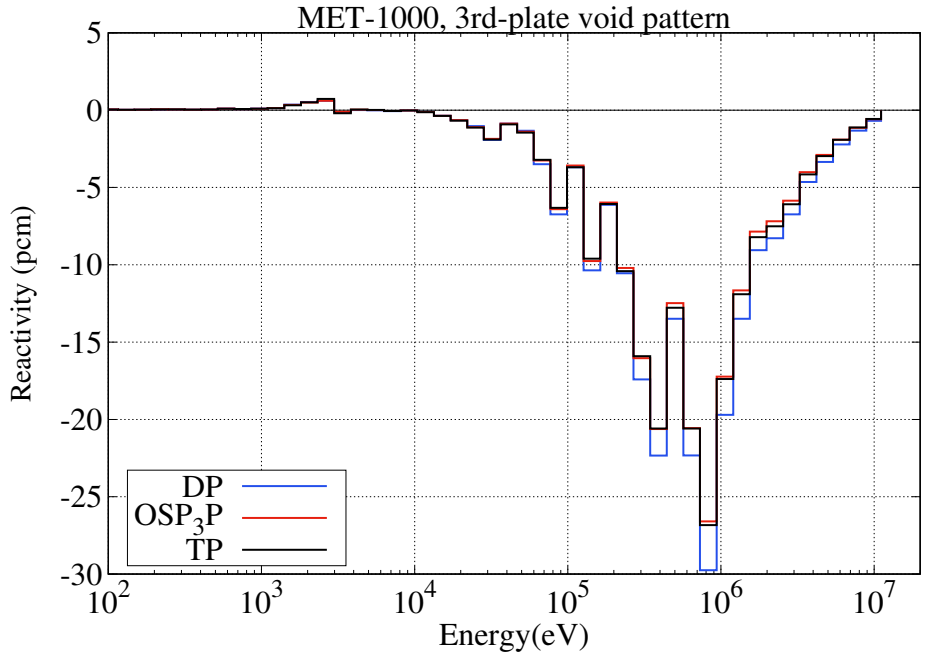

(d) Leakage component void reactivity.

Figure 3.9: (Cont.) MET-1000 core local void pattern energy-wise reactivity comparison.

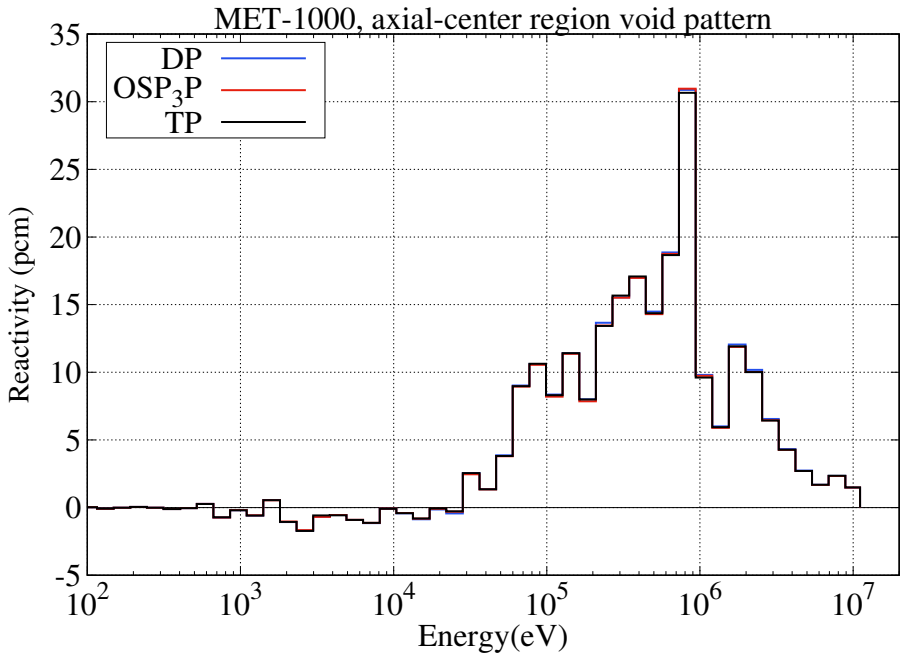

(e) Scattering component void reactivity.

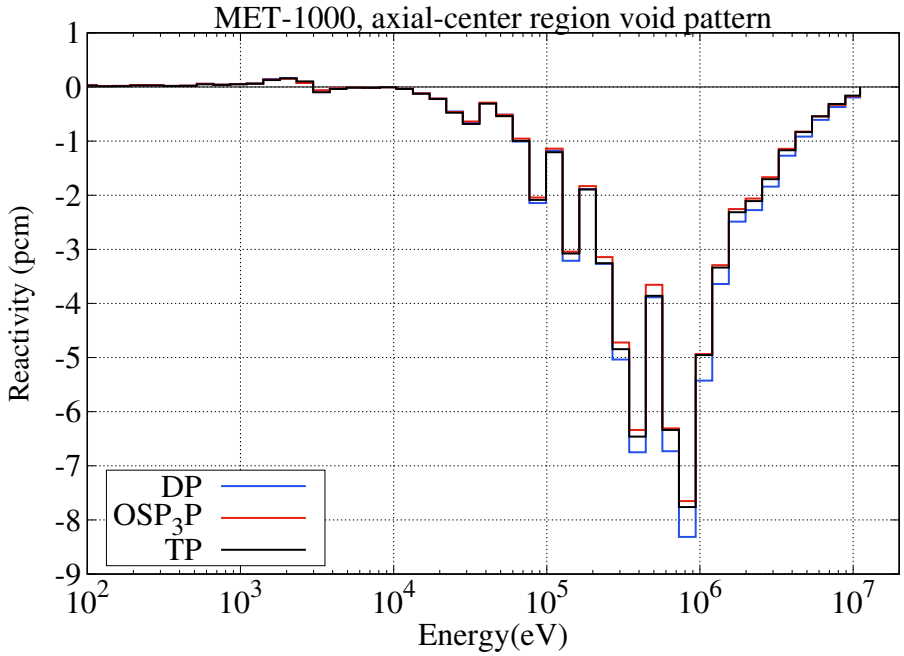

(f) Leakage component void reactivity.

Figure 3.9: (Cont.) MET-1000 core local void pattern energy-wise reactivity comparison.

scattering component reactivity and Figures 3.9 (b), (d), (f) are leakage component reactivity. It is notable that the DP method results display a relatively large bias on leakage component reactivity calculation for the third-plate void and axial-center region void patterns, while the OSP_3P method can give more accurate results on the whole. For the scattering component reactivity, we can refer to a partial enlargement figure (**Figure 3.10**) for a clear view. The enlarged energy range is 10^5 eV to 10^6 eV since the reactivity in this energy range is higher than other ranges. Although the bias of on each energy group is small, we can still say that the OSP_3P method gives more accurate result on the scattering component reactivity in general. Especially when the difference on bias for each energy group is summed together, the total difference is not negligible (**Figure 3.7**). Despite the magnitude of leakage compo-

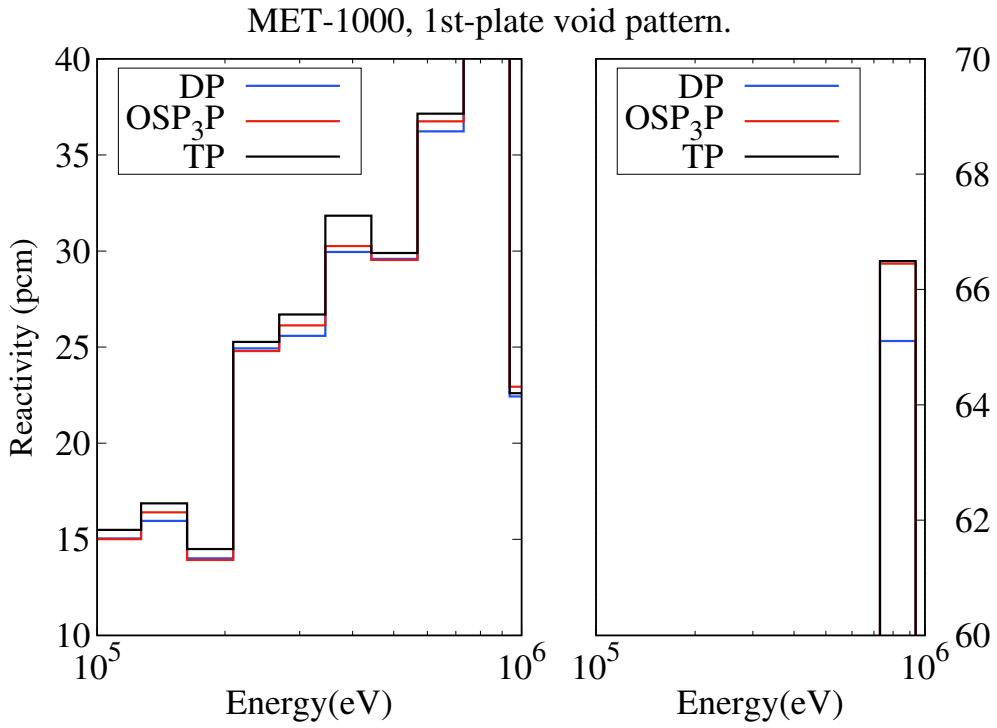

Figure 3.10: Partial enlargement of energy-wise scattering component reactivity, first-plate void case.

nent reactivity itself is not large, Figure 3.9 still presents the advantage of the OSP_3P

method on the scattering and leakage component reactivity calculation. Meanwhile, the results displayed in the previous section reveal that the bias on leakage component reactivity of the DP method is less than that of the SP_3P method, which is opposite to the results shown in this section. This opposite point is because the void pattern of calculations in these two sections are different. The whole core void pattern leads to more significant neutron leakage. The local void pattern calculation results suggest that the neutron leakage of voided region affects the OSP_3P methods significantly. For scattering component reactivity, the OSP_3P method shows advantage when neutron leakage is obvious. For leakage component reactivity, the OSP_3P method shows advantage when neutron leakage is not obvious.

Based on the calculations involved in the present work, the author concludes that the OSP_3P and OSP_3P methods show advantage on void reactivity calculation if the neutron leakage is significant.

3.4 Conclusion

A new method, SP_3P (OSP_3P), for fast reactor reactivity analysis based on the SP_3 and perturbation theories is proposed in this chapter. This new method is verified through comparing to direct calculation and transport (S_N) perturbation calculation with four fast reactor concepts which differ from each other in the fuel type and core size.

Firstly, the SP_3P results match the direct calculation results in all four fast reactor calculations, and this suggests the equations derivation is correct and the code implementation is successful. The biases of SP_3P results on non-leakage component reactivity calculation are 0.01%, 0.03%, 0.00% and -0.03%, respectively. Comparing to the biases of the DP method on non-leakage component, advantage of the SP_3P method is obvious. Then, the SP_3P method can substitute the DP method in fast reactor reactivity analysis, considering the computing time and calculation accuracy.

Secondly, the author solved the difficulty on categorizing the $\left\langle -\frac{2}{5}(\phi_{g'}^{2\dagger} - \phi_{g}^{2\dagger})\Delta\Sigma_{s,g'\to g}^{0}\phi_{g'}^{\prime 0} \right\rangle$ term through tracing the source of it. The sum of $\phi^{0\dagger}$-scattering and $\phi^{2\dagger}$-scattering components given by the SP_3P method equals to $\phi^{0\dagger}$-scattering component given by the OSP_3P method. This fact indicates that this innovative treatment solved the difficulty properly.

Thirdly, three different local void pattern problems are used to illustrate the advantage of the SP_3P method. Based on the calculation result with the designed void condition in the present work, the SP_3P method shows an advantage on scattering component reactivity prediction when the neutron leakage is relatively significant.

At the end of this research, considerations about potential future work are discussed here. Currently, there is no acceleration treatment for the SP_3 eigenvalue

calculation in CBZ, although the effect of acceleration is evaluated with diffusion solver with and without CMFD acceleration. The acceleration treatment on the SP_3 eigenvalue calculation should be benefit for CBZ. Additionally, the SP_3-perturbation method is developed based on the conventional SP_3 theory in this dissertation. There is a possibility that the SP_3P (OSP_3P) method could be improved with the rigorous SP_3 theory, but significant efforts are necessary.

Chapter 4

Conclusions

In this dissertation, a fast reactor analysis software, FRBurner, that meets various demands on new type fast reactor designs at different stages is developed and verified through a verification study, a multiple methods characteristic study, and an innovative reactivity calculation method study.

The verification of FRBurner suggests that this software can predict reactor physics key parameters like effective neutron multiplication factor, sodium void reactivity, Doppler reactivity, effective delayed neutrons fraction, and burnup reactivity accurately for general type of sodium-cooled fast reactors. The reliability of this module is clearly exhibited by the most rigorous option of the calculation method. Then, the multiple calculation methods characteristic study provides strong data support for choosing proper calculation for wide range utilization. As for the SP_3-based eigenvalue/flux calculation method, the proof about advantage of it through comprehensively comparing the calculation burden and accuracy with the transport and diffusion methods is a crucial part of work in this dissertation. It lays the data foundation for the subsequent SP_3-perturbation reactivity calculation research.

The study about the SP_3-perturbation reactivity calculation method is the most

important innovation in this dissertation. It fills the blank of SP_3 method utilization in fast reactor field research. Starting with the sodium void reactivity, the component-wise reactivity is discussed in depth. This dissertation points out a fact that widely-used form of the SP_3 equation set leads to an physical meaning unclear term in perturbation calculations, and this term can be eliminated with a form-changed SP_3 equations set. The comparison of prediction on scattering component reactivity between diffusion-perturbation, transport-perturbation, and SP_3-perturbation methods exhibits the advantage of the SP_3-perturbation method obviously. This advantage is discussed with three designed void pattern problems in this dissertation. Results indicate that the SP_3 method shows clear advantage in regions where neutron leakage is significant.

On the whole, the author has developed and verified a software applicable to various demands on fast reactor designs, and proposed a new method (SP_3-perturbation method) which is useful for the reactivity analysis. This software is useful for the new type fast reactor design in the future, and these two works together contribute to the nuclear engineering field greatly.

Bibliography

[1] G. Locatelli, M. Mancini, and N. Todeschini, "Generation IV nuclear reactors: Current status and future prospects," *Energy Policy*, vol. 61, pp. 1503–1520, 2013.

[2] IAEA, "Status of Fast Reactor Research and Technology Development (IAEA-TECDOC-CD–1691)," tech. rep., International Atomic Energy Agency (IAEA), 2013.

[3] G. I. Bell and S. Glasstone, "Nuclear reactor theory," tech. rep., US Atomic Energy Commission, Washington, DC (United States), 1970.

[4] D. G. Cacuci, *Handbook of Nuclear Engineering*. Springer Science & Business Media, 2010.

[5] Y. Nagaya, K. Okumura, T. Sakurai, and T. Mori, "MVP/GMVP Version 3: General Purpose Monte Carlo Codes for Neutron and Photon Transport Calculations Based on Continuous Energy and Multigroup Methods," tech. rep., JAEA, January 2017.

[6] W. S. Yang and M. A. Smith, "Theory Manual for the Fuel Cycle Analysis Code REBUS," Tech. Rep. ANL/NE-19/21, Argonne National Lab.(ANL), Argonne, IL (United States), 2020.

[7] B. J. Toppel, “User’s guide for the REBUS-3 fuel cycle analysis capability,” tech. rep., Argonne National Lab., IL (USA), 1983.

[8] G. Rimpault, D. Plisson, J. Tommasi, R. Jacqmin, J.-M. Rieunier, D. Verrier, and D. Biron, “The ERANOS code and data system for fast reactor neutronic analyses,” in *PHYSOR 2002-International Conference on the New Frontiers of Nuclear Technology: Reactor Physics, Safety and High-Performance Computing*, 2002.

[9] NEA, “NEA-1683 Eranos 2.3N. Modular code and data system for fast reactor neutronics analyses.,” 2022. https://www.oecd-nea.org/tools/abstract/detail/nea-1683/, Retrieved December 14, 2022.

[10] K. Yokoyama, T. Hazama, Y. Nagaya, G. Chiba, T. Kugo, M. Ishikawa, M. Tatsumi, Y. Hirai, H. Hyoudou, K. Numata, *et al.*, “Development of the next generation reactor analysis code system, MARBLE,” tech. rep., JAEA, 2011.

[11] K. Yokoyama, T. Hazama, K. Numata, and T. Jin, “Development of comprehensive and versatile framework for reactor analysis, MARBLE,” *Annals of Nuclear Energy*, vol. 66, pp. 51–60, 2014.

[12] K. Yokoyama, T. Jin, T. Hazama, and Y. Hirai, “Development of the versatile reactor analysis code system, MARBLE2,” tech. rep., Japan Atomic Energy Agency, 2015.

[13] K. Sugino and G. Rimpault, “Analyses of the JUPITER fast reactor experiments using the ERANOS and JNC code systems,” *ANS Int. Top. Mtg. on Advances in Reactor Physics and Mathematics and Computation into the Next Millennium (PHYSOR 2000)*, 2000.

[14] T. Hazama, G. Chiba, and K. Sugino, "Development of a fine and ultra-fine group cell calculation code SLAROM-UF for fast reactor analyses," *Journal of nuclear science and technology*, vol. 43, no. 8, pp. 908–918, 2006.

[15] K. Tada, Y. Nagaya, S. Kunieda, K. Suyama, and T. Fukahori, "Development and verification of a new nuclear data processing system FRENDY," *Journal of Nuclear Science and Technology*, vol. 54, no. 7, pp. 806–817, 2017.

[16] R. G. McClarren, "Theoretical aspects of the simplified Pn equations," *Transport Theory and Statistical Physics*, vol. 39, no. 2-4, pp. 73–109, 2010.

[17] G. Chiba and T. Endo, "Numerical benchmark problem of solid-moderated enriched-uranium-loaded core at Kyoto university critical assembly," *Journal of Nuclear Science and Technology*, vol. 57, no. 2, pp. 187–195, 2020.

[18] N. E. Stauff, T. K. Kim, T. A. Taiwo, L. Buiron, G. Rimpault, E. Brun, Y. Lee, I. Pataki, A. Kereszturi, A. Tota, *et al.*, "Benchmark for neutronic analysis of sodium-cooled fast reactor cores with various fuel types and core sizes," tech. rep., Organisation for Economic Co-Operation and Development, 2016.

[19] B. Igor'I, *Group constants for nuclear reactor calculations*. Consultants Bureau, 1964.

[20] V. Gopalakrishnan and S. Ganesan, "Self-shielding and energy dependence of dilution cross-section in the resolved resonance region," *Annals of Nuclear Energy*, vol. 25, no. 11, pp. 839–857, 1998.

[21] G. Chiba and T. Narabayashi, "Advanced Bondarenko method for resonance self-shielding calculations in deterministic reactor physics code system CBZ," *Annals of nuclear energy*, vol. 96, pp. 277–286, 2016.

[22] R. E. MacFarlane, “NJOY99.0: code system for producing pointwise and multigroup neutron and photon cross sections from ENDF/B data,” *US: Los Alamos National Laboratory*, 1999.

[23] R. Macfarlane, D. W. Muir, R. M. Boicourt, A. C. Kahler, III, and J. L. Conlin, “The NJOY Nuclear Data Processing System, Version 2016,” Tech. Rep. LA-UR-17-20093, Los Alamos National Laboratory, 1 2017.

[24] T. Tone, “A numerical study of heterogeneity effects in fast reactor critical assemblies,” *Journal of Nuclear Science and Technology*, vol. 12, no. 8, pp. 467–481, 1975.

[25] Y. Kawamoto, G. Chiba, M. Tsuji, and T. Narabayashi, “Numerical solution of matrix exponential in burn-up equation using mini-max polynomial approximation,” *Annals of Nuclear Energy*, vol. 80, pp. 219–224, 2015.

[26] G. Chiba, Y. Ohoka, K. Yamamoto, and H. Nagano, “Revisiting mini-max polynomial approximation method for nuclear fuel depletion calculation,” in *Proc. Int. Conf. on Math. Comp. Methods Applied to Nucl. Sci. Eng.*, 2019.

[27] K. Shibata, O. Iwamoto, T. Nakagawa, N. Iwamoto, A. Ichihara, S. Kunieda, S. Chiba, K. Furutaka, N. Otuka, T. Ohsawa, *et al.*, “JENDL-4.0: a new library for nuclear science and engineering,” *Journal of Nuclear Science and Technology*, vol. 48, no. 1, pp. 1–30, 2011.

[28] A. Santamarina, D. Bernard, P. Blaise, M. Coste, A. Courcelle, T. Huynh, C. Jouanne, P. Leconte, O. Litaize, S. Mengelle, *et al.*, “The JEFF-3.1.1 nuclear data library,” *JEFF report*, vol. 22, no. 10.2, p. 2, 2009.

[29] H. Greenspan, C. N. Kelber, and D. Okrent, *Computing Methods in Reactor Physics*. Gordon and Breach Science Publishers, 1970.

[30] K. D. Lathrop and B. G. Carlson, "Discrete ordinates angular quadrature of the neutron transport equation," tech. rep., Los Alamos Scientific Lab., N. Mex., 1964.

[31] E. M. Gelbard, "Application of spherical harmonics method to reactor problems," *Bettis Atomic Power Laboratory, West Mifflin, PA, Technical Report No. WAPD-BT-20*, 1960.

[32] E. W. Larsen, J. E. Morel, and J. M. McGhee, "Asymptotic derivation of the multigroup P1 and simplified PN equations with anisotropic scattering," *Nuclear science and engineering*, vol. 123, no. 3, pp. 328–342, 1996.

[33] O. Iwamoto, N. Iwamoto, K. Shibata, A. Ichihara, S. Kunieda, F. Minato, and S. Nakayama, "Status of JENDL," in *EPJ Web of Conferences*, p. 239, 2020. 09002-1-6.

[34] D. A. Brown, M. Chadwick, R. Capote, A. Kahler, A. Trkov, M. Herman, A. Sonzogni, Y. Danon, A. Carlson, M. Dunn, *et al.*, "ENDF/B-VIII. 0: The 8th major release of the nuclear reaction data library with CIELO-project cross sections, new standards and thermal scattering data," *Nuclear Data Sheets*, vol. 148, pp. 1–142, 2018.

[35] A. J. Plompen, O. Cabellos, C. De Saint Jean, M. Fleming, A. Algora, M. Angelone, P. Archier, E. Bauge, O. Bersillon, A. Blokhin, *et al.*, "The joint evaluated fission and fusion nuclear data library, JEFF-3.3," *The European Physical Journal A*, vol. 56, no. 7, pp. 1–108, 2020.

[36] W. Van Rooijen and G. Chiba, “Diffusion coefficients for LMFBR cells calculated with MOC and Monte Carlo methods,” *Annals of Nuclear Energy*, vol. 38, no. 1, pp. 133–144, 2011.

[37] Y.-A. Chao, “A new and rigorous SPN theory for piecewise homogeneous regions,” *Annals of Nuclear Energy*, vol. 96, pp. 112–125, 2016.

[38] S. Jeon, H. Hong, N. Choi, and H. G. Joo, “GPU Acceleration of the Prototype Pinwise Core Analysis Code VANGARD,” in *International Conference on Mathematics and Computational Methods Applied to Nuclear Science and Engineering (M&C 2021), Virtual Meeting*, 2021.

[39] S. Jeon, H. Hong, N. Choi, and H. G. Joo, “Methods and performance of a GPU-based pinwise two-step nodal code VANGARD,” *Progress in Nuclear Energy*, vol. 156, p. 104528, 2023.

[40] A. Vidal-Ferràndiz, S. González-Pintor, D. Ginestar, C. Demazière, and G. Verdú, “Pin-wise homogenization for SPN neutron transport approximation using the finite element method,” *Journal of Computational and Applied Mathematics*, vol. 330, pp. 806–821, 2018.

[41] Q.-Q. Pan, T.-F. Zhang, X.-J. Liu, H. He, and K. Wang, “SP3-coupled global variance reduction method based on RMC code,” *Nuclear Science and Techniques*, vol. 32, no. 11, pp. 1–10, 2021.

[42] A. E. Waltar, D. R. Todd, and P. V. Tsvetkov, *Fast spectrum reactors*. Springer, 2011.

[43] M. Tatsumi and A. Yamamoto, “Advanced PWR core calculation based on multi-group nodal-transport method in three-dimensional pin-by-pin geome-

try," *Journal of Nuclear Science and Technology*, vol. 40, no. 6, pp. 376–387, 2003.

[44] R. J. Stammler and M. J. Abbate, *Methods of steady-state reactor physics in nuclear design*. Academic Press London, 1983.

[45] Y.-A. Chao, "A new and rigorous SP_N theory–Part III: A succinct summary of the GSP_N theory, the P_3 equivalent $GSP_3^{(3)}$ and implementation issues," *Annals of Nuclear Energy*, vol. 119, pp. 310–321, 2018.